THE STRUCTURE OF COMPACT RADIO SOURCES AT 606 MHz

Thesis by

George H. Purcell, Jr.

In Partial Fulfillment of the Requirements

for the Degree of

Doctor of Philosophy

California Institute of Technology

Pasadena, California

1973

(Submitted May 14, 1973)

ACKNOWLEDGMENTS

Those who contributed most profoundly to this research project gave more of themselves than of their expertise. The inspiring teachers and exemplars of many years, as well as those who gave sympathetic encouragement at difficult times, will be unnamed here, but not forgotten.

Among the people and institutions that contributed directly, I am especially grateful to the National Science Foundation, which supported my graduate education;

To the Owens Valley Radio Observatory and the National Radio Astronomy Observatory, for the use of their facilities;

To the consulting staff at the W. H. Booth Computing Center, Caltech, for their friendly advice on numerous programming problems;

To Wayne Cannon, Ian Lockhart, John Broderick, and Bob Mutel, who helped make the observations;

To Ron Allen, Chuck Spencer, and Craig Moore, for engineering assistance at the Observatories;

To Barry Clark and George Grove of NRAO, who initiated me into the mysteries of the Mark II VLBI System;

To Drs. Ken Kellermann, Malcolm Longair, Randy Jokipii, James Gunn, Dave Jauncey, Maarten Schmidt, Jerry Kristian, and Bill Wright, for illuminating discussions,

data in advance of publication, and miscellaneous favors;

To my friend and colleague Dave Shaffer, for reliable help and thoughtful advice at every stage of the experiment;

And most of all to my thesis advisor, Professor Marshall Cohen, whose patient encouragement and wise counsel went far beyond the call of duty.

ABSTRACT

Long-baseline interferometry has been used to study the structure of thirteen compact radio sources at 606 MHz. The baseline was 3324 kilometers long and nearly east-west in orientation, so that the maximum angular resolution was about a hundredth of a second of arc for each source.

There were two series of observations, made on June 29 to July 1, 1971, and February 3 to 6, 1972. For most of the sources observed in each session, the correlated flux was measured from ten to forty times over a wide range of hour angle, with a standard error for each measurement of about 0.12 flux unit. A few sources were observed less often. Simple source models were then fitted to the data and compared to the models proposed by other observers.

The data for most of the sources were found to be consistent with models containing an elliptical halo concentric with an unresolved core. 3C 147, 3C 273, and 3C 279 appear to be more complicated, however. The observations of 3C 84, 3C 279, and 3C 345 also show evidence of weak structure at relatively large distances from the strong central components.

P1345+12 and CTD 93 were observed only in the first session, and 3C 120 and 3C 286 only in the second session. CTA 21, 3C 84, 3C 147, 3C 273, 3C 279, 3C 345, 3C 380,

CTA 102, and 3C 454.3 were observed in both sessions, and all but CTA 21 and 3C 380 gave strong evidence of changes in flux or structure during the interim. These changes appear to be intrinsic to the sources, and not the result of instrumental effects or scintillation phenomena.

CONTENTS

CHAPTER 1

INTRODUCTION AND THEORY

Introduction About fifteen years ago conventional ideas of galactic evolution began to undergo a profound change. At that time astronomers thought of galaxies, generally speaking, as massive condensations of matter whose angular momentum and mass had attained equilibrium distributions billions of years ago and could be expected to persist unchanged for billions of years to come. The shortest time scales associated with important changes in structure or external appearance were considered to be those connected with the evolution of the stellar content and the associated distributions of gas and dust; consequently one pictured galactic evolution as proceeding with majestic deliberation over intervals of millions of human lifetimes.

More recently, however, we have come to believe that in the dense central parts of galaxies and quasi-stellar objects significant evolutionary events can occur much more rapidly, on time scales of millions or thousands of years, or even less. Indeed, it appears that in some objects consequential developments can take place -- *have* taken place -- within the experience of a single observer. This revelation has been a dramatic one for observational

astronomers, and theoreticians too; but at the same time it has not, as yet, become revolutionary in the sense of introducing new principles or novel physical processes. Rather, it has come about primarily through the accumulation of a large and growing, though still very poorly understood, body of observations.

Although the evidence accumulated slowly at first, a definite trend had certainly developed by 1959, the year in which the Burbidges and Prendergast's reinvestigation of NGC 1068 *(16)*, together with Woltjer's theoretical speculations *(107)*, spurred a renewed interest in Seyfert galaxies. By 1963 a spectacular series of developments culminated in a comprehensive review article by Burbidge, Burbidge, and Sandage *(20)*, in which the authors brought together for the first time all the evidence of violent activity in galactic nuclei (including quasars), clearly defined the problems involved, and pointed out their enormous importance. Now, almost ten years later, we are more acutely aware than ever of the crucial role played by galactic nuclei in almost every phase of extragalactic astronomy. Yet new and puzzling discoveries continue to follow one another with such bewildering rapidity that even now we are better able to measure our progress by the questions we have learned to ask than by those we have been able to answer. As Geoffrey Burbidge put it in a 1970 review paper *(18, p. 453)*, "Clearly we are only at the beginning as far as both

observations and theory are concerned. Further studies of nuclei are essential if we are ever to make real progress in understanding the formation and evolution of galaxies, the overall energetics of the Universe, and cosmology."

Throughout the brief history of these studies radio observations have occupied a position of special importance. In the beginning, the detection of nonthermal radio emission was often the first indication of violent activity in extragalactic sources, and served to draw attention to whole classes of interesting objects. More recently radio methods owe their ascendancy to their superior resolving power, which can be exploited by three different kinds of observations: lunar occultation, scintillation, and interferometry. (Cohen's review article *(29)* delves into the history and techniques of all three.) The first two methods, though, are strictly limited in their scope by the uncontrollable and usually inconvenient parameters of the measuring apparatus -- namely the moon and the interplanetary plasma. For resolutions better than 0".2 or so, or for carefully controlled, reproducible studies of arbitrarily chosen sources, long-baseline interferometry is really the only practical alternative.

Interferometric methods have been used to study radio source structure since 1946, but the baselines of conventional systems are severely restricted by the need for a direct electrical connection between the two stations

during the observations. As a result the angular resolution of these systems is limited, for practical purposes, to about 0".01 even at short centimeter wavelengths. Shortly after the discovery of quasars, however, it became apparent that many compact sources were likely to have diameters of 0".001 or less, so that new techniques would be required in order to study them. In subsequent years several such systems have been developed *(29)*, all of which employ independent local oscillators at the two observing stations and use magnetic tape to preserve the output waveforms for later correlation. Since these systems are limited in resolution only by the accessibility of remote sites, the technique has come to be known, regrettably, as "very-long-baseline interferometry" or VLBI -- a term that misses the essential point completely. "Independent-oscillator interferometry" would be more apropos, but the current terminology is firmly entrenched and not likely to be supplanted.

During the past five years VLBI has contributed greatly to our knowledge of compact sources, yet the technique is far from realizing its full potential. It has been used at frequencies ranging from 18 to 22,200 MHz and on baselines of 200 meters (for tests) to 10,600 km, with most of the observations devoted to compact extragalactic objects. Resolutions of 0".001 or less, sufficient to detect structure as small as a parsec at the distance of the

Perseus cluster, are commonplace. Optical methods cannot as yet even approach this resolution for objects as faint as quasars, and so VLBI will remain for some time to come our only means of probing many of the most interesting compact objects.

On the other hand much of the work to date has been exploratory, and many of the results rather crude. The first studies were principally surveys designed to test the equipment and to determine the approximate sizes of a large number of sources. More recently interest has concentrated on a relatively small number of the most interesting sources -- principally those whose smallest-scale structure varies markedly in time. As a result the bulk of these more detailed observations have been made at the relatively short wavelengths, less than 21 cm, at which the variability was thought to be most pronounced. Increasingly, the emphasis has been on combining results from different baselines and frequencies to produce crude maps of the source structure.

My own program, the subject of the chapters that follow, has been an attempt to build on the earlier work by selecting a few of the strongest and most interesting sources and observing them as thoroughly as possible (on a single baseline) at a frequency and resolution that had previously been neglected. The NRAO-Cornell-Caltech group had already amassed a large body of data at 6, 13, and

18 cm *(22,23,24,33,34,58,59,60)*, along with sparser gleanings at 2.8 and 3.8 cm *(9,30,31,97)*; and the Canadian team had published a sizable mass of observations at 67 and 73.5 cm *(11,12,13,28,45)*. Between 18 and 67 cm, however, was a wide lacuna containing only a single small set of published results *(55)*. To help bridge this gap I selected an observing frequency of 606 MHz (49.47 cm wavelength). This frequency was convenient because it lies in a protected band and because appropriate radio-frequency amplifiers were readily available. In addition I hoped it would allow a really fruitful comparison with the Canadian results, in which I was particularly interested. Together with the antennas selected, the 130-foot at Owens Valley Radio Observatory and the 140-foot at NRAO, the frequency established a baseline having a maximum resolution of about $0''.01$.

The objective of the program was to learn something about the structure of the sources observed, by fitting simple models to the data and comparing those models to the ones proposed by other observers. Therefore I tried to design the experiment in such a way as to make the models as veritable as possible and to escape some of the difficulties encountered in previous work. More than anything else I wanted to avoid the uncertainties involved with interpreting a heterogeneous collection of data assembled from observations made on different baselines, using different equipment, at epochs months apart. Formerly, when a

given source was customarily observed only a few times in each observing session, one sometimes had to proceed in this way in order to put together enough information to derive a model; but the calibration problems entailed by such a procedure are formidable at best, and if time-varying components are involved they can become intractable.

In this second-generation experiment it was possible to proceed more systematically. All the observations were made on the same baseline using virtually the same equipment and were reduced uniformly. Furthermore, although there were two observing sessions separated by seven months, each of the sessions was designed to be complete in itself, so that the data from each could be reduced and interpreted independently. As originally conceived the purpose of the first session was to obtain fairly complete data and a preliminary model for each source, and to identify especially complex or otherwise interesting sources requiring more exhaustive study. Then the second series of observations would be used to fill gaps in the first series, resolve discrepancies, examine the most interesting objects in more detail, and possibly to look at some additional sources. The unexpected appearance of changes in the apparent structure of several of the sources during the interval between the two series later modified this plan, but it also justified my concern with the problem of assembling a self-consistent body of observations.

In selecting sources I relied mainly on the previous results cited above but also drew on other observations when possible. Since I planned to construct source models it was also necessary to choose from the strongest sources, in order that the correlation amplitudes remain well above the noise level even when the sources were fairly well resolved. This restriction narrowed the field of candidates considerably but left a group of twelve that seemed almost certain to have measurable structure in the range being investigated: CTA 21, 3C 84, P0403-13, 3C 119, 3C 147, 3C 273, 3C 279, 3C 287, 3C 286, 3C 309.1, 3C 380, and 3C 410. Ten further sources comprised a list of secondary interest: 3C 48, 3C 120, 3C 343, 3C 343.1, 3C 345, P2127+04, P2135-14, NRAO 667, P2203-18, and 3C 446. Table 1-1 lists the sources that were actually observed in one or both sessions, along with their redshifts and 606-MHz fluxes.

Theory Several authors have written excellent summaries of radio interferometry and aperture synthesis techniques. Perhaps those of Bracewell *(8)* and Swenson *(102)* are among the best. Here it will suffice to point out that what one observes directly with a two-element interferometer is a single point in the Fourier transform of the (two-dimensional) brightness distribution of the source. That is,

TABLE 1-1

The Sources Observed, with

Their Redshifts and Fluxes

SOURCE	REDSHIFT (z)	FLUX (606 MHz)
CTA 21	?	9.2
3C 84	0.018	24
3C 120	0.033	5.4
3C 147	0.545	38
3C 273	0.158	46
3C 279	0.536	11.3
3C 286	0.846	19
P1345+12	?	7.7
CTD 93	?	3.9
3C 345	0.594	8
3C 380	0.691	26
CTA 102	1.037	6.7
3C 454.3	0.859	13

$$V(u,v) = \frac{\int_{-\infty}^{\infty}\int_{-\infty}^{\infty} B(x,y)e^{-i2\pi(ux + vy)}\,dx\,dy}{\int_{-\infty}^{\infty}\int_{-\infty}^{\infty} B(x,y)\,dx\,dy} \qquad (1\text{-}1)$$

In this formula $V(u,v)$ is the observed quantity, usually called the complex visibility function, and $B(x,y)$ is the corresponding brightness distribution over the source. As formulated here x and y are in radians. The transform variables u and v are physically the components in the east-west and north-south directions, respectively, of the projection of the interferometer baseline (see below) onto a plane perpendicular to the line of sight to the source. Their units are wavelengths at the observing frequency, and they can be expressed in terms of the interferometer and source parameters as

$$u = \frac{D}{\lambda} \cos \delta_i \cos \theta \qquad \text{and} \qquad (1\text{-}2a)$$

$$v = \frac{D}{\lambda} (\sin \delta_i \cos \delta_s + \cos \delta_i \sin \delta_s \sin \theta) \qquad (1\text{-}2b)$$

where D and λ are the length of the baseline and the wavelength, respectively,

δ_i and δ_s are the latitude of the baseline and the declination of the source, respectively, and

θ is an angle usually called the "interferometer hour angle," or IHA.

In terms of more familiar quantities,

$$\theta = GST - \phi_i - \alpha_s - \frac{\pi}{2} \qquad (1\text{-}2c)$$

where GST is the Greenwich sidereal time,

ϕ_i is the longitude of the baseline, and

α_s is the right ascension of the source.

Observe that (1-2a,b) are the parametric equations of an ellipse, with θ as the parameter. Thus, as the earth and baseline rotate the observation point describes an ellipse in the transform plane.

Finally, note that the word *baseline*, as used here, means formally the line segment drawn from some reference point at one of the two telescopes, to the corresponding point at the other telescope. For convenience one often thinks of the baseline as having been translated (without rotation) so that its center lies at the center of the earth. The *longitude* and *latitude* of the baseline then refer to the axis along which the baseline lies.

CHAPTER 2

EQUIPMENT AND OBSERVING PROCEDURES

Equipment All the equipment was virtually identical in the two observing sessions. Figure 2-1, which applies to both stations, indicates schematically the arrangement of the main components. The following paragraphs describe each of these components in more detail.

The two telescopes were the 140-foot diameter paraboloid at the National Radio Astronomy Observatory in Green Bank, West Virginia, and the 130-foot paraboloid of the Owens Valley Radio Observatory near Big Pine, California. Table 2-1 lists the important parameters of the instruments and the baseline. The local horizon generally limited observations at both stations to zenith distances less than 75 degrees, and the hour-angle limit of the NRAO instrument (at seven hours) further restricted observation of the most northerly sources.

The feeds, designed at NRAO, were identical at the two stations. They consisted of two center-fed half-wave dipoles mounted perpendicular to one another over a ground plane, and connected through a hybrid junction in such a way as to receive radiation right-circularly polarized (according to the IEEE convention) at the source.

Circularly polarized feeds are required in order to

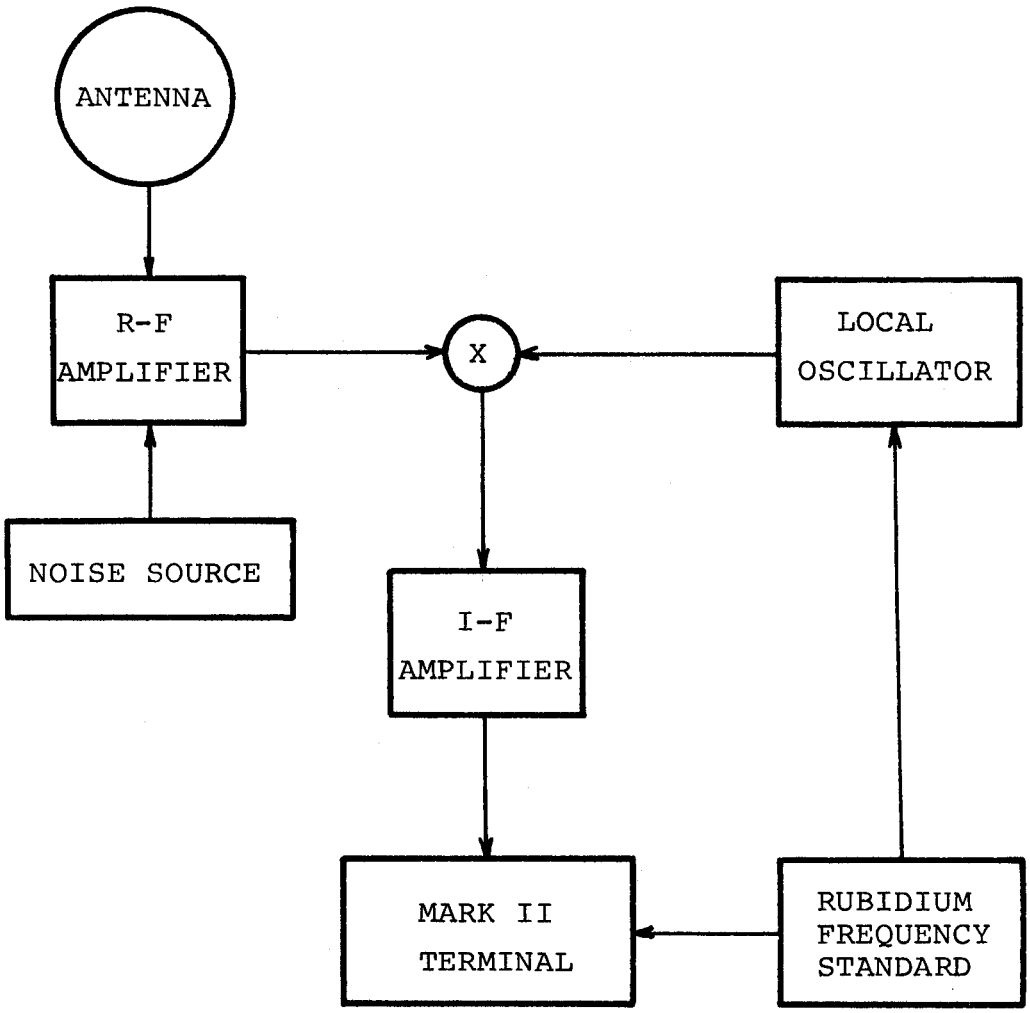

Figure 2-1. Simplified block diagram of the receiver.

TABLE 2-1

Parameters of the Telescopes and Baseline

PARAMETER	NRAO	OVRO
Aperture diameter (m)	42.7	39.6
Aperture efficiency (606 MHz)	≃50%	≃50%
Longitude	79°50'09".5	118°16'55".0
Geodetic latitude	+38°26'15"	+37°15'54"
Geocentric latitude	+38°15'02"	+37°02'47"
Geocentric radius (m)	6,370,816	6,371,635
Height above mean sea level (m)	826	1216

	BASELINE*
Longitude	7°43'00".0
Geocentric latitude	+1°49'09".6
Length (m)	3,324,155
Length in wavelengths (606 MHz)	6,719,442

*The baseline coordinates were determined interferometrically. The values quoted are nearly, but not exactly, consistent with the station coordinates.

avoid the decorrelation of linearly polarized signals caused by differential Faraday rotation. Late in the morning, at a frequency of 606 MHz, the difference in rotation between the two antennas could conceivably exceed half a radian. Unfortunately it is difficult to design a circularly polarized feed that illuminates the dish efficiently. Despite the fact that the dipole arms were tilted back slightly toward the ground plane in an attempt to narrow the beam, these feeds picked up about 100 K of spillover, a substantial fraction of the total system temperature.

The radio-frequency amplifiers were identical one-stage transistor amplifiers designed and built at the National Astronomy and Ionosphere Center. They contributed about 18 dB gain.

After being heterodyned down to an intermediate frequency of 30 MHz (at NRAO, 150 MHz) and further amplified, the signals at both stations entered Mark II VLBI recording terminals. These terminals, together with a "reproduce terminal" (described in Chapter 3) and a set of computer programs, comprise a complete system for recording and analyzing VLBI data. Since this system has been described in detail elsewhere *(26)*, I shall here merely outline the operation of the record terminal.

Figure 2-2 is a considerably simplified block diagram of the Mark II terminal. The i-f signal, at 30 MHz, first enters a section called the i-f converter. Here the

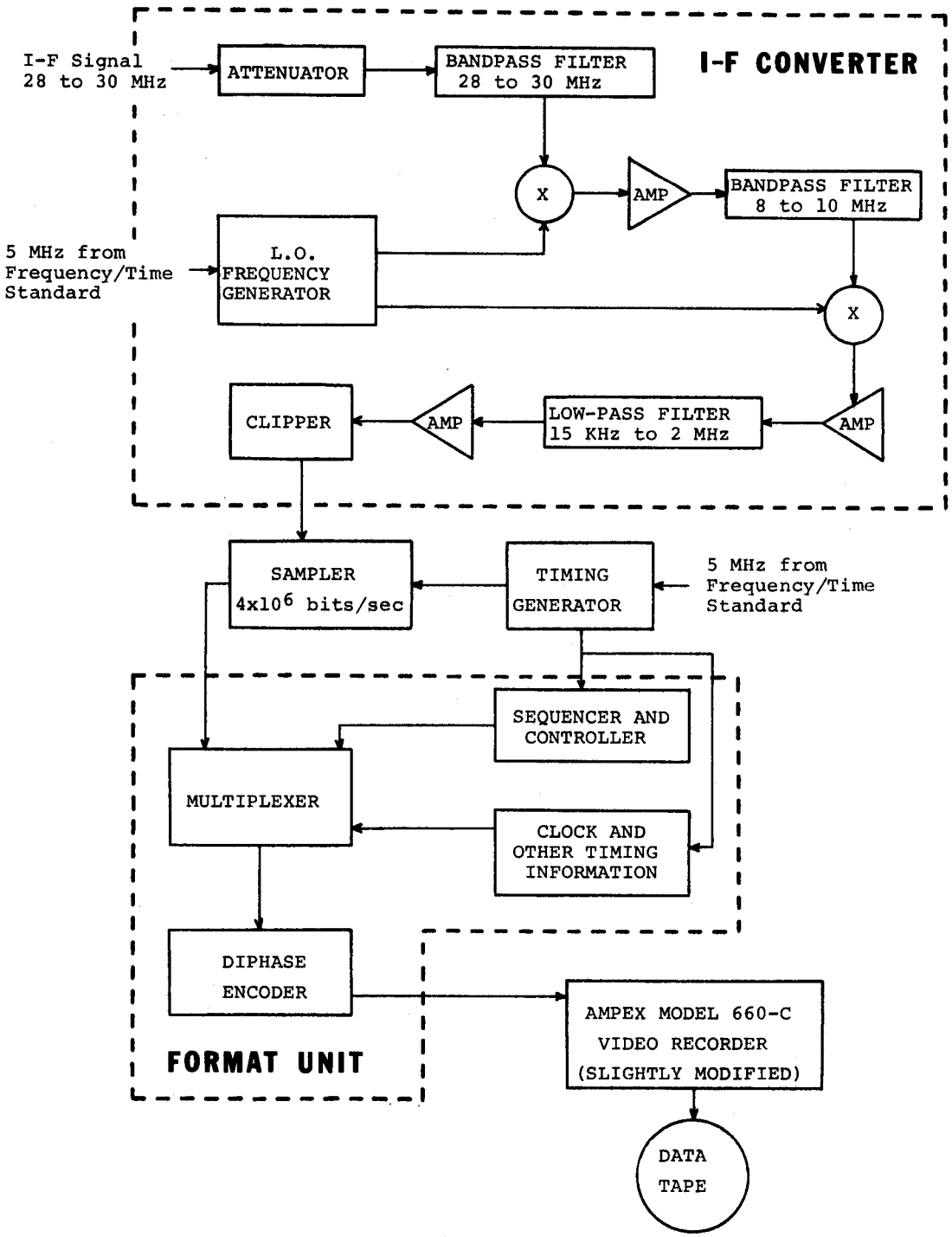

Figure 2-2. Simplified Block Diagram of the Mark II Record Terminal

signal passes through two additional mixing stages, with amplifiers and filters, which reject the upper side band (in this case the r-f signal between 607 and 609 MHz) and translate the lower side band, originally 605 to 607 MHz, to the video band extending from 2 MHz down nearly to zero. A clipper then transforms the video signal into a square waveform suitable for sampling.

In the next stage a sampler, carefully synchronized with the other functions of the terminal, samples the sign of the clipped video at intervals of a quarter of a microsecond (the Nyquist rate for a 2-MHz bandwidth) and sends the digital data on to the format unit.

The function of the format unit is to prepare the data for recording on video tape. The format itself is largely imposed by two dominant considerations: the electrical and mechanical aspects of the recording process, and the need for precise synchronization when two tapes are correlated. The recorder used in the terminal is the Ampex VR660-C, a commercial model designed for television work.

The tape, two inches wide, moves at 3.7 inches per second along a helical path around a cylindrical drum. Inside the drum, spinning at 30 revolutions per second, is a circular disk in which two recording heads are mounted on opposite sides. The two heads write alternately on the tape, for intervals of a sixtieth of a second. As it writes, each head follows a diagonal path about eleven inches long,

nearly from one edge of the tape to the other. Thus the basic unit of recording time is a sixtieth of a second (a "frame" in television parlance), and one function of the format unit is to insert patterns of synchronizing bits at the beginning and end of each frame. For convenience at playback, coarse timing information of the same precision is also recorded along an audio track near one edge of the tape.

Since the coherence time of the video data is only half a microsecond, however -- and since the recording and playback processes are less than perfectly stable -- it is necessary to supply timing information to the playback processor more often than sixty times a second. Therefore the format unit injects another short pattern of synchronizing bits into the data every 512 microseconds. All the timing bits displace data, of course, but the fraction lost is negligible.

The last function of the format unit is made necessary by the fact that the frequency spectrum of the data waveform, extending over many octaves, is unsuitable for recording. In the diphase encoder this waveform is transformed to a higher frequency range where it occupies only about one octave. The resulting signal, after being clipped, is finally used to hard-drive the heads of the recorder.

Among the remaining elements of the receiver,

the most critical of all is the frequency standard. When VLBI experiments fail the cause, more often than not, is in the phase stability of the receivers or in the timing. In this experiment both stations used Hewlett Packard Model 5065A rubidium vapor frequency standards. The 5-MHz output from these standards served to phase-lock the frequency synthesizers which generated the local oscillator signals, to synchronize the various functions of the Mark II record terminals, and to drive auxiliary clocks. Using these standards at an observing frequency of 606 MHz, one might hope to integrate the fringes for several minutes without appreciable loss of coherence. Actually, in this experiment ionospheric fluctuations were probably the principal factor limiting the coherent integration time, at least during the day.

The only other part of the system worthy of particular attention is the noise diodes used to calibrate the system temperature. VLBI observations are insensitive to receiver gain variations, but the total system temperature is a parameter that affects the results directly, and so it must be monitored. In theory one could use calibrated noise sources to measure the system temperature directly, but in practice it is difficult to make a reliable determination. Even without accurate calibration, however, *relative* system temperature measurements are easy and for my

purposes were adequate.

Estimates of the *absolute* system temperature were made in two ways -- by assuming an effective temperature for the noise source, and by observing sources of known flux density with an assumed aperture efficiency of fifty percent. The results of the two methods were consistent and indicated that the total system temperature at OVRO was near 600 K during both observing sessions, while the temperature at NRAO was in the neighborhood of 350 K. Of the total, perhaps 15 K can be attributed to sky background, 100 K to spillover, 200 or 250 K to the r-f amplifier, and the remainder to later stages of the receiver, notably the first mixer and the first i-f amplifier.

Observing Procedures The first observing session began at UT 1200 June 29, 1971, and ended at UT 2000 July 1, 1971. Between UT 1200 and 2000 on June 30 there was an eight-hour interruption for the weekly preventive maintenance at NRAO, so that 48 hours remained for set-up, tests, and observations.

The main objective of the observations was to measure the visibility amplitudes of CTA 21, 3C 84, 3C 147, 3C 273, 3C 279, 3C 345, and 3C 380 as thoroughly as possible as a function of hour angle, and the observing schedule was organized so as to make the measurements efficiently. In order to minimize the amount of time spent slewing

the telescopes I grouped the sources in close pairs -- for instance 3C 273 and 3C 279, 3C 345 and 3C 380 -- and generally observed each pair in alternation. This stratagem usually kept the transit time between sources under four minutes, although it failed badly when CTA 21 and 3C 84 crossed the meridian on opposite sides of the zenith at OVRO (where the telescope is on an altazimuth mount).

Certainly the most important question in planning the schedule was how long to make the individual observations. Several factors influenced the decision. Before each observation the observers at both stations fired their noise tubes momentarily to measure the system temperature. This measurement took a minute or so, and in order to include the source contribution it had to be made after the telescope was properly pointed. Hence the minimum interval between observations was sometimes as long as five minutes, and it would have been inefficient to make the observations shorter than the gaps. The requirement that the errors in the measurements be smaller than five percent also imposed a lower limit at about the same level, six or seven minutes.

On the other hand it is desirable to alternate between sources as rapidly as possible for two reasons: first, to observe the accessible hour-angle range as uniformly as possible, avoiding gaps in the data which would obscure or confuse part of the source structure; and second, to make as many independent measurements as possible, so as to have

enough redundancy to be able to recognize occasional bad data.

Weighing the various considerations I settled on ten minutes as a standard observation time. This choice made it possible to observe most of the sources twice an hour with adequate precision. Occasionally the schedule allowed longer observations, up to an hour in several instances.

In addition to the seven principal sources there were four presumed calibrators on the schedule -- P1345+12, CTD 93, CTA 102, and 3C 454.3 The presumption was that at least one or two of the four would be completely unresolved, would yield a constant fringe amplitude independent of hour angle, and could be used to establish the flux scale for the other sources. But all four turned out to have interesting structure, which in at least two cases varies markedly in time. This development was exciting, but it interfered badly with the flux calibration, as discussed in Chapter 3. In any case I observed these sources less often than the rest, emphasizing disparate baselines to assure that they really were unresolved. Furthermore I observed them for only five minutes at a time instead of ten, hoping that each source could be represented by a single average fringe amplitude.

The second set of observations lasted from UT 1300 February 3, 1972, until UT 1300 February 6, 1972, although

it was interrupted several times by bad weather and attendant problems at NRAO. It closely resembled the first series, and the few changes were more tactical than strategic. The basic observation interval remained ten minutes, and we still monitored the system temperature by firing a noise source just before each observation. Of the sources from the first session the principal seven (CTA 21, 3C 84, 3C 147, 3C 273, 3C 279, 3C 345, and 3C 380) were again on the schedule, now joined by 3C 120 and 3C 286. I had given up as hopeless the notion of calibrators, and abandoned P1345+12 and CTD 93 entirely; but CTA 102 and 3C 454.3 returned as interesting objects in their own right.

The additional observing time in the second session made it possible not only to repeat most of the observations from the first, and to fill in gaps, but also -- as I had hoped -- to reexamine some of the most complicated sources in more detail. In fact, there was enough time to observe 3C 84, 3C 147, and 3C 279 continuously through an entire apparition.

Tables of all the observations, for both sessions, will be found in Chapter 4 along with the source models.

CHAPTER 3

REDUCTION PROCEDURES

The reduction of the data on the video tapes involves three distinct phases which I shall describe in turn: recovery of the fringes, calculation of the fringe amplitude, and application of several correction and calibration procedures.

It would not be far from right to say that there are no data on the video data tapes -- nothing in the way of information about radio source structure, at least. Rather, the information resides in the relation *between* the tapes -- to be precise, in the correlation coefficient of the two bit streams. This fact is brought home with crushing clarity, from time to time, to the hapless "VLBer" who runs an ostensibly perfect experiment only to discover that he doesn't know the time, or perhaps the baseline, well enough to recover the fringes. Half a loaf is better than none, but half an interferometer is more on a par with half a pair of pliers or half a telephone number; and even two halves won't work unless they are fitted together in just the right way.

In the Mark II VLBI system the unit that does this fitting, or correlation, is the reproduce terminal. The reference previously cited *(26)* describes the terminal

thoroughly, and Appendix A discusses a few of the features relevant to statistical considerations. To summarize, the terminal consists of two tape players, a correlator, and other digital hardware, including a Varian 620-I computer that performs various control functions and writes out the calculated correlations on a standard nine track tape for further processing. An ASR 33 teletype also is available for auxiliary input-output functions. The tape players are Ampex VR660-C's, practically identical to the ones used in the record terminals.

When the processor correlates a pair of tapes, the computer begins by reading in the baseline parameters, source position, observation time, and other information needed to control the processor. This information has been written in advance on the first few inches of the "output" tape. Then the data tapes begin to run. Reading first the coarse and then the fine timing information, the processor aligns the tapes in time, offsetting them just enough to compensate for the difference in propagation time from the source to the two stations, and for any difference between the station clocks.

As the processor reads the two data tapes it first decodes them and then sends each of the resulting sequences of bits into a buffer. Operationally each of the buffers is like a circular array of 2048 bits, with a load pointer going round and round dropping successive bits into

consecutive storage locations. At the same time an *unload* pointer follows along about half a cycle behind, picking up the same sequence of bits. This device stabilizes the correlators against small fluctuations in the rates at which the data come off the tapes.

Leaving its buffer, one of the bit streams next encounters a phase rotator, which supplies two auxiliary bit streams approximating sine and cosine waves at the natural fringe rate. The input string is multiplied by each of these auxiliary sequences, and the two outputs go to the correlators. This manipulation reduces the apparent fringe rate to a value near zero, making it possible to accumulate correlations over hundreds of thousands of bits without smearing over an appreciable fraction of a fringe. Since the phase of the fringes is still unknown, both the sine and the cosine mixing are necessary in order to recover that phase and the full fringe amplitude in the subsequent processing.

In the correlators the outputs from the phase rotator finally meet the output from the other buffer. The present configuration uses thirty-one adjacent delay channels, permitting an uncertainty of plus or minus four microseconds in the overall timing. A thirty-second channel stores the total number of pairs of bits correlated, for normalization. The correlations are accumulated for a fifth of a second; at the end of that interval the contents

of all sixty-four channels (thirty-two sine and thirty-two cosine channels) are written onto the output tape along with some identification words and error information. This entire process continues to the end of the data on the input tapes, when the processor automatically stops.

The second stage of reduction is the recovery of the fringes. First, in many cases, it is possible to compress the data even further by averaging the correlation coefficients over an interval of a second or two using a program in the Mark II package called VLBAVG. In addition to the averaging, which saves time -- and money! -- further down the line, the program also can perform certain editing and correcting operations. (Reference *(26)* gives details of all the programs.)

Next the data tape passes to a program called VLBAMP, which averages the fringes coherently for a predetermined interval by doing a fast Fourier transform on the sequence of correlation coefficients. This process entails a search for the fringes through some range of residual delay and fringe rate, but at this stage one usually knows the delay within a microsecond, and the rate within perhaps forty millihertz, so that the search is not very extensive. For each integration interval the program computes and prints the time, the length of the integration, the fringe rate and delay, the fringe amplitude and phase,

and other information, including a summary of the errors detected in that interval during the first stage of reduction. The more important quantities also are punched on cards.

The choice of an integration interval is important. It must be long enough so that the signal emerges clearly above the noise, but not so long that fluctuations in the fringe rate reduce the coherence appreciably. Often there is considerable latitude in the choice. I used fifteen seconds in the first series of observations and reduced most of the second with both fifteen and seventy-five second integrations. The longer interval introduced a decorrelation of about two percent, but it reduced the noise level substantially and produced slightly better estimates of the fringe rate and delay. Because of their lower noise level I used the results of the seventy-five second integrations in the succeeding steps.

The next step is to edit the cards from VLBAMP. I began by partitioning the longer observations into sub-observations about ten minutes long, each of them destined to be a single point on the final visibility curves. Then I removed the obviously "bad" data. Some cards were merely redundant, the result of multiple first-stage processing. When something had been manifestly wrong during the observation -- a telescope mis-pointed, say, or a noise tube inadvertently left on for a minute -- naturally the

corresponding cards were rejected. Others were thrown out because of dangerously high error rates during correlation. In still other cases the data themselves supplied the only indication of pathology. Wildly discordant delays and fringe rates, accompanied by fringe amplitudes near the noise level, were the usual symptoms. Some of these anomalies probably resulted from momentary instability in one of the local oscillators, others possibly from undiagnosed errors in correlation.

Despite this careful pruning some bad data inevitably got through. Mild decorrelation of unknown cause is impossible to detect at this point. Only in the visibility curves does it become manifest, and sometimes not then. Nearly every VLBI experiment produces a few observations in which the correlation amplitude is unaccountably five, fifteen, possibly forty percent lower than it "ought" to be. The four points clustered around -5 hours in Figure 4-11b are an obvious case, as is the point at 3.1 hours in Figure 4-5a. But the two points at the far right in Figure 4-1b are more in doubt.

After editing, the cards in each sub-observation go into a program that computes the weighted mean values and standard errors of the important parameters of the observation: the residual delay, residual fringe rate, and correlation amplitude. Except for the amplitude, these values are final. In addition the program determines the mean time of

the observation, its length, and its mean coordinates in the visibility (u,v) plane.

The third and last stage of the reduction procedure applies three corrections to the raw correlation amplitudes, attempts to establish the relation between the amplitude scales for the two sets of observations, and finally tries to relate these correlation scales to an absolute flux scale.

Appendix A deals with the correction procedure in painstaking, if not painful, detail. Here it will suffice to observe that three corrections are necessary. First, the seventy-five-second coherent averages must be increased 1.8 percent to compensate for the empirically determined decorrelation due to small fluctuations in the apparent fringe rate. The decorrelation of the fifteen-second averages is negligible. Second, the presence of noise in the measured correlation coefficients causes the derived correlation amplitudes to be, on the average, a little too large. A small downward correction counteracts this effect. Third, all the amplitudes have to be scaled upward by a factor proportional to the geometric mean of the total system temperatures at the two stations (see equation (A-17)).

The estimated errors in the final, corrected correlation amplitudes are a by-product of the same analysis that produced the corrections. Apart from a scaling factor these

errors are exactly the ones that appear in the data tables and visibility curves of Chapter 4, and that determine the weighting factors in the model calculations. They account *only* for the statistical uncertainties inherent in the measurement of a signal in the presence of noise. In particular they include no contribution due to the uncertainty in the measurement of the relative system temperature, a factor that was occasionally significant during the second observing session. Nor do they account for sporadic or systematic errors such as would result from temporary instability in a local oscillator or from antenna gain varying as a function of zenith distance. Fortunately these additional contributions to the measurement error are generally either negligibly small or so large that they command individual attention.

More interesting than the correction factors, from a scientific standpoint, is the calibration of the two observing sessions against each other and against an absolute flux scale. During the planning of the experiment it seemed natural to suppose that these calibrations would be more or less trivial. The flux and structure of the sources would remain constant; therefore the shape of the visibility curves would be the same for both sets of observations. If the estimates of the system temperatures for the two sets were consistent, then the curves would be identical. Otherwise they would differ only by a scaling

factor that would be apparent from the curves. With nine pairs of curves to compare (one for each of the nine sources common to both sessions) one could determine the scaling factor quite accurately even if several of the curves were incomplete.

The flux scale was to have come from the calibrators in an equally direct way. The dearth of previous observations at comparable wavelength and resolution made the choice of calibrators difficult, to the extent that the best information about some candidates came from scintillation surveys. Nevertheless four sources seemed more promising than the rest: P1345+12, CTD 93, CTA 102, and 3C 454.3. If any one of these four had been completely unresolved -- and constant in flux -- it would have established the ratio of correlated flux to correlation amplitude and thereby solved all the calibration problems at a single stroke.

This simple-minded scheme disintegrated rapidly. The first series of observations revealed that none of the four calibrators was even close to being unresolved. Worse, the results of the second series showed definite evidence of changes in structure in five sources, with a sixth (3C 147) so equivocal as to be useless for calibration purposes. To complete the disaster, only two of the remaining three sources common to both sets of observations could be put on a flux scale consistent with the first set. It was clearly going to be necessary to resort to indirect means to

establish the calibrations.

The more crucial problem was the establishment of internal consistency between the two parts of the experiment, because that calibration would affect directly the character and interpretation of the temporal variations. I began by making the simplest possible hypothesis independent of the observations -- namely, that no calibration was needed. More precisely, I supposed that the best (lowest) geometric mean system temperature measured during the first part was equal to the best temperature measured during the second part. This assumption was plausible because, after all, the systems were virtually identical. The estimates of absolute system temperature made at both stations during the two sets of observations provided additional support. Of course, it wouldn't do to compare arbitrarily chosen observations from the two series, since the temperatures were rather worse at some times than at others; but it seemed reasonable to suppose that *at its best* the system would be about equally good in the two sessions.

This hypothesis drew more compelling corroboration from the observations. Of the three sources that had not shown evidence of changes in structure, 3C 380 was the most thoroughly observed in both parts of the experiment. For this source at least, the provisional normalization produced excellent agreement between the two sets of points.

The agreement was especially heartening since 3C 380 is a relatively large source with apparently simple structure and a history of only marginal variability even at high frequency *(61, p. 425)*. Among all the sources observed, 3C 380 would have to be considered one of the least likely to change appreciably during a seven-month interval.

The observations of a second source, CTA 21, also were consistent with the provisional normalization, although the second set of data was woefully incomplete. For the third source, 3C 273, the agreement was less good. It appeared that if the structure had remained constant the total flux must have increased by about ten percent (see Figure 4-5). On the other hand the long gap in the data from the second series made it impossible to rule out the possibility that there had been a change in structure as well. Moreover, 3C 273 is known to be an extremely active variable source at short centimeter wavelengths *(106,31)* with at least one component smaller than 0".005 *(58,60)*. Compared to 3C 380, at least, 3C 273 seems a relatively likely candidate for rapid variations at 606 MHz. Relying on the preponderance of the evidence, I adopted the provisional normalization permanently.

The flux calibration posed a more perplexing problem. The ideal calibrator would have been a completely unresolved source of known flux; unfortunately the observations discovered no such source. In fact it is quite

possible that no good calibrator exists for an experiment at this frequency, resolution, and sensitivity.

The next best calibrator would be a source of known flux and structure in which all the flux is in incompletely resolved components. In that case one could derive the correlation amplitude of the unresolved source from the model. Several sources in this experiment satisfied at least the requirement that none of the components be completely resolved. The problem is that in no case is the structure known precisely enough to assure that the model provides a reliable value of the unresolved correlation amplitude. Specifically, almost all of the models involve extended components for which the flux depends sensitively on the size.

A more embarrassing difficulty is that no one knows just what the fluxes of some of the sources (in particular, the calibrators) were at the epochs of the observations. In retrospect, we should have measured the fluxes ourselves, concurrently with the interferometry. At the time, though, flux measurements seemed superfluous: the sources all had been measured carefully before, and it was "well known" that at the low frequency of 606 MHz the fluctuations were slow and small. Not until I had read a preprint of Hunstead's paper *(54)* describing large changes in the total flux of CTA 102 and 3C 454.3 on a time-scale of months, did I begin to have confidence in my own observations of rapid

variations -- and to realize the full dimensions of the calibration problem. The irony was (what is really quite natural) that my two most compact sources, which still held out the best chance for an accurate flux calibration, were the very ones that were varying most erratically.

For a time there seemed to be some hope of finding the needed fluxes by extrapolating from neighboring epochs or frequencies. Hunstead's published fluxes at 408 MHz extend from mid-1967 to late 1970 for CTA 102, and from mid-1967 to mid-1971 for 3C 454.3. He also quotes two isolated measurements of 3C 454.3 at 610 MHz, made at Jodrell Bank in 1969 and 1970. In addition the group at Arecibo has measured the fluxes of both sources at irregular intervals, at frequencies of 318, 430, and 606 MHz. Figure 3-1 summarizes the few available observations made since the middle of 1969. Although the trends at the several frequencies are fairly clear, the relation between variations at different frequencies is obscure. There certainly is no way to estimate what the 606-MHz flux of either source was in 1971.5 or 1972.1, with a probable error less than fifteen percent.

None the less a flux calibration was vital to the experiment, and there was no choice but to rely on the four original calibrators in working it out. The other sources were simply too far resolved for their models to account reliably for all the flux. Even in one of the most favorable

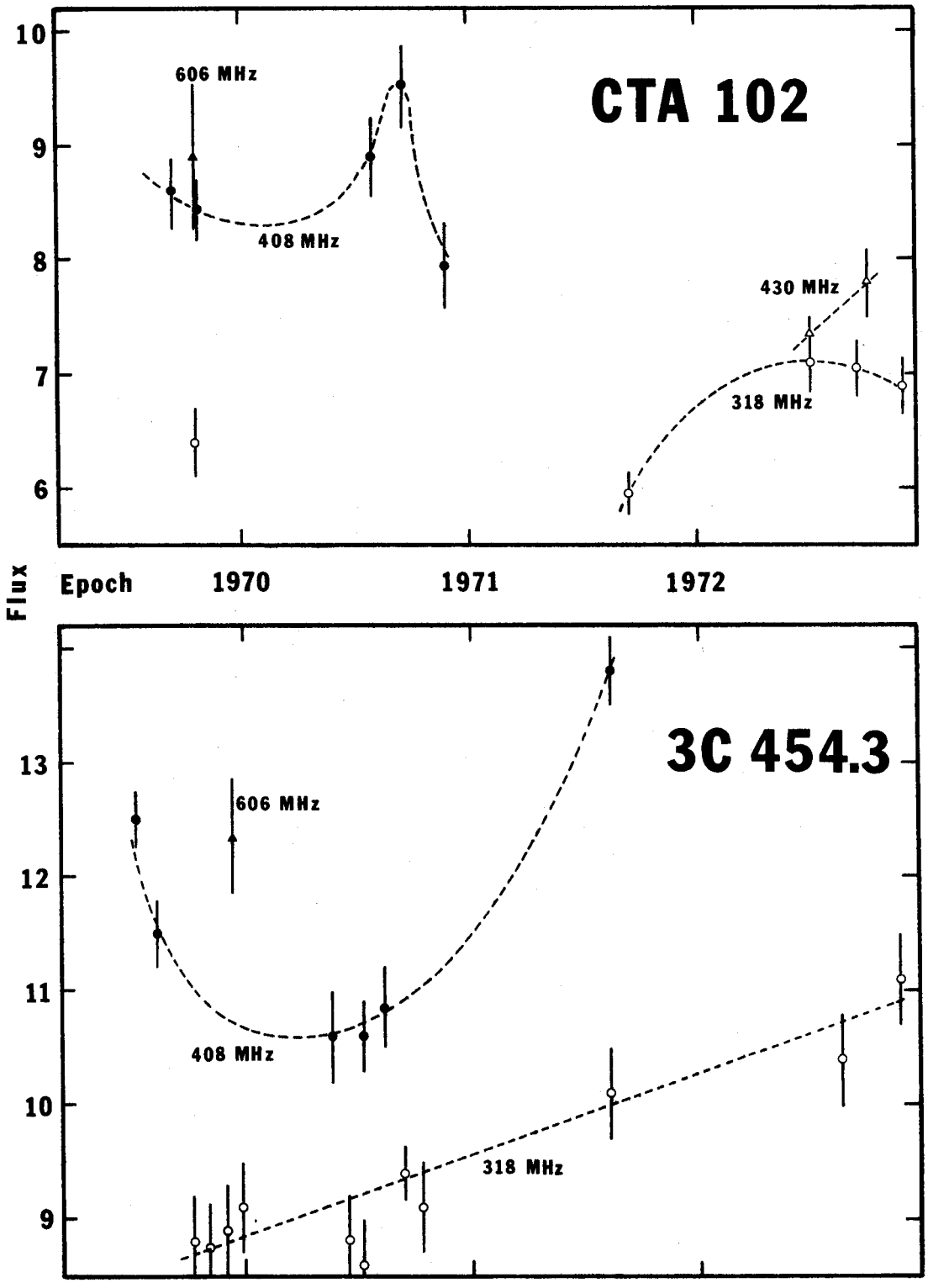

Figure 3-1. Recent flux variations in CTA 102 and 3C 454.3

cases, 3C 345, the model flux could easily be in error by fifty percent. The calibrators, by contrast, were much less resolved and the model fluxes correspondingly more trustworthy. The paucity of observations and the uncertainty in the fluxes of CTA 102 and 3C 454.3 were damaging handicaps to be sure, but by no means lethal ones.

Table 3-1 lists the calibration data, while the sections in Chapter 4 on the calibrators give the observations and the models. The tabulated values of the correlation coefficient corresponding to one flux unit of correlated flux, for the four sources, are remarkably consistent with the exception of the second value for 3C 454.3. This single discordance is hardly surprising in view of the marked change in source structure -- and flux -- that seems to have taken place during the seven months between the two sets of observations. The mean of the remaining values is 21.86, and I set the calibration factor equal to 22.0; that is, a correlated flux of one flux unit produces a (fully corrected) correlation coefficient of 0.00022. All the flux tables in Chapter 4 were computed from the corrected correlation coefficients by applying this conversion factor.

The error in this determination is due, as we have seen, to uncertainties in both the models and the source fluxes. Inspection of the numbers in Table 3-1 suggests an error of about ten percent if we agree to ignore the entry

TABLE 3-1

Flux Calibration Data

SOURCE	FLUX (f.u.)	CORRELATION UNITS* IN MODEL	CORRELATION UNITS PER FLUX UNIT
P1345+12	7.5	169.1	22.5
CTD 93	3.9	76.7	19.7
CTA 102 (1971)	6.7	162.6	24.2
CTA 102 (1972)	6.7	150.2	22.4
3C 454.3 (1971)	13.0	266.3	20.5
3C 454.3 (1972)	13.0	175.1	13.5

*One correlation unit corresponds to a correlation coefficient of 10^{-5}.

13.5, which is surely irrelevant. Considering the probable errors in the models and fluxes, however, I suspect that the consistency in the Table is partly fortuitous, and that fifteen percent is a more realistic estimate of the error. If the tabulated flux of CTD 93 is correct then the value 19.7 is certainly a lower limit, since the model was completely unresolved at the time of one of the observations (at +2.2 hours in Figure 4-10). We can also compute an upper limit on the conversion factor by using formula (A-17), because observed correlations are invariably smaller than the formula predicts. Substituting 0.5 for η_1 and η_2, 350 K for T_1, and 600 K for T_2, we find $\rho/S = 0.0003342$.

CHAPTER 4

SOURCE MODELS

Preliminary Considerations The need to proceed from visibility curves to source models arises from the motivation for the experiment -- our desire to understand the physical processes occurring in the source. In order to do so we want to know what the source "looks like" -- that is, what is the brightness distribution over its surface. Ideally, with a large (but finite) number of well chosen observations one could perform a complete aperture synthesis and compute the brightness distribution directly to some limiting resolution. This technique is standard in short-baseline interferometry.

In long-baseline work, on the other hand, one has very little freedom to choose his observations. The immobility of the antennas restricts the observation point in the Fourier transform plane to the single elliptical path (for each pair of antennas) given by formula (1-2). Furthermore, present techniques allow only the amplitude, and not the phase, of the fringes to be measured. Even with continuous measurements along the track, then, direct computation of the source brightness distribution by inversion of the visibility function is out of the question.

At the same time it is evident that even the few

data available conceal considerable information about the source structure. One might hope at least to discover whether the source is simple or compound in structure; and possibly to find out something about the number, size, shape, arrangement, and relative strengths of the components. Model-fitting techniques have proven themselves to be a useful, though indirect and hazardous, means of extracting some of this information.

The following section will expose some of the liabilities of the method. For the present, several desirable features are apparent: it provides a way to proceed where none existed; it is intuitively plausible; and it lends itself readily to analytic mathematical treatment and to systematic statistical procedures like least-squares analysis. In addition it allows us to incorporate other information obtained independently. We already know from previous observations, for example, that most extended radio sources consist of one or two, or rarely three, more or less discrete components, with the flux in each component concentrated toward the center. Indeed, the essential accuracy of early crude determinations of the structure of these extended sources is the principal justification for faith in the results of model-fitting on compact sources.

Additional information can be incorporated into the model too. Most sources containing compact components have

complicated spectra which give reliable information about the number and size of the components. Equally important are previous models of the same source, even at different frequencies. At the present primitive stage in the development of VLBI technique it is not always apparent what relation observations made at 18 cm wavelength in 1968, say, bear to observations at 50 cm in 1972. Gradually these relations are being sorted out, however, and frequently they provide valuable clues.

The Modeling Procedure Physical plausibility and mathematical tractability were the paramount considerations in deciding on the general form of the models. Four types of components, all with elliptical isophotes, were available to the fitting program: uniformly illuminated disks, limb-darkened disks, rings, and Gaussians. However, for the limited range of baselines spanned by the observations, the first three kinds proved virtually indistinguishable from the Gaussians, which I used exclusively in the final models. Each source, then, is supposed to consist of a small number (generally not more than three) of elliptical components with Gaussian brightness distributions. Each component, in turn, is specified completely by six parameters: its amplitude (or flux), the distance and position angle of its center with respect to some arbitrary origin in the source, the length of its major axis, its axial

ratio, and the position angle of its major axis. Models constituted in this way are versatile and easy to manage, and they conform well to the known brightness distributions of extended sources.

Appendix B deals with the mathematical features of the model-fitting scheme. Briefly, it is an iterative, nonlinear least-squares procedure: it attempts to vary the parameters in such a way as to find the model that reproduces the observations as faithfully as possible. As a starting point for the iteration, the program requires a moderately good initial guess. At the end of the computations it produces estimates of the standard errors in the parameter values it has determined, along with an error correlation matrix which is invaluable in assessing the model. The program also allows one to hold any desired parameters fixed -- to require that a particular component be circular, for instance, or that all the components lie along some given line.

In judging the results of the modeling procedure one principle prevails: the best model is the simplest one providing a reasonable fit to the data and consistent with trustworthy independent information about the source. An excellent numerical criterion for a model is its chi-square per degree of freedom (see formula (B-19) and the accompanying discussion). For a correct model, with accurate error

estimates, its value should be near one. The square root of this quantity, which I have called the "error factor," is given with each of the models in the final section of this chapter.

Behind this simple principle lurk various traps. Many of these problems have their origin in the initial model. In contrast to other situations in which least-squares analysis is habitually applied, the theory here gives no specific idea of what kind of fitting functions one should use. One obvious effect of this uncertainty is a weakening of the assumptions underlying the least-squares analysis. Another is that it is hard to know where to begin the iteration. Because of the nonlinear nature of the problem it is entirely possible for two or more dissimilar models to fit the observations equally well. It often happens, for instance, that several combinations of separation and position angle fit a double source equally well. The two models of CTA 21 (A and B in Table 4-2) exemplify another kind of ambiguity. One of the two may be correct; at least one is utterly wrong; yet the experiment fails to discriminate between them. The implication for the other models is perfectly clear. (Of course the likelihood of this kind of duplicity increases rapidly as the number of variable parameters approaches the number of data points, one reason why simple models are inherently preferable.)

A more likely situation occurs when the errors in some of the derived parameter values are highly correlated. The flux and size of an extended component generally fall into this category, as do the separation and orientation of a double source when the observations span only a small range of position angles. In these cases there can be a whole continuum of indistinguishable models.

Another ambiguity applies to almost all the models, and the reader should keep it in mind. Because the phase of the fringes is unknown, any model can be rotated through 180° to give a completely equivalent model. Ordinarily this rotation is of little interest, as its effect on the structure is nugatory; but when the model consists of a single strong component and two or more much weaker ones, any of the weak components can be rotated to the opposite side of the strong component to give a model that is *nearly* equivalent. Such a partial rotation does change the structure materially. The three-component models of 3C 279 (Table 4-11) are good examples.

Despite these various hazards source models can be enormously useful. The point is, that one must interpret a model skeptically, realizing that at best it can provide only a good approximation to the structure of a source. Often it is just a single representative from a considerable family of equally plausible relatives. At worst it

may misrepresent the source entirely.

The Models In this section are presented the complete data from all the observations in both series, along with the most likely model, or models, and a brief discussion of each source. For those sources that were observed in both sessions I computed first the models for the larger set of data and then used the results as starting points in fitting the smaller set.

The following Key explains the organization of the data in the different tables and figures.

- -

Key to the Tables and Figures

Tables of the Observations The data are arranged in five columns:

Column 1 contains the mean interferometer hour angle (IHA) for the observation, expressed in hours. It is identical to the angle θ in formula (1-2).

Columns 2 and 3 contain u and v, the coordinates of the observation point in the visibility plane. These coordinates are defined in formulas (1-2a,b).

Column 4 contains the observed correlated flux, expressed in flux units (10^{-26} watts per square meter per hertz). An asterisk following the flux indicates that the value is suspect and has been ignored in the model-fitting.

Column 5 contains the estimated standard error, in flux units, of the flux in column 4. These estimates are based on the statistical considerations discussed in Appendix A.

Tables of the Models Each component occupies two lines. The first line lists the parameter values, in ordinary type, and the second gives the corresponding error estimates, when applicable, in italics. In all cases the units of the error are the same as those of the parameter to which it refers.

The tabulated errors are standard deviations based on the linearized least-squares analysis described in Appendix B. Often when several parameters are highly correlated the errors computed in this way carry the model far beyond the valid range of the linear approximation. In these cases I have simply put "*L*" for the error, to indicate a large value. Occasionally an error was difficult to estimate for some other reason, and in such cases the column contains a question mark to indicate an unknown but presumably moderate-sized value. Where no error entry appears the parameter was not considered variable and was held constant during the fitting.

(A final warning: the error estimates, particularly when they are small, tend to invest the parameter values with a meretricious infallibility. Remember that unless

the model represents the source correctly, the parameter values and their errors are equally meaningless.)

The meanings of the column headings are as follows:

Column 1 is simply a serial number for reference.

Column 2 contains the component flux, in flux units.

Columns 3 and 4 contain the polar coordinates of the center of the component. r is expressed in seconds of arc, and θ in degrees. The origin is arbitrary but usually has been placed at the center of the strongest component. North corresponds to $\theta = 0°$, east to $\theta = 90°$.

Column 5 gives x, the full component length to half-maximum intensity along the major axis. The units are seconds of arc.

Column 6 contains α, the axial ratio ($0 \leq \alpha \leq 1$).

Column 7 gives ζ, the position angle of the major axis, in degrees. In accordance with the usual convention north is 0°, east 90°.

Figures In the figures the data are presented together with the corresponding models. Interferometer hour angle, in hours, is plotted along the abscissa, and flux, in flux units, along the ordinate. Note that the flux scale does not, in general, begin at zero. The error bars attached to the data are the same standard deviations that appear in the tables.

The meanings of the plotting symbols are as follows:

o data from the first series, June 29 to July 1, 1971;

△ same as o, but data not used in model computations;

● data from the second series, February 3 to 6, 1972;

▲ same as ●, but data not used in model computations.

CTA 21

A certain aura of mystery surrounds CTA 21, the strongest source at intermediate radio frequencies without an optical identification. Despite the renewed efforts of Kristian *(65)*, who has probed to twenty-second magnitude, the visual counterpart of this source remains as elusive as ever.

A less romantic reason for interest in the structure of CTA 21 is the fact that it was the primary calibrator in the extensive survey of radio scintillation made at Arecibo between 1965 and 1968 *(32,49)*. At that time the source was still completely unresolved *(1,79,4,40)*, and the investigators at Arecibo assumed that its scintillation index (that is, the fraction of the source scintillating) was 1.0 at 430 and 611 MHz. The discovery of appreciable structure larger than a few hundredths of a second of arc would invalidate that assumption and upset the entire calibration.

CTA 21's curved spectrum *(35,57)*, which peaks at about 900 MHz, suggests the presence of two compact components. Both are self-absorbed at 606 MHz, but the larger component can be expected to dominate the flux. At progressively higher frequencies the smaller component should become more and more prominent, causing the apparent size of the source to diminish.

Previous VLBI observations support this model. Observations at 18 cm *(23,24)* indicate a size near 0".01. Kellermann and others, combining data at 6 and 18 cm, derived a size of 0".008 for a simple source model *(58)*, but later, with more extensive data, suggested a core-halo structure in which the halo is about 0".01 in diameter, while the core is less than 0".002 *(60)*. Broderick and others *(10)* laudably forebore to propose a model based on their scanty data, but their 13-cm observations indicate a size somewhat smaller than 0".01.

Data at relatively low frequencies, including the present observations, imply a somewhat larger size in agreement with the core-halo model. Early Canadian work *(12)* suggested a diameter of about 0".02 in position angle 95°. The same group's more recent model, however, is rather different: two equally intense unresolved components separated by 0".11 in position angle 70° *(28)*. This model is founded on a larger but less homogeneous body of data *(11)* than the earlier one. The large separation is definitely inconsistent with other observations.

The 606-MHz data are listed in Table 4-1 and plotted in Figure 4-1. The hour-angle coverage in 1971 was fairly complete, although the point at -2.82 hours is unquestionably bad. In the 1972 data there are only four reliable points, so that it was impossible to do more with

them than check for consistency with the earlier observations. A sizable fraction of the data after 3.8 hours had to be deleted because of anomalously low correlation amplitudes, and evidently the same contagion, whatever it was, infected the rest of the observation as well. The apparent maximum in the visibility is therefore almost certainly spurious.

Modeling was difficult because the visibility curve is of a particularly simple form that submits to a variety of interpretations. (Note, however, that circularly symmetric forms are impossible.) Model A (Table 4-2), an equal point double, fits well but has a serious deficiency: it accounts for only about 66 percent of the flux. Model B, an elliptical model that fits equally well and accounts for all the flux, is more consistent with the earlier observations, although it lacks an unresolved core. Similar models with a core do equally well however: model B' (which is not plotted) shows that as much as 20 percent of the source flux can be concentrated at the center of the elliptical halo without disturbing the observed visibilities in the least. The large error estimates in this model reflect the uncertainty in the flux distribution.

Thus, while the observations confirm the trend of earlier work, they still fail to define clearly the structure of the source. If one allows the model to supply less

than the total source flux a variety of equal and unequal double models are possible in addition to the simple elliptical forms, with and without cores.

In fitting models to the four points from the second session I simply tried to verify that the data were compatible with models A and B. For each model only the flux was allowed to vary, and the resulting small changes and excellent fits show that the data are indeed compatible with the prior models. This absence of secular variation is also consistent with the total-flux observations at Arecibo, in which no significant changes have been seen at 318, 430, or 606 MHz over a period of several years *(56)*.

TABLE 4-1

Observations of CTA 21

EPOCH	IHA	u ($\lambda \times 10^6$)	v ($\lambda \times 10^6$)	CORR. FLUX	ERROR
1971	-3.824	3.622	-1.390	5.11	0.10
	-2.822	4.966	-1.070	3.97*	0.10
	-1.784	5.997	-0.648	4.36	0.10
	-0.951	6.509	-0.262	3.97	0.10
	+0.054	6.715	+0.232	4.11	0.10
	0.720	6.597	0.559	4.19	0.10
	1.974	5.839	1.140	5.08	0.10
	2.136	5.693	1.209	5.05	0.10
	2.302	5.533	1.278	5.08	0.10
	2.470	5.360	1.345	5.07	0.10
	2.638	5.178	1.410	5.34	0.10
	2.761	5.037	1.457	5.23	0.14
	3.056	4.678	1.563	5.33	0.10
	3.222	4.465	1.619	5.55	0.10
	3.388	4.243	1.672	5.69	0.10
	3.557	4.009	1.724	5.78	0.10
	3.723	3.771	1.771	5.71	0.10
1972	1.342	6.306	0.856	4.53	0.12
	2.344	5.490	1.295	4.77	0.11
	2.845	4.937	1.488	5.14	0.11
	3.348	4.297	1.660	5.51	0.11
	3.959	3.420	1.834	5.24*	0.18
	4.178	3.084	1.887	5.34*	0.11

TABLE 4-2

Models of CTA 21

	COMP.	FLUX	r	θ	x	α	ζ
1971, Model A Equal Point Double Error Factor 1.13	1	3.04 *L*	0.0	---	0.0	---	---
	2	3.04 *L*	0.010 *0.0004*	125.4 *3.7*	0.0	---	---
1971, Model B Elliptical Gaussian Error Factor 1.14	1	9.2	0.0	---	0.037 *0.001*	0.386 *0.011*	173.5 *0.4*
1971 Model B' Gaussian with Core Error Factor 1.15	1	1.84	0.0	---	0.0	---	---
	2	7.36	0.0	---	0.043 *0.001*	0.402 *0.013*	172.5 *0.5*
1972 Model A Equal Point Double Error Factor 1.05	1	2.93 *0.07*	0.0	---	0.0	---	---
	2	2.93	0.010	125.4	0.0	---	---
1972 Model B Elliptical Gaussian Error Factor 1.10	1	8.88 *0.11*	0.0	---	0.037	0.386	173.5

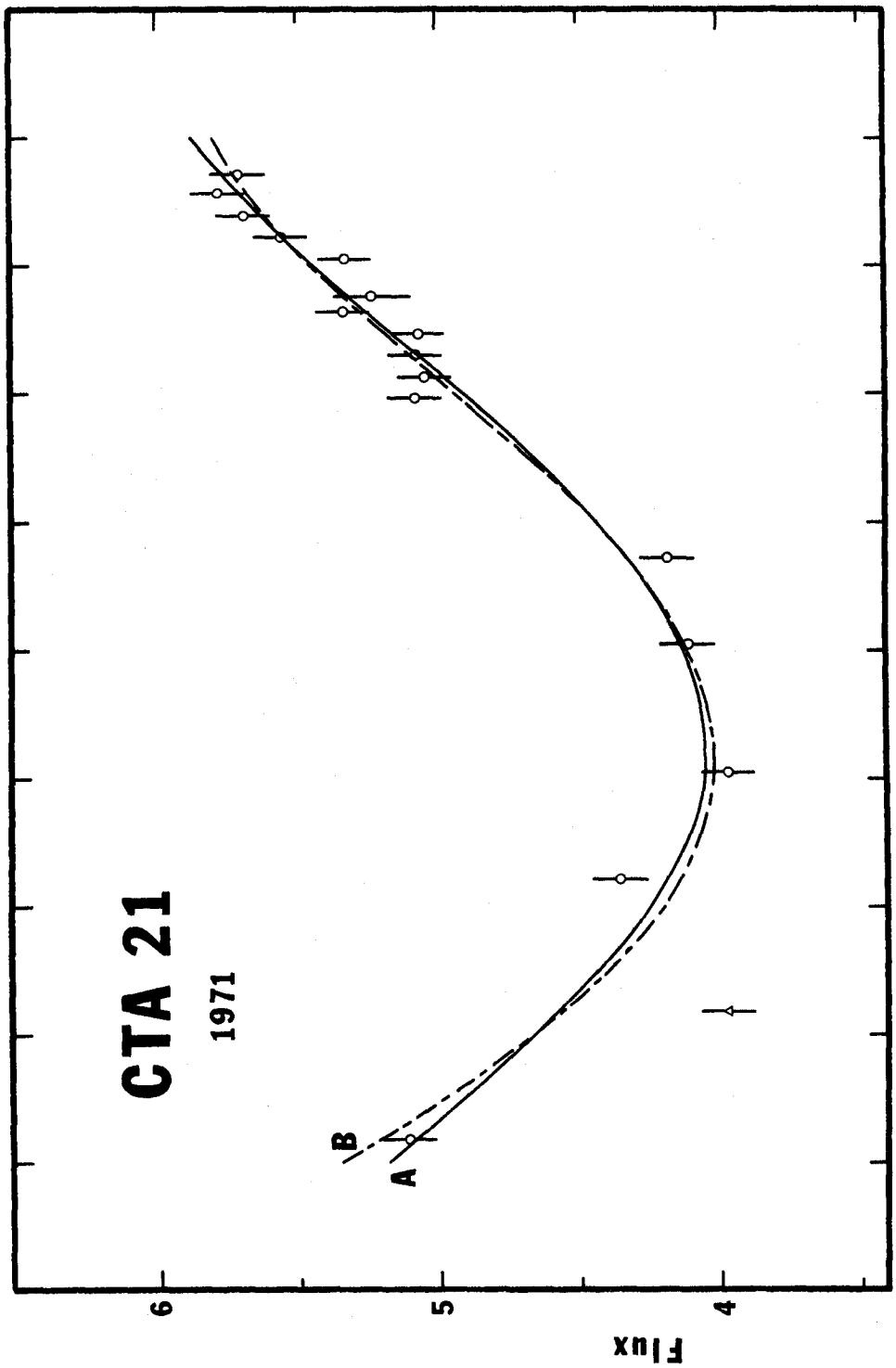

Figure 4-1a. Observed correlated fluxes and predictions of models for CTA 21. Epoch 1971. Key on page 49.

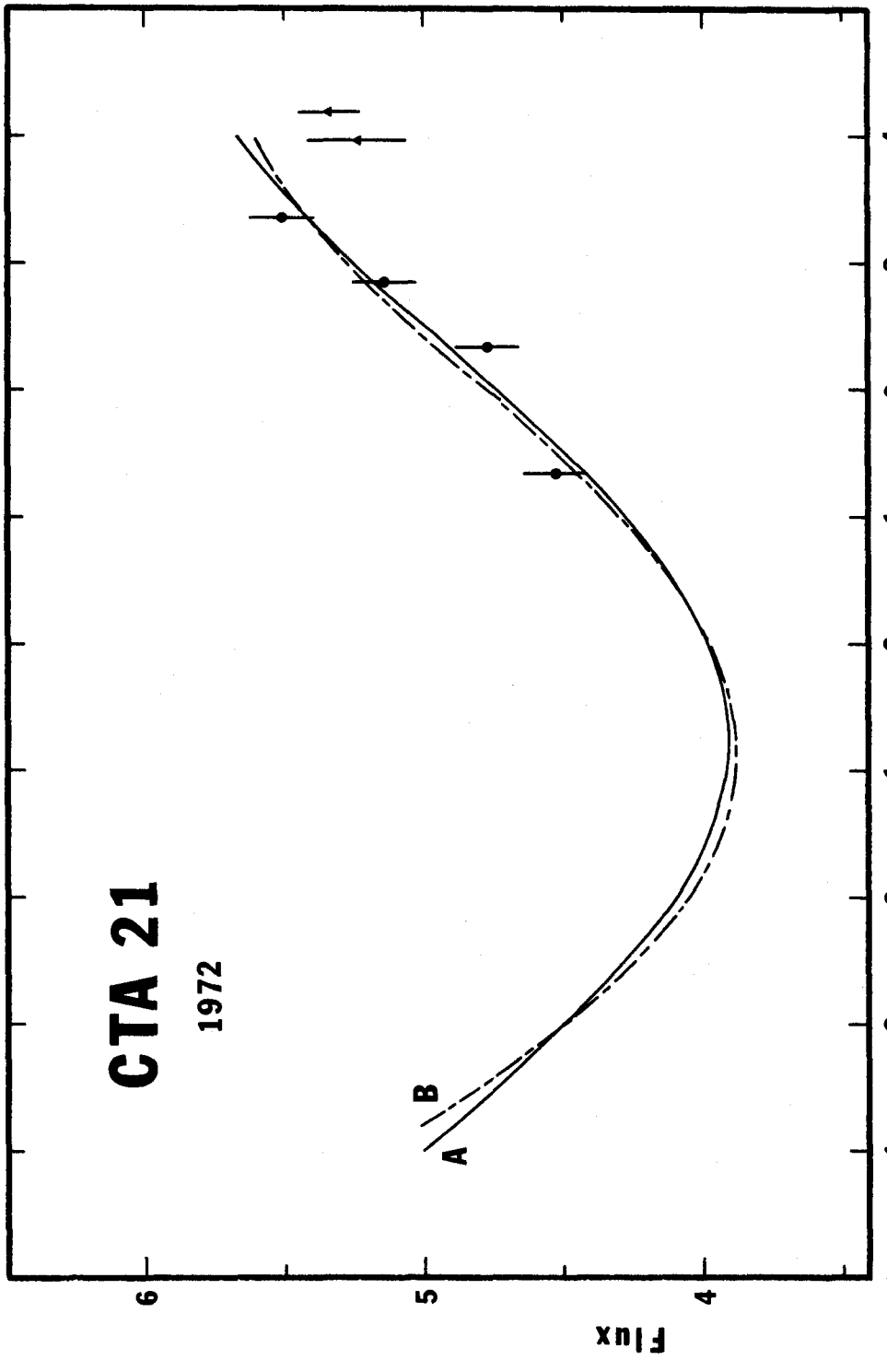

Figure 4-1b. Observed correlated fluxes and predictions of models for CTA 21. Epoch 1972. Key on page 49.

3C 84

Optical astronomers are more familiar with 3C 84 as NGC 1275. The brightest member of the Perseus cluster, it is a classical Seyfert galaxy *(96)*, but one with some rather bizarre refinements all its own. Unlike the other classical Seyferts, which are all relatively nearby spiral systems, it defies precise classification, but it clearly is neither a regular spiral nor an elliptical *(74)*. Easily its most remarkable feature is the enormously extended and rapidly moving system of filamentary structures that seems to have been ejected from the nucleus *(73,14)*. As Lynds *(68)* points out, his Hα interference photograph centered at 6694 Å bears a striking resemblance to the Crab nebula -- on a vastly greater scale.

The radio source in the neighborhood of NGC 1275 is no less extraordinary. On the largest scale there seems to be an extended source of low surface brightness spread over a large part of the whole Perseus cluster *(83)*. Centered on the galaxy is a smaller component about 5' across having a considerably steeper spectrum. This component is typical of strong radio galaxies. Finally, at or near the optical nucleus are two compact components both of which vary in time *(61, p. 438)*.

The smaller of the two compact components is more actively variable and dominates the flux at wavelengths

shorter than 11 cm. Early measurements at Jodrell Bank *(5,79,40)*, made at 21, 11, and 6 cm, established progressively smaller upper limits on its size and ultimately showed it to be smaller than 0".01 at 6 cm. As VLBI observations accumulated at 6 and 18 cm *(58,24,60)* a model consistent with Kellermann's partition of the curved spectrum emerged, in which the smaller component has a size near 0".001 while the larger has a diameter of 0".02 to 0".03. Other observations, however, indicate that the smallest-scale structure may be more complicated, with several components in the 0".001 range *(31)*.

At frequencies between 300 and 1400 MHz the larger compact component should predominate, but the Canadian model *(28)* takes no cognizance of it, proposing instead a double source consisting of two equal components 0".0008 in diameter separated by 0".037 in position angle 175°. Such a structure is difficult to reconcile with the source's highly suggestive flux spectrum, not to mention the extensive interferometry at short centimeter wavelengths.

The 606-MHz data (Table 4-3 and Figure 4-2) are incompatible with a point double source, but a single elliptical component fits them, and Kellermann's flux partition, rather well. As usual in a model of this sort the estimates of size and flux are closely interdependent, and foreknowledge of the flux is a great help. In the case of

3C 84 we know from the spectrum that the extended component contributes about eight flux units at 606 MHz, so that the model needs to supply only about sixteen.

The 1971 data (Figure 4-2a) deviate about twice as far from model A (Table 4-4) as one would like, but the correspondence of overall trends is clear. Besides, even the largest deviations amount to only about three percent of the total flux in the compact components, and so the departures from a perfectly smooth gaussian brightness distribution, needed to produce them, are very small. It would be easy to dismiss the two low points at 1.29 and 2.35 hours as examples of mild anomalous decorrelation, except for the fact that they coincide so well with minima in the more complete 1972 data.

The 1972 data (Figure 4-2b) are systematically and unmistakably different from the 1971 set, strong evidence that a change in structure has taken place. Yet surprisingly, the change in model A required to reproduce the change in the visibility curve is rather small. In fact, a shortening of the major axis by six percent is the only significant difference. In deriving this model I assumed that the flux had remained constant. Those who prefer that their sources expand, rather than contract, can achieve the same effect by making the minor axis -- or, if you like, both axes -- longer and increasing the flux at the same

time. The increase will have to be uncomfortably large, though, and the whole procedure violates the principle that models for the two epochs should be as nearly alike as possible.

Model B in Figure 4-2b was inspired by the fact that the discrepancies between the data and the simple elliptical source model were smaller and more systematic in the second session. The locations and shapes of the two additional components are quite uncertain and definitely not to be taken seriously. At the same time the ripples in the data appear to be authentic, and the model gives a good idea of the amount of flux and the distances involved in accounting for them. A single extra component matches admirably the data after -1 hour but is inevitably 180° out of phase with the four points at the far left.

TABLE 4-3

Observations of 3C 84

EPOCH	IHA	u ($\lambda \times 10^6$)	v ($\lambda \times 10^6$)	CORR. FLUX	ERROR
1971	-5.473	0.923	-4.240	3.87	0.10
	-5.308	1.209	-4.210	3.66	0.10
	-5.146	1.490	-4.172	3.89	0.10
	-4.974	1.781	-4.123	3.86	0.10
	-4.808	2.061	-4.068	3.74	0.10
	-4.677	2.280	-4.018	3.80	0.13
	-4.084	3.230	-3.735	3.93	0.10
	-3.582	3.973	-3.422	4.01	0.10
	-2.553	5.271	-2.593	4.28	0.10
	-2.046	5.775	-2.108	4.00	0.10
	-1.216	6.379	-1.230	4.08	0.10
	-0.255	6.701	-0.137	4.52	0.10
	+0.029	6.716	+0.194	4.68	0.10
	0.568	6.642	0.819	4.81	0.10
	1.066	6.456	1.383	5.07	0.10
	1.294	6.334	1.636	4.33	0.10
	1.663	6.090	2.033	4.94	0.10
	2.348	5.486	2.722	4.29	0.13
	3.026	4.717	3.322	4.74	0.14
	3.722	3.772	3.835	4.16	0.10
	4.087	3.224	4.057	4.10	0.13
	4.217	3.023	4.127	4.00	0.10
	4.292	2.904	4.165	3.96	0.10
	4.383	2.759	4.210	4.03	0.10
	4.550	2.489	4.286	3.93	0.10
	4.716	2.215	4.354	3.77	0.10
	4.854	1.985	4.404	3.82	0.10
	4.928	1.860	4.428	3.38	0.12

TABLE 4-3 -- Continued

EPOCH	IHA	u ($\lambda \times 10^6$)	v ($\lambda \times 10^6$)	CORR. FLUX	ERROR
1971	+5.081	1.601	4.474	3.44	0.10
	5.254	1.304	4.518	3.32	0.11
	5.419	1.018	4.551	3.25	0.12
1972	-4.572	2.453	-3.975	4.42	0.14
	-4.399	2.733	-3.898	4.63	0.13
	-4.222	3.015	-3.810	4.92	0.12
	-3.997	3.362	-3.686	4.71	0.13
	-0.942	6.513	-0.925	4.41	0.12
	-0.780	6.577	-0.741	4.55	0.12
	-0.613	6.630	-0.549	4.58	0.12
	-0.450	6.669	-0.363	4.51	0.12
	+0.224	6.705	+0.420	5.07	0.12
	0.391	6.681	0.614	4.87	0.12
	0.558	6.645	0.806	4.86	0.12
	0.725	6.595	0.998	5.02	0.12
	0.892	6.534	1.188	4.69	0.12
	1.059	6.460	1.376	4.60	0.12
	1.254	6.357	1.593	4.60	0.14
	1.400	6.270	1.753	4.61	0.12
	1.568	6.158	1.932	4.73	0.12
	1.735	6.035	2.109	4.75	0.12
	1.902	5.901	2.282	4.47	0.12
	2.064	5.759	2.446	4.41	0.13
	2.250	5.584	2.628	4.41	0.15
	2.396	5.438	2.767	4.24	0.13
	2.563	5.260	2.922	4.52	0.13
	2.730	5.072	3.072	4.53	0.13
	2.897	4.875	3.216	4.11	0.13

TABLE 4-3 -- Continued

EPOCH	IHA	u ($\lambda \times 10^6$)	v ($\lambda \times 10^6$)	CORR. FLUX	ERROR
1972	+3.064	4.669	3.353	4.34	0.13
	3.441	4.170	3.643	4.25	0.10
	3.650	3.876	3.788	4.48	0.13
	3.818	3.632	3.897	4.40	0.13
	3.985	3.381	3.998	4.24	0.13
	4.152	3.124	4.092	4.04	0.13
	4.301	2.889	4.170	4.35	0.14
	4.745	2.168	4.365	4.02	0.19
	4.912	1.888	4.423	4.02	0.19
	5.079	1.604	4.474	3.80	0.19
	5.246	1.317	4.516	3.86	0.19
	5.406	1.041	4.549	4.01	0.20

TABLE 4-4

Models of 3C 84

	COMP.	FLUX	r	θ	x	α	ζ
1971, Model A Elliptical Gaussian Error Factor 1.87	1	16.0	0.0	---	0.0300 *0.0001*	0.601 *0.005*	174.3 *0.5*
1972, Model A Elliptical Gaussian Error Factor 1.40	1	16.0	0.0	---	0.0282 *0.0002*	0.638 *0.005*	178.0 *0.5*
1972, Model B Three Components	1	16.0	0.0	---	0.0282 *0.0002*	0.638 *0.005*	178.0 *0.7*
	2	0.15 *0.08*	0.154 *0.009*	121.3 *3.2*	0.0	---	---
Error Factor 1.12	3	0.46 *L*	0.170 *0.003*	129.2 *3.6*	0.0281 *L*	0.3 *L*	55.1 *L*

(For explanation see key on page 48.)

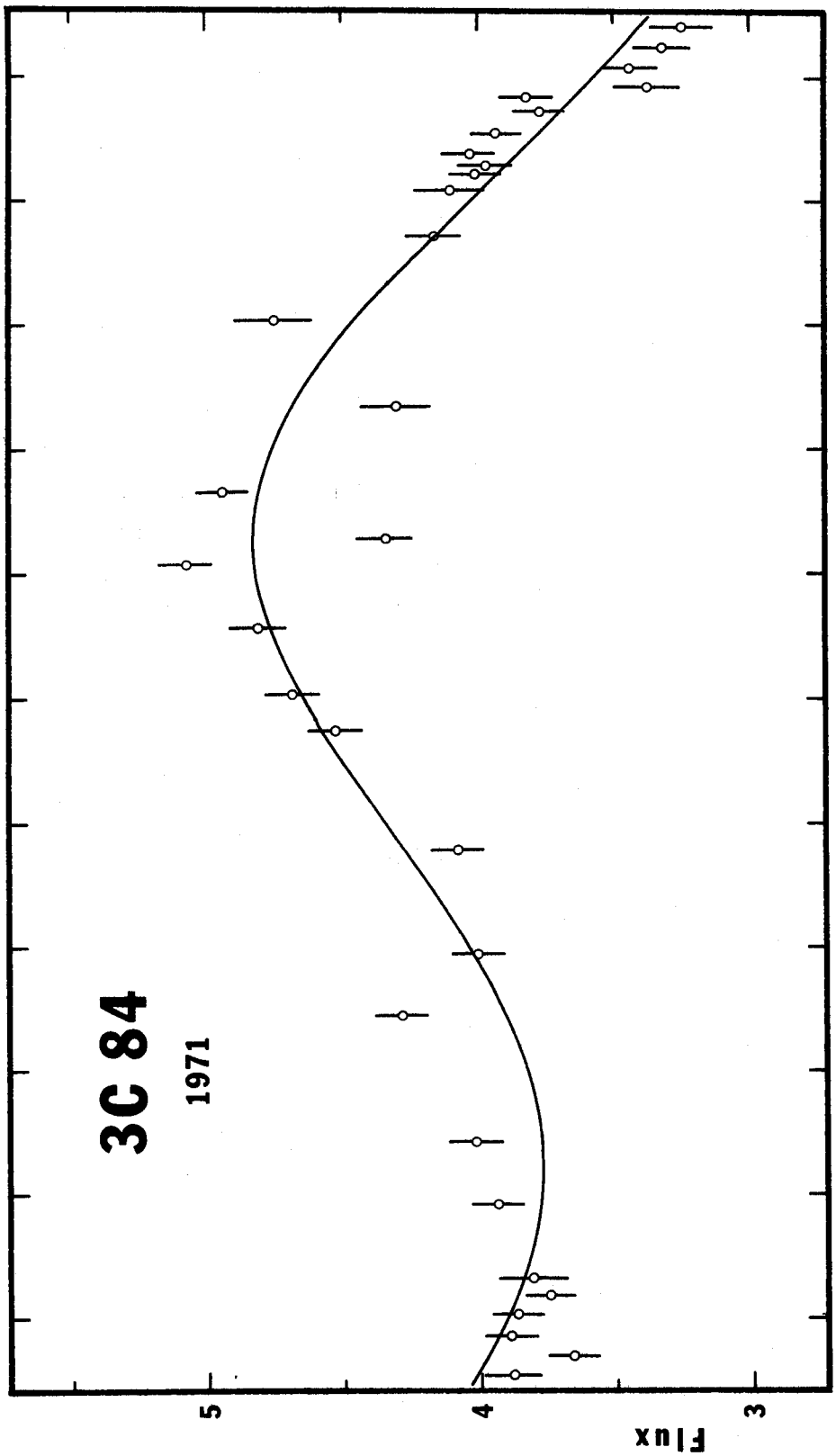

Figure 4-2a. Observed correlated fluxes and predictions of models for 3C 84. Epoch 1971. Key on page 49.

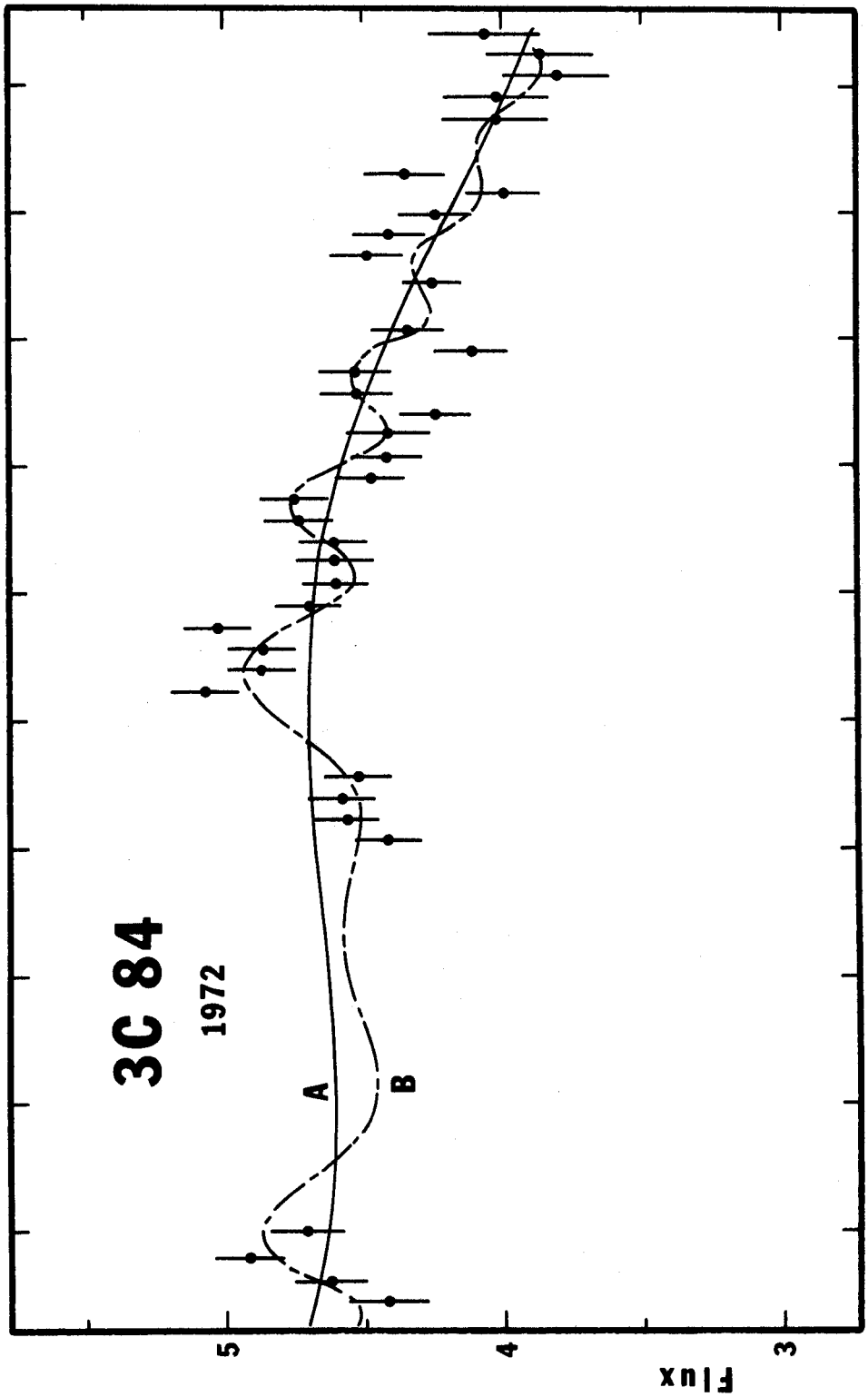

Figure 4-2b. Observed correlated fluxes and predictions of models for 3C 84. Epoch 1972. Key on page 49.

3C 120

Shimmins, Clarke, and Ekers *(98)* identified 3C 120 with a galaxy of magnitude 14.4 whose stellar nucleus and strong, broad emission lines make it appear to be an unusually luminous Seyfert galaxy *(89)*.

At short centimeter wavelengths this object has a complicated history of violent variability involving components ranging from a few thousandths of a second in diameter on down *(80,60,97)*. There is also an extended component about 10' in diameter that has a spectrum typical of radio galaxies *(43)*. This component predominates at low frequencies but of course is completely resolved in all VLBI measurements.

Between these two extremes is another component, denoted "B" by Kellermann and others *(58)*, which they characterize as quiescent or slowly varying. Its size is uncertain but probably less than 0".003, and its strength at 606 MHz must be in the neighborhood of one or two flux units *(80)*. According to Kellermann's model this is the only component one would expect to see in low-frequency VLBI, and the few observations seem to bear the model out. The Canadians' two reliable measurements at 448 MHz *(11,28)* establish only that the correlated flux is less than two flux units; but Jauncey and others, at 610 MHz, measured about 1.7 flux units on baselines between four and five

million wavelengths *(55)*.

The source is really too weak to belong in the present program. I added it to the second session only to fill in some spare time, and then lost most of the observations anyway because of bad weather in West Virginia. The six surviving measurements appear in Table 4-5 and Figure 4-3. Despite a hint of varying resolution the point-source model is really the only one justified by the data and the preexisting evidence. It corresponds well to the B component, although the flux seems a little smaller than that measured by Jauncey's group a little more than three years earlier.

- -

TABLE 4-5

Observations of 3C 120

EPOCH	IHA	u ($\lambda \times 10^6$)	v ($\lambda \times 10^6$)	CORR. FLUX	ERROR
1972	-0.152	6.711	0.188	1.27	0.12
	1.347	6.303	0.427	0.93	0.18
	1.855	5.940	0.502	1.07	0.14
	2.392	5.441	0.576	1.09	0.18
	3.276	4.394	0.681	1.45	0.09
	3.635	3.898	0.717	1.42	0.09

TABLE 4-6

Model of 3C 120

	COMP.	FLUX	r	θ	x	α	ζ
1972 Point Source Error Factor 1.59	1	1.31 *0.08*	0.0	---	0.0	---	---

(For explanation see key on page 48.)

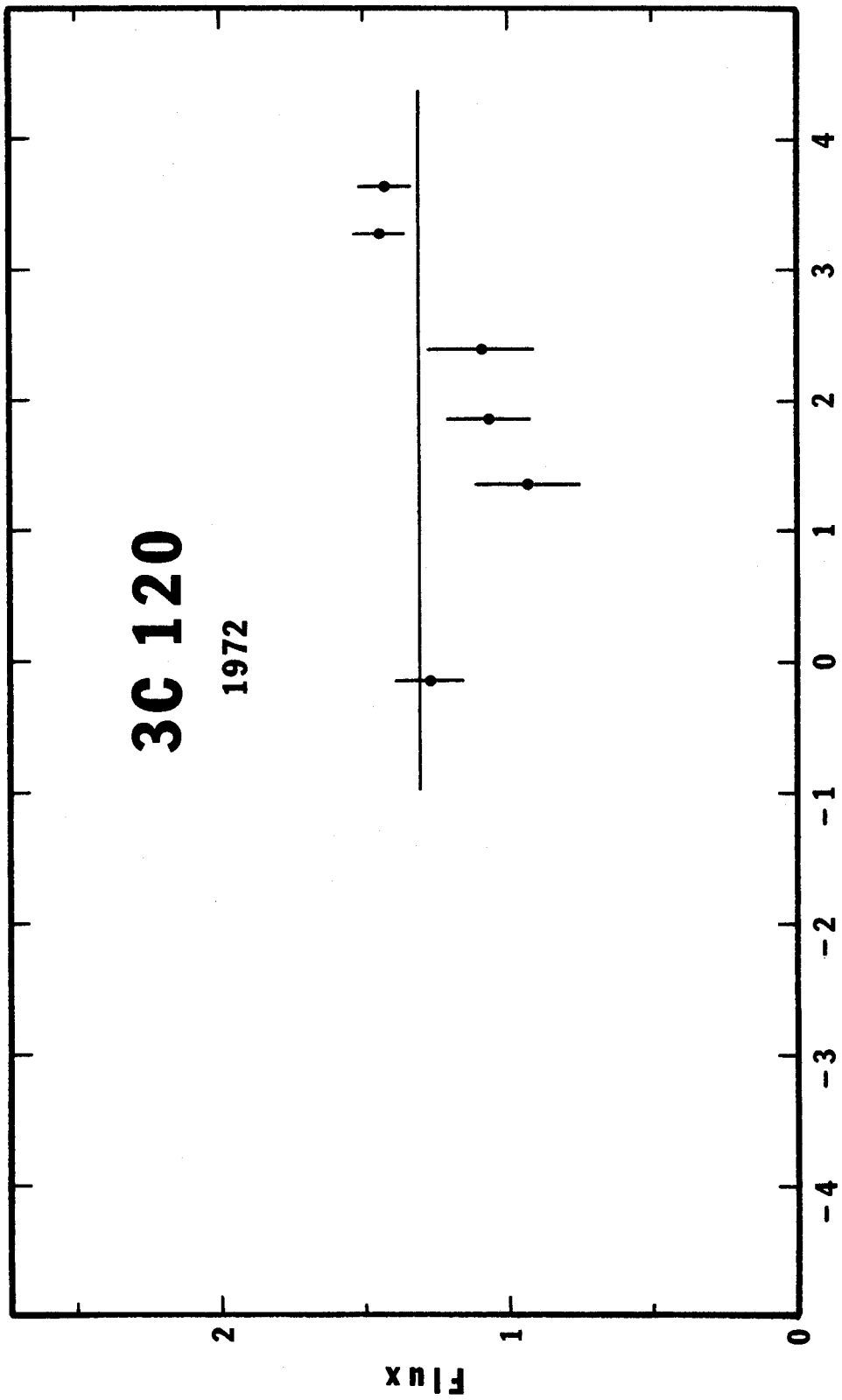

Figure 4-3. Observed correlated fluxes and prediction of model for 3C 120. Epoch 1972. Key on page 49.

3C 147

3C 147 was identified by Schmidt and Matthews *(95)* with a nondescript quasar of visual magnitude 16.9 *(19)*.

The radio observations are thoroughly confusing, if not contradictory. Most of the early work concentrated on low frequencies. Rowson, at Jodrell Bank, proposed a double structure at 158.6 MHz with more or less unresolved components separated by $2\overset{''}{.}4$ in position angle 35° *(82)*; and subsequent scintillation studies by Hewish and others, at 178 MHz, confirmed the presence of structure rather smaller than a second *(51)*. However recent VLBI measurements, made at 121.6 MHz on a baseline comparable to Rowson's, find the source completely unresolved and thus cast doubt on the larger-scale structure *(42)*.

At a somewhat higher frequency, 408 MHz, Anderson and Donaldson *(4)* proposed an elliptical gaussian structure $0\overset{''}{.}52 \times \underline{<}0\overset{''}{.}21$, elongated in position angle 55°. Their data are also consistent with a double structure of somewhat smaller elongation, but not with the one propounded by the Canadian group *(11,28)*. In the latter model, based mostly on 448-MHz data, half the flux comes from a completely resolved component between one and two seconds in size; and the rest is divided equally between two unresolved components separated by $0\overset{''}{.}24$ in position angle 85°.

Observations at still higher frequencies only

aggravate the atmosphere of uneasy accommodation among the various results. The most thorough and accurate study of 3C 147 to date is that of Donaldson and Smith *(79,41)*, who obtained continuous, twenty-four-hour observations on the Malvern-Jodrell Bank baseline at wavelengths of 21 and 11 cm. In their model 80 percent of the total source flux comes from a region they call 3C 147B, consisting of two elliptical gaussian components, $0\overset{''}{.}07 \times 0\overset{''}{.}04$, separated by $0\overset{''}{.}14$ in position angle 55°. The individual components are elongated along the separation axis, and their flux ratio is 1.3 to 1. The remaining flux emanates from a less well defined region called 3C 147A, about $0\overset{''}{.}55$ away in position angle 28°. It too is elliptical, but much larger, about $0\overset{''}{.}6 \times 0\overset{''}{.}15$, with the major axis near position angle 4°. While this model bears a suggestive resemblance to some of those described above, the authors' assertion that their 3C 147B is consistent with the Canadians' 448-MHz data is something of a surprise -- particularly when it comes coupled with the remark that the separation seems to be smaller at the lower frequency, perhaps as small as $0\overset{''}{.}09$. Such are the vagaries of model-fitting!

The only other significant body of data at a comparable frequency is that of Clark, Kellermann, and others at 18 cm *(24,60)*. These investigators, who are seldom at a loss for an explanation, say only, "This source does not

appear to possess symmetry about either the position angle of 55° suggested by Anderson and Donaldson (1967) or the angle of 85° suggested by the 75-cm data. It is clear that in both position angles there is structure at least as large as 0".07 as well as appreciable structure smaller than 0".02" *(60, p. 15)*.

My own observations, unfortunately, contribute nothing to relieve the confusion. The 1971 data (Table 4-7 and Figure 4-4a) evidence unusually complex structure, apparently involving more than two discrete parts. But the points are so few, and so scattered compared to the scale of significant variation, that it would be hopeless to try to fit a model to them. In 1972 I attempted to fill in the visibility curve by observing the source continuously through an entire apparition, a period of over eleven hours. Fate intervened, however, in the form of a slowly failing battery and inexorably rising receiver temperature at the focus of the 140-foot telescope. As a result more than two hours of observations were lost completely and the value of the preceding three hours badly compromised. These data are plotted in Figure 4-4b.

The trustworthy data, principally those before -1 hour, fully confirm the impression created by the earlier set. If the source can be characterized as an ensemble of discrete components then surely there are at least three of

them. Some of them, or at least the source as a whole, must be larger than $0''.03$ in order to be so highly resolved. (The largest visibility, at -3.42 hours, is only 0.12.) The rapid alternation of extrema, too, implies component separations of at least $0''.08$. On the other hand there appears also to be structure on rather smaller scales, and the deep minima, if real, argue against a large number of strong components.

In spite of these tantalizing indications I have been unable to put together any adequate model. Variations of the Canadian and Donaldson-Smith schemes, although they resemble the observations in character, fail to match them in detail. So do numerous other attempts. Partly this failure reflects the inadequacy of the data; but the main problem is clearly that the source is exceptionally complex and contains significant compact structure spanning a wide range of scale sizes. To complicate the picture even more, this structure seems likely to be a strong function of frequency, or time, or both. Notice in this connection the poor correspondence between the data of Figures 4-4a and b. Further detailed studies of 3C 147 are going to produce some exceedingly interesting results.

TABLE 4-7

Observations of 3C 147

EPOCH	IHA	u ($\lambda \times 10^6$)	v ($\lambda \times 10^6$)	CORR. FLUX	ERROR
1971	-5.779	0.388	-4.987	2.45	0.10
	-4.694	2.252	-4.698	3.05	0.13
	-3.885	3.531	-4.228	3.01	0.11
	-2.594	5.226	-3.087	2.71	0.12
	-2.066	5.757	-2.505	3.05	0.11
	-2.002	5.815	-2.431	3.11	0.10
	-1.556	6.167	-1.896	2.55	0.14
	-1.330	6.313	-1.614	2.79	0.11
	-1.061	6.459	-1.270	2.80	0.13
	-0.816	6.563	-0.951	2.19	0.13
	-0.374	6.684	-0.365	2.78	0.13
	+0.230	6.704	+0.446	2.94	0.19
	1.022	6.477	1.495	2.76	0.13
	1.631	6.113	2.263	2.64	0.12
	2.182	5.650	2.913	2.77	0.11
	2.760	5.037	3.532	2.22	0.19
	2.873	4.904	3.645	2.04	0.15
	3.046	4.691	3.811	2.19	0.15
	3.683	3.829	4.354	3.48	0.10
	3.850	3.583	4.479	3.49	0.10
	4.002	3.355	4.584	3.36	0.12
	4.738	2.179	4.993	3.20	0.10
	4.907	1.896	5.061	4.05	0.10
1972	-4.965	1.798	-4.808	3.42	0.13
	-4.766	2.132	-4.730	3.58	0.15
	-4.599	2.408	-4.654	3.48	0.15
	-4.432	2.680	-4.569	2.88	0.15
	-4.262	2.952	-4.473	3.28	0.15
	-3.613	3.930	-4.025	4.28	0.13

TABLE 4-7 -- Continued

EPOCH	IHA	u ($\lambda \times 10^6$)	v ($\lambda \times 10^6$)	CORR. FLUX	ERROR
1972	-3.425	4.193	-3.872	4.65	0.15
	-3.257	4.418	-3.728	4.12	0.15
	-3.065	4.667	-3.553	3.70	0.17
	-2.919	4.849	-3.414	2.44	0.15
	-2.752	5.047	-3.248	3.25	0.15
	-2.585	5.236	-3.076	3.56	0.15
	-2.418	5.415	-2.898	3.59	0.15
	-2.252	5.582	-2.717	3.79	0.15
	-1.916	5.888	-2.331	3.88	0.14
	-1.749	6.024	-2.132	3.61	0.14
	-1.582	6.148	-1.928	2.88	0.14
	-1.415	6.260	-1.721	3.03	0.14
	-1.248	6.361	-1.510	3.28	0.14
	-1.085	6.447	-1.301	3.15	0.15
	-0.889	6.535	-1.047	2.60	0.16
	-0.754	6.586	-0.868	2.15	0.16
	-0.576	6.640	-0.634	2.24	0.14
	-0.419	6.676	-0.425	2.36	0.15
	-0.255	6.701	-0.205	1.58	0.20
	-0.082	6.715	+0.028	2.55	0.14
	+0.109	6.713	0.285	3.72	0.23
	0.224	6.704	0.439	3.23	0.21
	0.430	6.674	0.714	1.63	0.28
	0.579	6.639	0.913	1.95	0.22
	0.744	6.589	1.132	2.84	0.20
	0.908	6.527	1.346	1.59	0.26
	1.247	6.361	1.784	3.36	0.22
	1.435	6.247	2.021	3.37	0.22
	1.592	6.141	2.215	4.27	0.20
	1.767	6.011	2.428	4.31	0.22

TABLE 4-7 -- Continued

EPOCH	IHA	u ($\lambda \times 10^6$)	v ($\lambda \times 10^6$)	CORR. FLUX	ERROR
1972	+1.926	5.880	2.618	3.75	0.20
	2.084	5.741	2.801	3.22	0.22
	4.428	2.687	4.842	2.56	0.10
	4.592	2.420	4.925	2.20	0.10
	4.760	2.143	5.002	1.91	0.10
	5.347	1.142	5.196	2.75	0.12

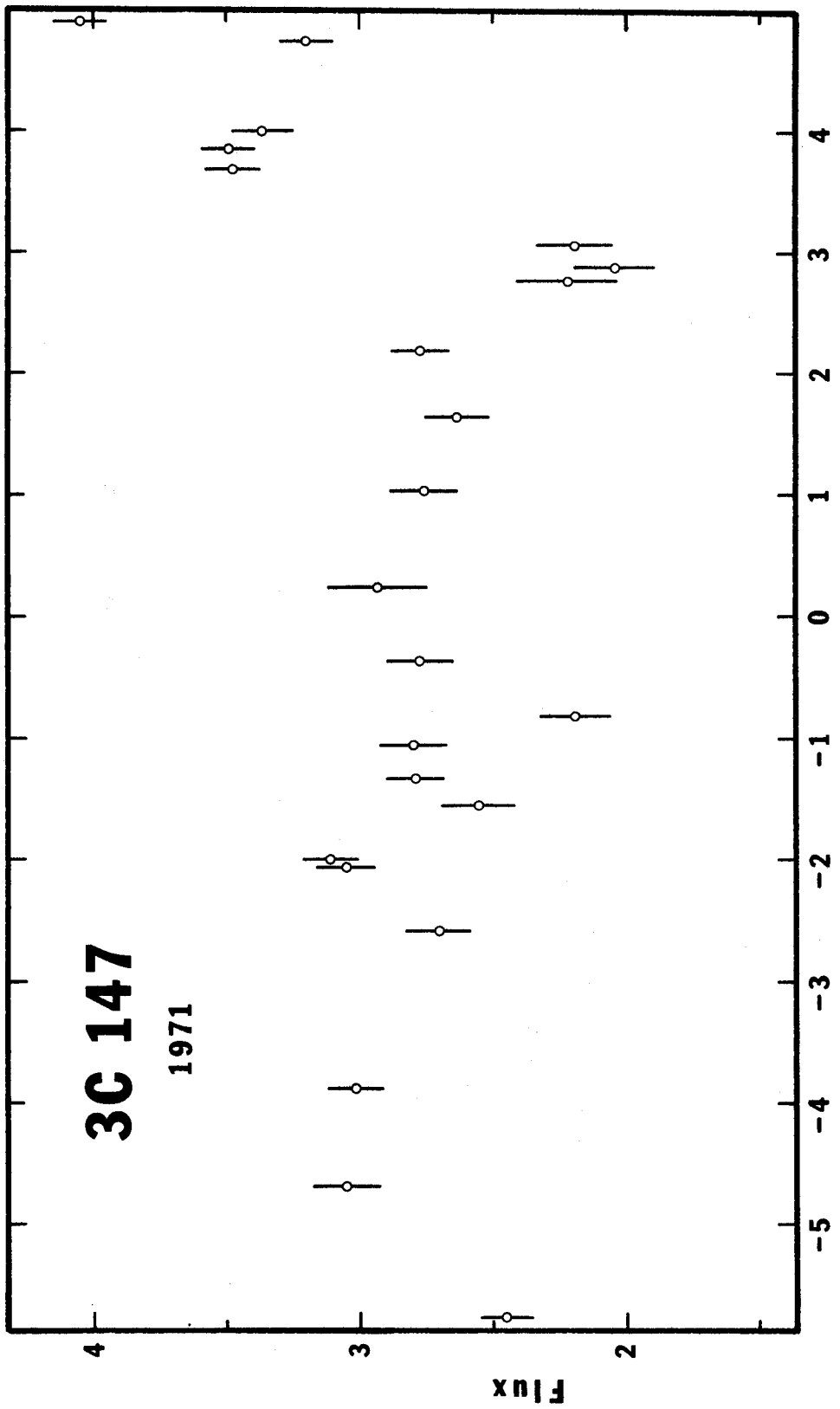

Figure 4-4a. Observed correlated fluxes for 3C 147. Epoch 1971. Key on page 49.

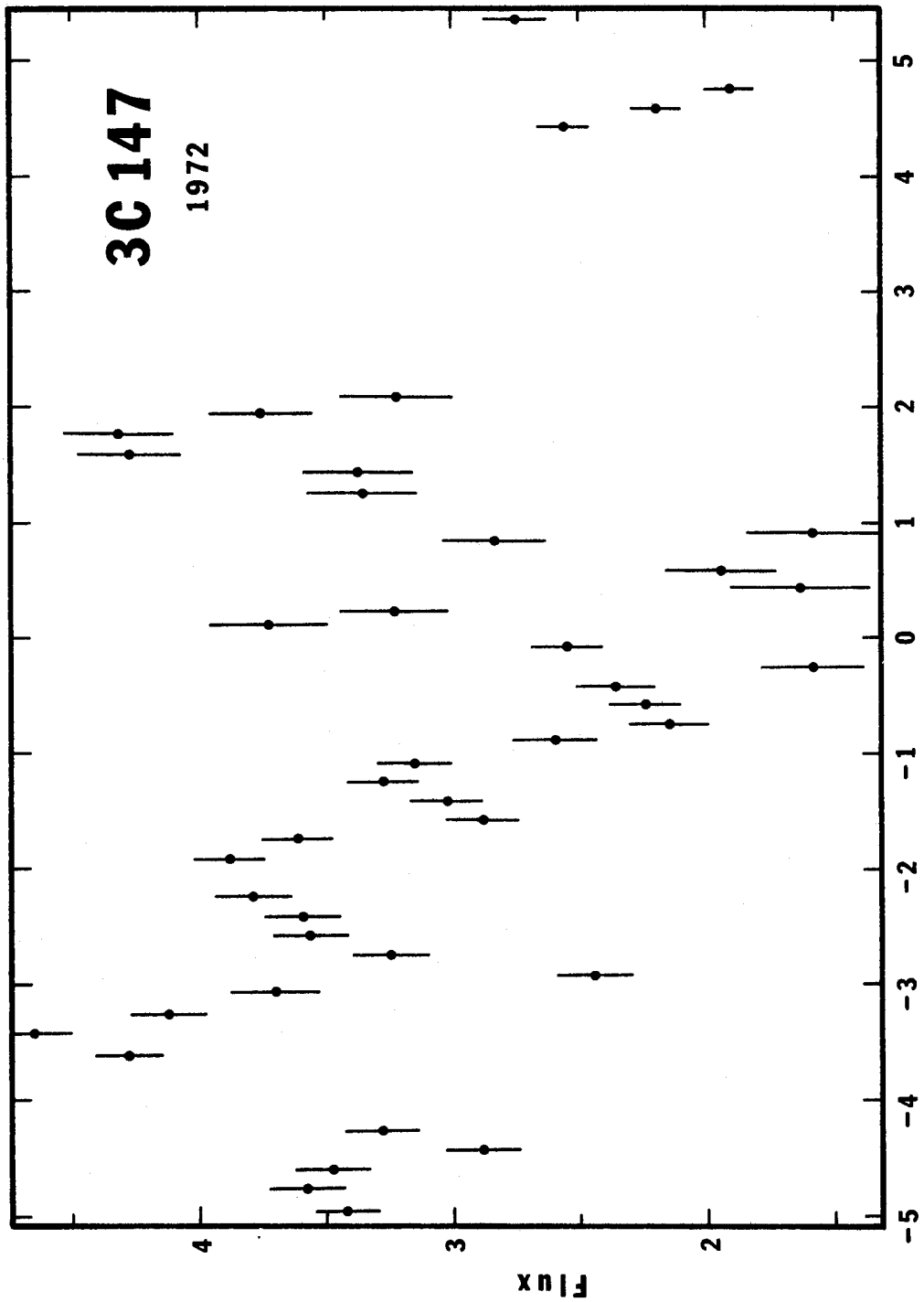

Figure 4-4b. Observed correlated fluxes for 3C 147. Epoch 1972. Key on page 49.

3C 273

3C 273 is the quasar nonpareil. In both the optical and radio realms its fund of exciting surprises seems inexhaustible. Since Schmidt's explication of its line spectrum in 1963 *(92)* it has led the way in optical *(101)* and radio *(38,61)* variability, in VLBI *(13)*, and, with 3C 279, in the controversy over anomalous rates of expansion *(106,31)*.

The radio structure of 3C 273 is complex, like that of 3C 147, but presumably somewhat better understood. Early occultation observations *(50,52)*, supplemented later by intermediate-baseline interferometry *(4)*, showed that the largest-scale structure corresponds to the optical features noted by Schmidt *(92)*. There is a compact source (3C 273B) at the position of the quasar, and a much more diffuse component (3C 273A) situated close to the far end of the jet, about 20" away in position angle ∿44°.

3C 273A is completely resolved by all VLBI, but the B source has been studied thoroughly. After a false start *(1,5)* the British group, working at 21, 11, and 6 cm, found it unresolved, and hence smaller than 0".01, at their highest resolution *(79,40)*. An extensive series of 6-, 13-, and 18-cm observations with the Mark I system *(22,23,24,58,59,60)* established that the B source is itself compound and contains at least three parts: B, which has taken over

the old designation, has a size of about 0".022, C is ∿0".002, and D must be ≤0".0004.

The relative positions of these subcomponents are less clear. In reference *(60)* the authors opined that all the components are contained in a region comparable in size to component B; but after considering additional data they were more circumspect *(10)*. There is also evidence of changes in the flux and structure of the source *(46 (but see also 76),106,31)*. These observations show that the smallest components, especially, are evolving on time scales of months. They move rapidly relative to one another, and new ones seem to be created.

The Canadian observations at 408 and 448 MHz *(12, 11,28)* introduce further complications. Interpretation of their data is hampered by the circumstance that most of the observations are near position angle 90°; however, at least two models fit reasonably well. In the first, sixty percent of the flux is in a component 0".10 x <0".04, and the rest is in a component 0".027 x <0".01; both are elongated along position angle 33°. The unsettling thing about this model is that although the second component resembles B, the first is like nothing seen at higher frequencies. In the alternate model two identical components about 0".01 in diameter are separated by 0".08 in position angle ∿100°. The dissimilarity of the two models is a measure of the

ambiguity of the data; nevertheless the two have an arresting feature in common: structure on a scale considerably larger than had previously been observed.

Table 4-8 and Figure 4-5 show the present observations. They share the shortcoming of the Canadian data in being clustered tightly around position angle 90°. The 1972 observations suffer also from a long gap and some anomalously low points. I deleted those at 0.03 and 2.87 hours from the model-fitting, though it is mildly disturbing that the latter point falls so close to the low point in the 1971 data at 3.12 hours.

Since the data are ambiguous I restricted the search for models to three particular types: those resembling component B as described above, those resembling the Canadians' models, and those highly elongated along position angle $\sim$44°, the axis of the gross radio and optical structure. Starting with the first-session data, I tried unsuccessfully a variety of single components, core-halos, and doubles in other configurations. Model B (Table 4-9, not plotted) is the only one of this type that performed tolerably well. Model A, involving three point sources, fits equally well, but unlike model B it adapts readily to the 1972 data. Notice that the strength of the second component is the only parameter that changes markedly. Model B, in contrast, firmly resisted all attempts to twist it

into a form compatible with the 1972 data. For this reason, at least, it seems much less plausible than model A.

Model A itself is far from compelling, however, and we ought to ask ourselves which of its features are essential and which possibly accidental. The total flux is probably not far from right, though only about half the amount implied by the spectrum *(60)*. One could restore part of the deficiency, if desired, by making the components slightly diffuse, or more neatly by positing an additional large, completely resolved component like the one in the Canadians' first model. Much smaller values, on the other hand, are definitely ruled out by the data.

The configuration and even the number of the components are very poorly determined. None the less we can draw one definite conclusion directly from the asymmetry of the visibility curves around hour angle zero. In a source so close to the celestial equator this asymmetry implies that there is important structure in the north-south direction at distances large compared to the typical resolution of the instrument. In this particular case the distances must be similar to those deduced by the Canadians, $0\overset{''}{.}06$ to $0\overset{''}{.}08$. More specific inferences are less reliable, although the rough alignment of the model along position angle 45° is certainly suggestive. Similar models in which all the components are forced to lie along a straight line do

nearly as well, especially when the position angle is near 40°.

TABLE 4-8

Observations of 3C 273

EPOCH	IHA	u ($\lambda\times10^6$)	v ($\lambda\times10^6$)	CORR. FLUX	ERROR
1971	-3.066	4.667	0.027	7.91	0.12
	-2.907	4.863	0.035	7.75	0.10
	-2.740	5.061	0.043	7.44	0.10
	-2.573	5.249	0.052	7.01	0.10
	-2.456	5.375	0.058	6.40	0.16
	-1.978	5.835	0.085	5.30	0.10
	-1.449	6.239	0.117	4.50	0.11
	-0.944	6.512	0.150	4.50	0.11
	-0.397	6.680	0.186	4.02	0.10
	+0.275	6.699	0.232	4.36	0.11
	0.856	6.548	0.271	4.11	0.10
	1.315	6.322	0.301	4.51	0.18
	1.863	5.933	0.335	4.71	0.10
	2.616	5.202	0.377	5.99	0.10
	3.122	4.595	0.402	4.95*	0.10
	3.708	3.793	0.427	7.56	0.10
1972	-3.335	4.315	0.015	9.18	0.14
	-3.178	4.523	0.022	8.82	0.13
	-3.011	4.735	0.030	8.59	0.13
	-2.844	4.939	0.038	8.41	0.13
	-2.718	5.086	0.044	8.39	0.19
	+0.030	6.716	0.215	3.58*	0.15
	0.601	6.633	0.254	4.48	0.13
	1.195	6.390	0.293	4.78	0.12
	1.796	5.987	0.330	5.73	0.12
	2.366	5.468	0.363	6.91	0.13
	2.867	4.912	0.390	6.65*	0.12
	3.458	4.147	0.417	7.89	0.12
	3.588	3.964	0.422	8.54	0.14

TABLE 4-9

Models of 3C 273

	COMP.	FLUX	r	θ	x	α	ζ
1971, Model A Three Point Sources	1	5.32 *1.63*	0.0	---	0.0	---	---
	2	2.09 *L*	0.050 *0.011*	52.4 *12.8*	0.0	---	---
Error Factor 1.67	3	1.81 *L*	0.080 *0.030*	39.4 *17.5*	0.0	---	---
1971, Model B Two Components	1	5.55 *0.65*	0.0	---	0.0	---	---
Error Factor 1.68	2	3.69 *L*	0.064 *0.013*	44.6 *10.0*	0.066 *L*	0.115 *L*	11.2 *L*
1972, Model A Three Point Sources	1	5.32 *L*	0.0	---	0.0	---	---
	2	4.26 *L*	0.052 *L*	52.5 *L*	0.0	---	---
Error Factor 2.62	3	1.86 *L*	0.090 *L*	39.3 *L*	0.0	---	---

(For explanation see key on page 48.)

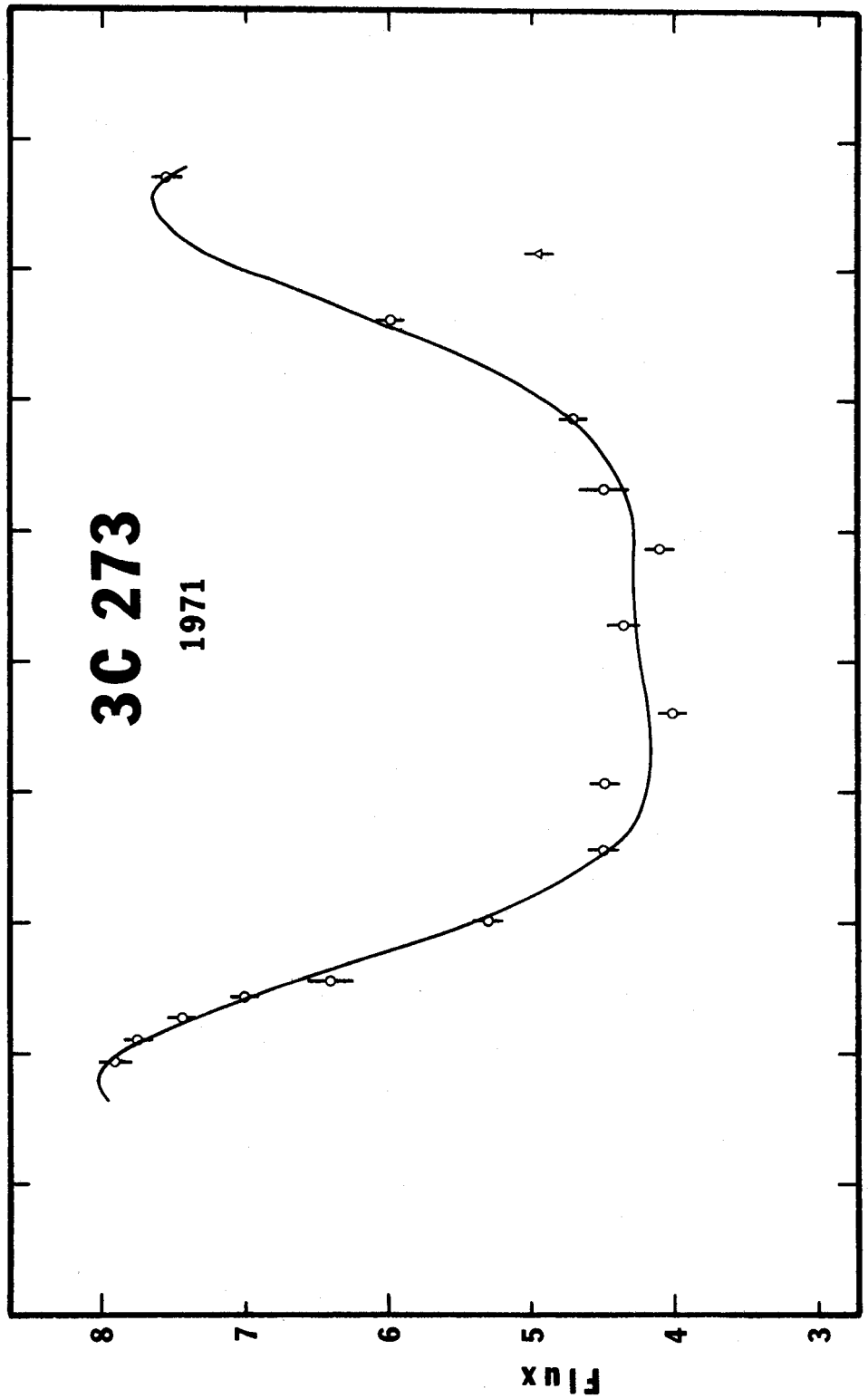

Figure 4-5a. Observed correlated fluxes and predictions of model for 3C 273. Epoch 1971. Key on page 49.

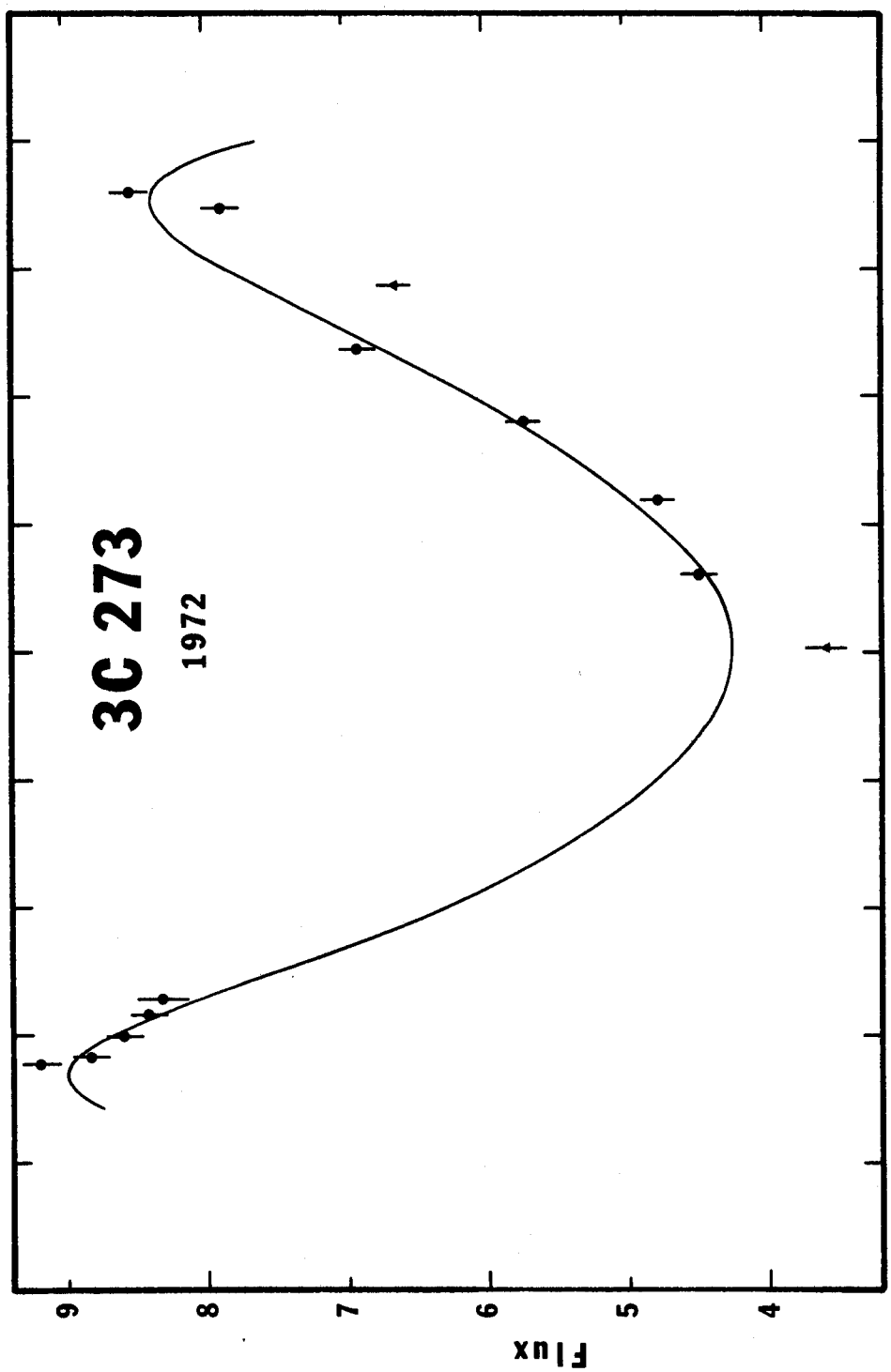

Figure 4-5b. Observed correlated fluxes and predictions of model for 3C 273. Epoch 1972. Key on page 49.

3C 279

3C 279 is a quasar remarkably similar in many respects to its neighbor 3C 273. Wyndham and others made the identification *(88,109,87)*, and Burbidge and Rosenberg measured the redshift *(17)*. At optical frequencies the source is strongly polarized, and both the brightness and polarization vary markedly in intervals as short as a week *(63)*. The radio flux too is highly variable, especially at short wavelengths *(61)*.

The radio spectrum (Figure 4-6) is complex and suggests the presence of four components *(58)*. The most extended, A, has a diameter of about half a minute of arc. It has a so-called normal radio spectrum and dominates at low frequencies *(2)*, but is invisible to VLBI. Components B, C, and D are much smaller. Pre-VLBI observations between Jodrell Bank and Malvern at 21, 11, and 6 cm *(5,79, 40)* failed to resolve them; however the Mark I observations at 6, 13, and 18 cm *(10,22,23,24,58,59,60)* showed that B is about $0\overset{''}{.}022$ in diameter while C is about $0\overset{''}{.}001$. D remained unresolved ($\leq 0\overset{''}{.}0004$), but more recent observations at 3.8 cm *(64,106,31)* show it to be compound and evolving rapidly.

According to this model component B should predominate at sufficiently low frequencies, a prediction apparently verified by the Canadian observations at 408 and 448 MHz. Preliminary measurements *(12)* suggested a size of

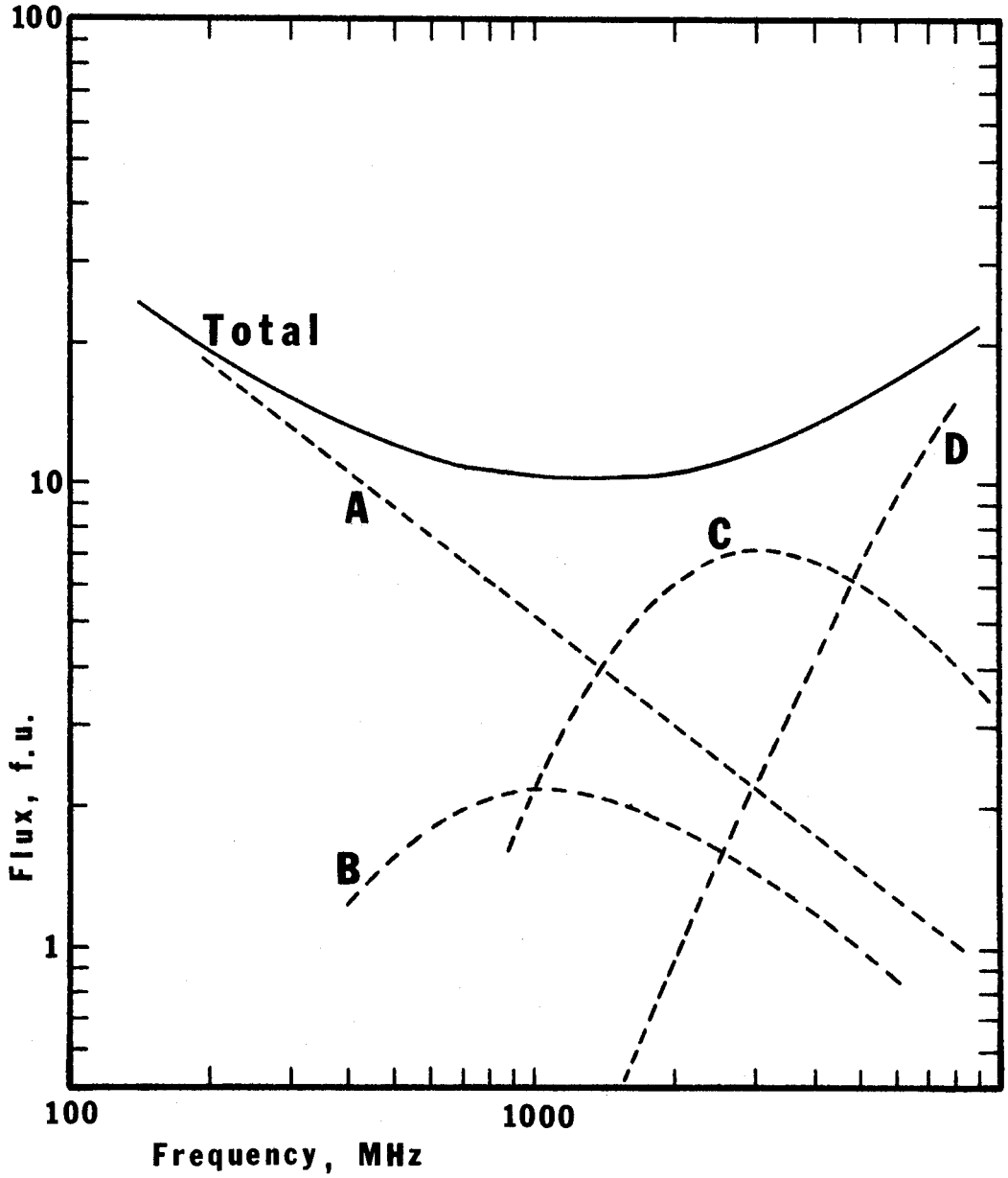

Figure 4-6. The flux spectrum of 3C 279, partitioned among the four components A, B, C, and D described in the text.

about $0''.03$, but more thorough observations indicate a diameter of $\sim 0''.01$ in position angle 90° ± 15° *(11,28)*.

In the present investigation 3C 279 produced some rather startling results. Whatever conviction these results carry is due in large measure to the excellent quality of the data (Table 4-10 and Figure 4-7). No points had to be rejected, and the hour-angle coverage was uniform in both sessions. Most important, in the second series of observations we were able to observe continuously from the time the source became visible at Owens Valley to the moment it passed out of range at NRAO.

Looking first at the 1972 data (Figure 4-7b), we notice two striking features. First, although the declination of the source is near zero, the visibility function is asymmetric around the interferometer meridian. Inasmuch as the sense of the asymmetry (higher amplitudes at positive hour angles) is opposite to that found for the nearby source 3C 273, an instrumental origin is practically out of the question. Hence we can conclude, as in the case of 3C 273, that 3C 279 contains significant structure in the north-south direction on a scale larger than $0''.05$. And second, there is an unmistakable small-scale ripple in the curve. This ripple is the signature of structure at an even larger distance.

Model A (Table 4-11 and Figure 4-7b) accounts for

both these features but requires careful interpretation. Keep in mind, to begin with, that the position-angle discrimination of the data is very poor. Nevertheless the distance between components 1 and 2 is so large that we can locate them fairly accurately with respect to one another. Their relation to the third component is more equivocal, however. The evidence that the component exists is strong. For the benefit of skeptics I have plotted model B, which is just A without the third component. (Not surprisingly it is also practically identical to the best-fitting two-component model.) Whether one gauges by eye or by error factor, the fit is not nearly as good. On the other hand the location of the third component is ambiguous. Although the quoted location gives the best fit, a position angle of about 82° (at the same distance) is also reasonable, and other locations are conceivable.

It is natural to ask whether this three-component model bears any comprehensible relation to the four-component model. On the basis of the spectrum plotted in Figure 4-6, at 606 MHz there should be about 6 flux units in component A and something like 5 flux units in the compact part of the source. Of this total component B should account for about 2 flux units and C for 3 or so, with D making up the scant remainder. Comparing this division with the present model, we find the correspondence almost

preternaturally good. Component 1 associates itself with C, 2 with B, and 3 with D. The size and flux of component 2 are closely interdependent, but the choice made gives excellent agreement with the expected values of both.

Consider now the observations from 1971. The character of the asymmetry seems different (see Figure 4-7a), and the details are less clear because there are fewer points. Nevertheless I used model A as a starting point and was surprised to see the model converge rapidly to the parameter values given in the Table.

Here again some comments are in order. Admittedly, the way in which the model fits the data looks a little peculiar -- possibly more like an aerial view of a slalom course than a legitimate example of curve-fitting. Quite likely this is not the model one would elect if the data began and ended with these ten points. Remember, though, that the model is merely a modification of a preexisting model for which the evidence is much more convincing. Observe too that the modification is not very drastic: only three of the parameters (the position of component 2 and the strength of component 3) had to be changed substantially in order to accommodate the new data. Besides, the fit is *remarkably* good -- notwithstanding the fact that there are only two more data points than variable parameters. Model B (which again is just model A without

component 3) now fares even worse by comparison to A than it did before, mainly because the third component seems to have been much stronger in 1971.

Taken at face value the fact that such similar models fit so well the rather different-looking visibility curves from the two epochs suggests that the models are authentic and that the apparent changes in source structure are real. I shall return to this point in Chapter 5. On the other hand skepticism guides any sensible discussion of source models, and model A certainly poses some perplexing questions. For example, is the model really isomorphic with the four-component model? If so, why have large component separations not been observed at higher frequencies? What kinds of motion are implied by the apparent changes in source structure, and what do they tell us about the nature of the source? Since questions like these apply to some of the other sources as well, I shall defer them, also, to Chapter 5.

TABLE 4-10

Observations of 3C 279

EPOCH	IHA	u ($\lambda \times 10^6$)	v ($\lambda \times 10^6$)	CORR. FLUX	ERROR
1971	-2.850	4.932	0.660	3.46	0.10
	-2.155	5.675	0.565	3.13	0.10
	-1.648	6.101	0.488	3.02	0.11
	-0.609	6.631	0.317	2.95	0.13
	+0.069	6.715	0.200	2.89	0.11
	0.657	6.617	0.099	3.12	0.10
	1.161	6.408	+0.015	3.67	0.10
	1.917	5.888	-0.105	4.05	0.10
	2.415	5.418	-0.177	3.81	0.10
	2.994	4.756	-0.253	3.87	0.10
1972	-2.872	4.905	0.663	3.50	0.13
	-2.705	5.101	0.642	3.47	0.13
	-2.538	5.287	0.619	3.28	0.13
	-2.371	5.463	0.596	3.55	0.13
	-2.204	5.629	0.572	3.15	0.13
	-2.054	5.768	0.550	2.93	0.15
	-1.868	5.929	0.522	2.97	0.14
	-1.711	6.053	0.498	3.12	0.13
	-1.544	6.175	0.472	3.06	0.13
	-1.377	6.284	0.445	3.00	0.13
	-1.210	6.382	0.418	2.67	0.13
	-1.055	6.461	0.392	2.91	0.14
	-0.865	6.545	0.360	2.54	0.15
	-0.708	6.601	0.334	2.78	0.14
	-0.541	6.649	0.305	2.53	0.14
	-0.374	6.684	0.277	2.80	0.14
	-0.207	6.706	0.248	3.05	0.14
	-0.052	6.715	0.221	2.99	0.15

TABLE 4-10 -- Continued

EPOCH	IHA	u ($\lambda \times 10^6$)	v ($\lambda \times 10^6$)	CORR. FLUX	ERROR
1972	+0.338	6.690	0.154	2.99	0.13
	0.505	6.658	0.125	2.69	0.13
	0.672	6.612	0.097	2.80	0.13
	0.839	6.555	0.069	3.06	0.13
	1.006	6.484	0.041	3.04	0.13
	1.186	6.395	+0.011	3.18	0.12
	1.420	6.257	-0.027	3.04	0.16
	1.556	6.167	-0.049	3.46	0.13
	1.723	6.044	-0.075	3.23	0.13
	1.890	5.910	-0.101	3.34	0.13
	2.057	5.765	-0.126	3.38	0.13
	2.224	5.610	-0.151	3.70	0.13
	2.440	5.392	-0.181	3.86	0.13
	2.607	5.212	-0.204	3.85	0.13
	2.778	5.016	-0.226	4.11	0.13
	2.952	4.808	-0.248	4.36	0.13
	3.115	4.604	-0.268	4.25	0.13

TABLE 4-11

Models of 3C 279

	COMP.	FLUX	r	θ	x	α	ζ
1971, Model A	1	3.54	0.0	---	0.0	---	---
		0.14					
Three Components	2	1.80	0.098	25.9	0.020	1.0	---
		L	*0.009*	*2.9*	*0.010*		
	3	0.34	0.304	250.6	0.0	---	---
Error Factor 0.93		*0.08*	*0.007*	*4.4*			
1971, Model B	1	3.54	0.0	---	0.0	---	---
		0.45					
Two Components	2	1.80	0.098	25.9	0.020	1.0	---
Error Factor 3.13		*L*	*0.020*	*6.7*	*L*		
1972, Model A	1	3.32	0.0	---	0.0	---	---
		0.28					
Three Components	2	2.14	0.061	46.8	0.022	1.0	---
		L	*0.004*	*7.4*	*0.013*		
	3	0.16	0.300	261.9	0.0	---	---
Error Factor 1.14		*0.04*	*0.003*	*5.5*			
1972, Model B	1	3.32	0.0	---	0.0	---	---
		0.33					
Two Components	2	2.14	0.061	46.8	0.022	1.0	---
Error Factor 1.35		*L*	*0.005*	*8.7*	*L*		

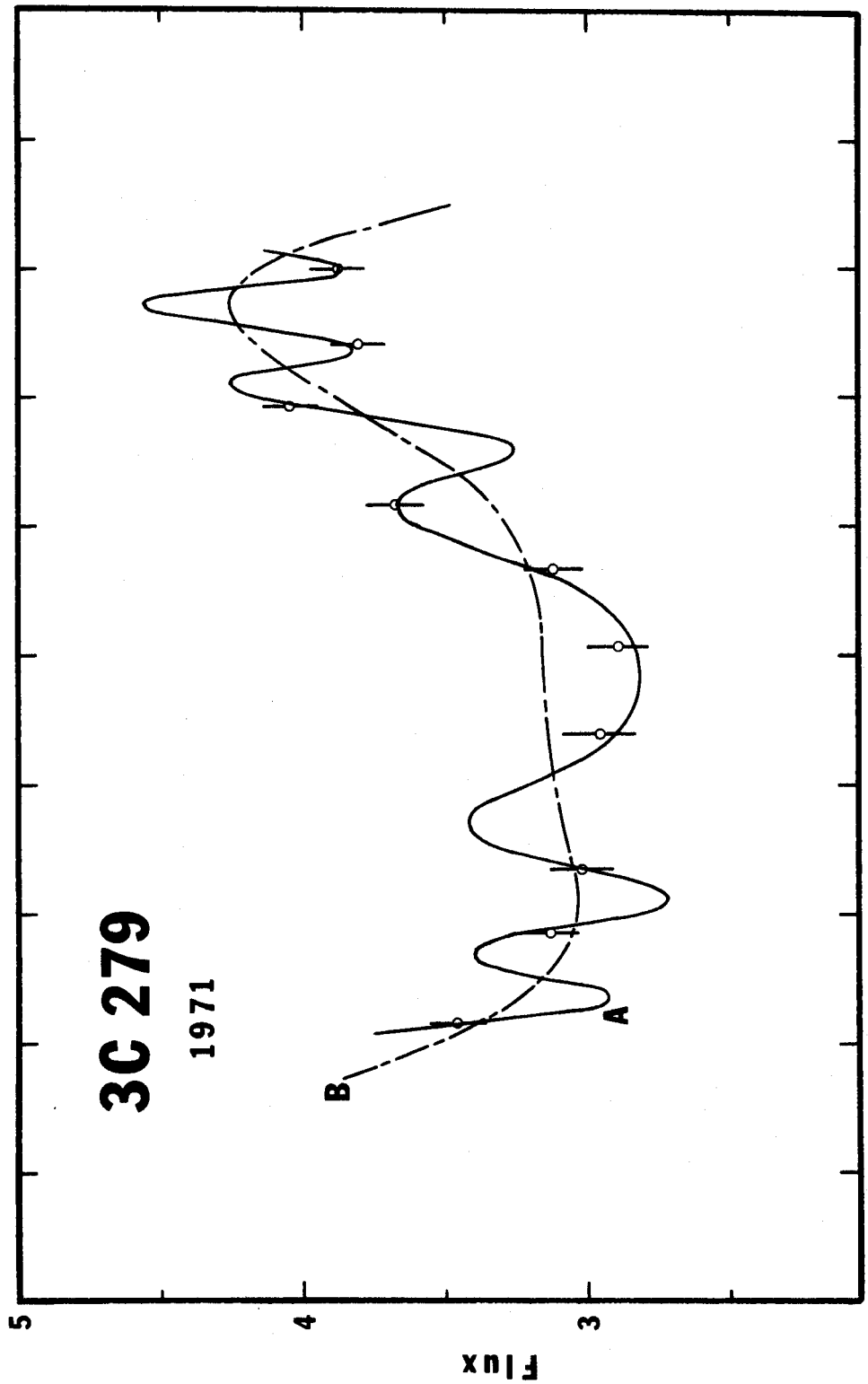

Figure 4-7a. Observed correlated fluxes and predictions of models for 3C 279. Epoch 1971. Key on page 49.

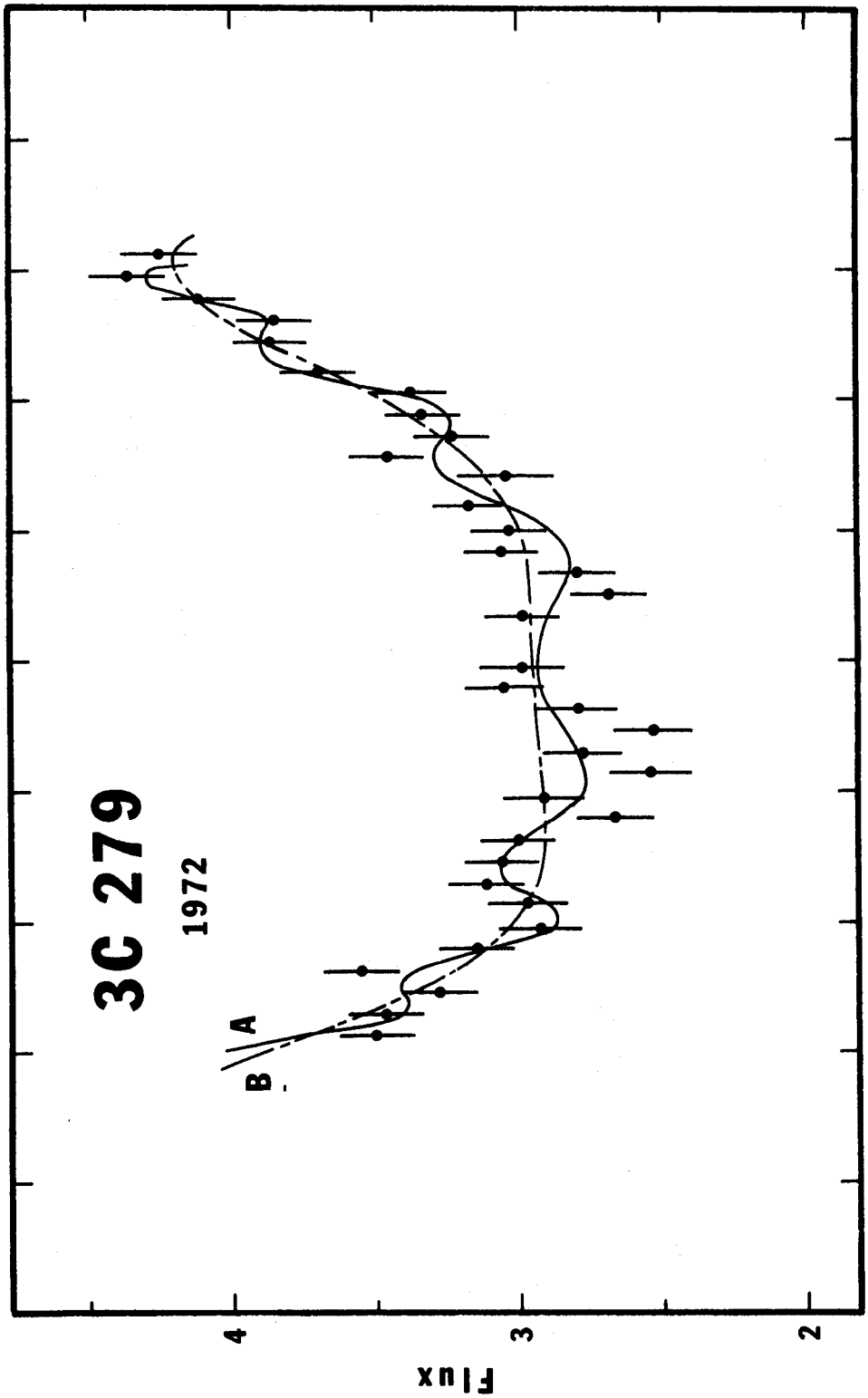

Figure 4-7b. Observed correlated fluxes and predictions of models for 3C 279. Epoch 1972. Key on page 49.

3C 286

3C 286 is an undistinguished quasar of visual magnitude 17.4 first identified by Matthews and Sandage *(71)*. Oke measured the redshift *(78)*.

Interferometrically the source has been studied at 6, 11, 21, and 73 cm at Jodrell Bank *(1,79,4)*, at 13 and 18 cm by the NRAO-Cornell-Caltech group *(24,59,60,10)*, and at 67 and 73 cm by the Canadians *(12,11,28)*. No variability has been detected *(38)*, and all the results agree in showing that the brightness distribution is generally smoother and larger in angular extent than in the typical source in this investigation -- more like 3C 380, say, than 3C 273 or 3C 279. The spectrum implies the presence of at least two components, the larger of which dominates at wavelengths longer than 70 cm *(4,60)* and has an overall extent of a few tenths of a second of arc. The smaller, which has a size on the order of $0\overset{''}{.}03$, is more prominent at higher frequencies *(79,24,60)*. There is some indication, however, that the distinction between the two components is fairly indefinite. Although the higher-frequency measurements show no evidence of structure $<0\overset{''}{.}002$, the Canadian observations do suggest the presence of a weak unresolved source. Their model, which seems consistent with all the previous studies, involves three components: A, accounting for 30 percent of the flux, is $>0\overset{''}{.}2$ in position angle 38°

and $\sim 0''.026$ in position angle 128°; B, elongated in the same direction, is $0''.053 \times 0''.026$ and contributes 60 percent of the flux; and C, which is $\leq 0''.005$, supplies the rest.

At 606 MHz I observed the source only in the 1972 observing session and was unable to obtain uniform hour-angle coverage even then. Nevertheless the visibility curve that resulted has a distinctive form that confirms the general features, if not the details, of the Canadian model (see Table 4-12 and Figure 4-8). A two-component model (Table 4-13) fits the data tolerably well, though the discrepancies between the model and the data are uncomfortably large, particularly along the low portion of the curve. These discrepancies may be due to measurement errors, but a more likely possibility, in my opinion, is that irregularities in the source structure are at least partly responsible.

Be that as it may, the data definitely show pronounced elongation in approximately the direction specified by the Canadian model, along with a weak, nearly unresolved core similar to theirs. I was compelled to endow the core with a little structure, however, in order to reproduce the slight slope in the low portion of the curve. Unfortunately the parameters of each of the elliptical components are extremely interdependent; consequently the fluxes, sizes, and position angles are really only plausible guesses chosen to be consistent with the previous observations.

TABLE 4-12

Observations of 3C 286

EPOCH	IHA	u ($\lambda \times 10^6$)	v ($\lambda \times 10^6$)	CORR. FLUX	ERROR
1972	-4.687	2.264	-3.040	11.16	0.12
	-4.526	2.528	-2.989	10.99	0.11
	-4.374	2.774	-2.935	10.58	0.15
	-4.190	3.065	-2.863	9.88	0.12
	-3.886	3.530	-2.729	9.12	0.09
	-0.744	6.589	-4.794	1.99	0.12
	-0.142	6.711	+0.056	2.01	0.12
	+0.491	6.661	0.622	2.85	0.16
	1.050	6.464	1.113	2.71	0.14
	1.579	6.150	1.559	3.24	0.15
	2.164	5.667	2.021	2.95	0.13
	2.829	4.957	2.494	3.45	0.13
	2.986	4.767	2.595	3.41	0.12
	3.153	4.555	2.699	3.12	0.12
	3.349	4.296	2.815	3.39	0.10

TABLE 4-13

Model of 3C 286

	COMP.	FLUX	r	θ	x	α	ζ
1972 Core and Ell. Halo	1	3.89 *L*	0.0	---	0.018 *L*	0.491 *L*	145.9 *?*
Error Factor 2.47	2	15.54 *L*	0.0	---	0.046 *L*	0.473 *L*	46.0 *?*

(For explanation see key on page 48.)

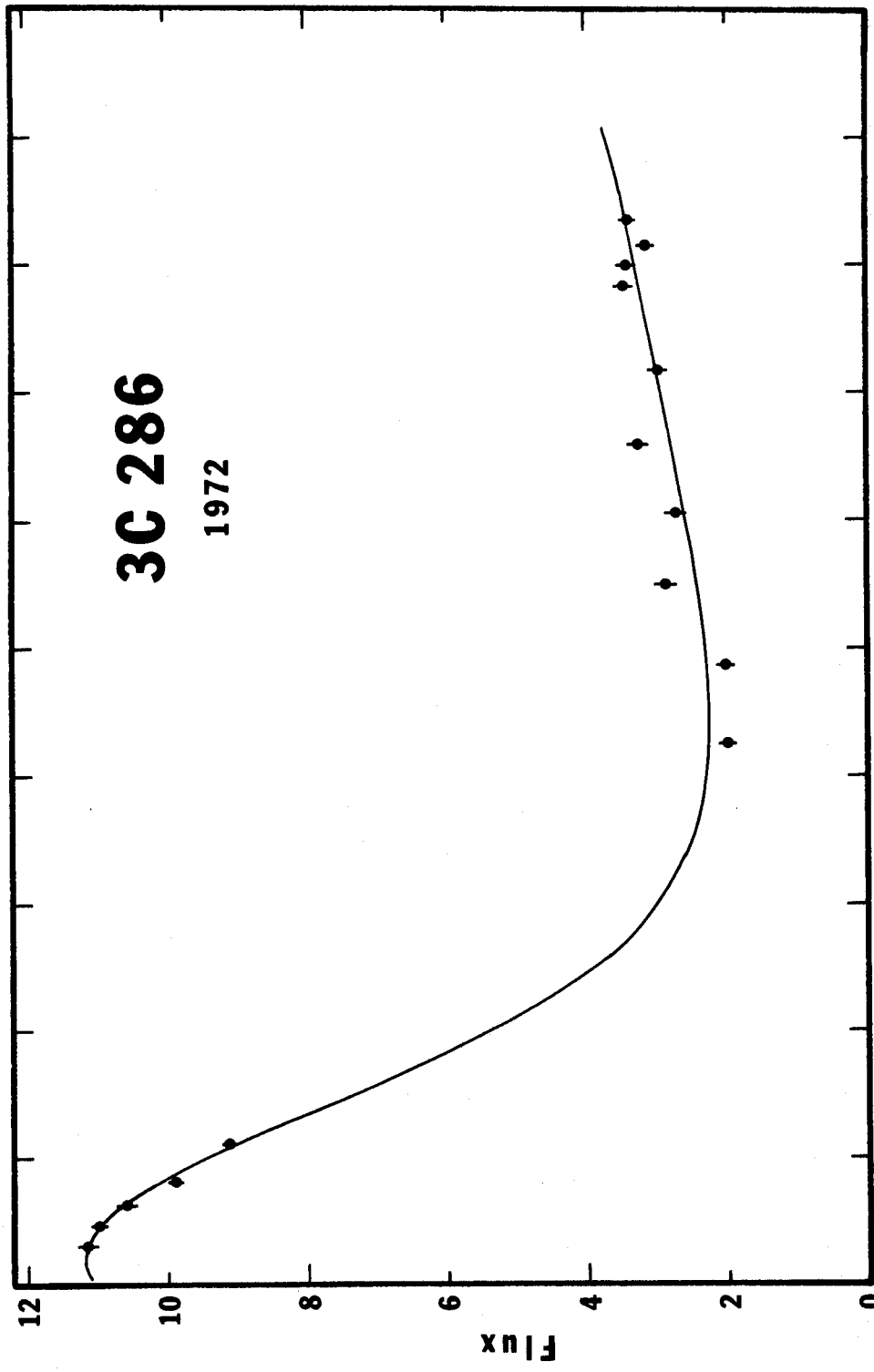

Figure 4-8. Observed correlated fluxes and predictions of models for 3C 286. Epoch 1972. Key on page 49.

P1345+12

Clarke, Bolton, and Shimmins *(27)* identified P1345+12 with a galaxy of photographic magnitude 17, which they characterized as S0 to indicate a spherical system with a suggestion of a dust lane. It is known to be a strong scintillator *(32)* and hence smaller than about $0\overset{''}{.}2$; but it appears to have been completely resolved in high-resolution VLBI measurements at 13 cm *(47,59)*, so that it must be larger than $0\overset{''}{.}001$.

Although the source seems to be of little intrinsic interest, I included it in the first series of observations in the hope that it would serve as a calibrator. It turned out not to be unresolved, but the few observations (Table 4-14 and Figure 4-9) are consistent with a simple elliptical structure (Table 4-15). The parameters of the ellipse are quite uncertain, especially the position angle of the major axis and the axial ratio. A circular form is apparently out of the question, however, and the size is fairly well determined if we assume that the observed component accounts for the total flux.

TABLE 4-14

Observations of P1345+12

EPOCH	IHA	u ($\lambda \times 10^6$)	v ($\lambda \times 10^6$)	CORR. FLUX	ERROR
1971	-3.499	4.090	-0.938	5.26	0.15
	-1.241	6.365	-0.253	3.28	0.15
	+0.844	6.553	+0.525	2.44	0.15
	2.607	5.212	1.120	3.23	0.16

TABLE 4-15

Model of P1345+12

	COMP.	FLUX	r	θ	x	α	ζ
1971 Elliptical Gaussian Error Factor 1.77	1	7.7	0.0	---	0.029 *0.011*	0.543 *0.19*	15.3 *17.7*

(For explanation see key on page 48.)

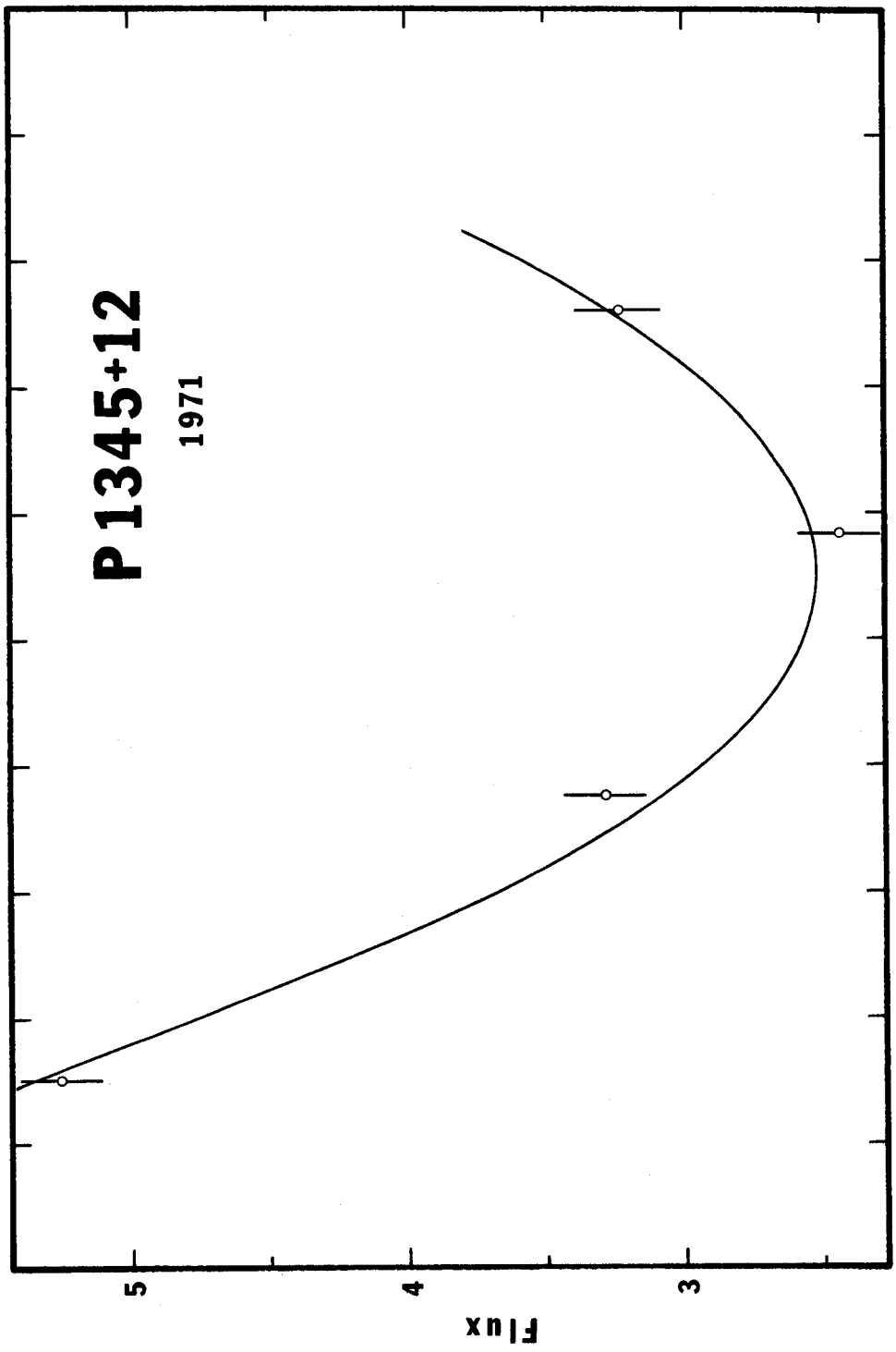

Figure 4-9. Observed correlated fluxes and predictions of model for P1345+12. Epoch 1971. Key on page 49.

CTD 93

Merkelijn's original identification of CTD 93 with a faint stellar object *(72)* was incorrect, as the object is definitely a star *(94)*. The correct identification is apparently an even fainter galaxy about half a minute of arc southwest of the star.

Like P1345+12, CTD 93 seems to be of little interest in its own right; but previous VLBI measurements at 13 and 18 cm *(58,59)* had shown it to be 0".003 or smaller at those wavelengths, and so I included it in the first observing session as a possible calibrator.

The observations (Table 4-16 and Figure 4-10) seem to indicate a compound rather than simple structure; indeed, the point double model proposed in Table 4-17 fits the data rather well. There are grounds for considerable doubt about this interpretation, however. In the first place the spectrum, which peaks around 900 MHz, gives no hint of compound structure; and the previous observations, while extremely limited, also are consistent with a single component. Moreover, three of the five observations in the present group are compatible with a point source. Only the points at -1.12 and +0.49 hours are out of line, and on them rests the present interpretation. On the other hand the previous data are insufficient to rule out the double model, and the coincident observational errors required to

produce the two vagrant points, while not impossible, are rather unlikely.

- -

TABLE 4-16

Observations of CTD 93

EPOCH	IHA	u ($\lambda \times 10^6$)	v ($\lambda \times 10^6$)	CORR. FLUX	ERROR
1971	-4.337	2.832	-2.552	3.37	0.18
	-1.117	6.431	-0.681	0.87	0.36
	+0.486	6.662	+0.575	1.92	0.20
	2.182	5.650	1.825	3.61	0.30
	4.810	2.059	3.069	3.23	0.14

TABLE 4-17

Model of CTD 93

	COMP.	FLUX	r	θ	x	α	ζ
1971	1	2.09 *0.60*	0.0	---	0.0	---	---
Point Double Error Factor 1.35	2	1.39 *0.74*	0.049 *0.004*	117.8 *7.8*	0.0	---	---

(For explanation see key on page 48.)

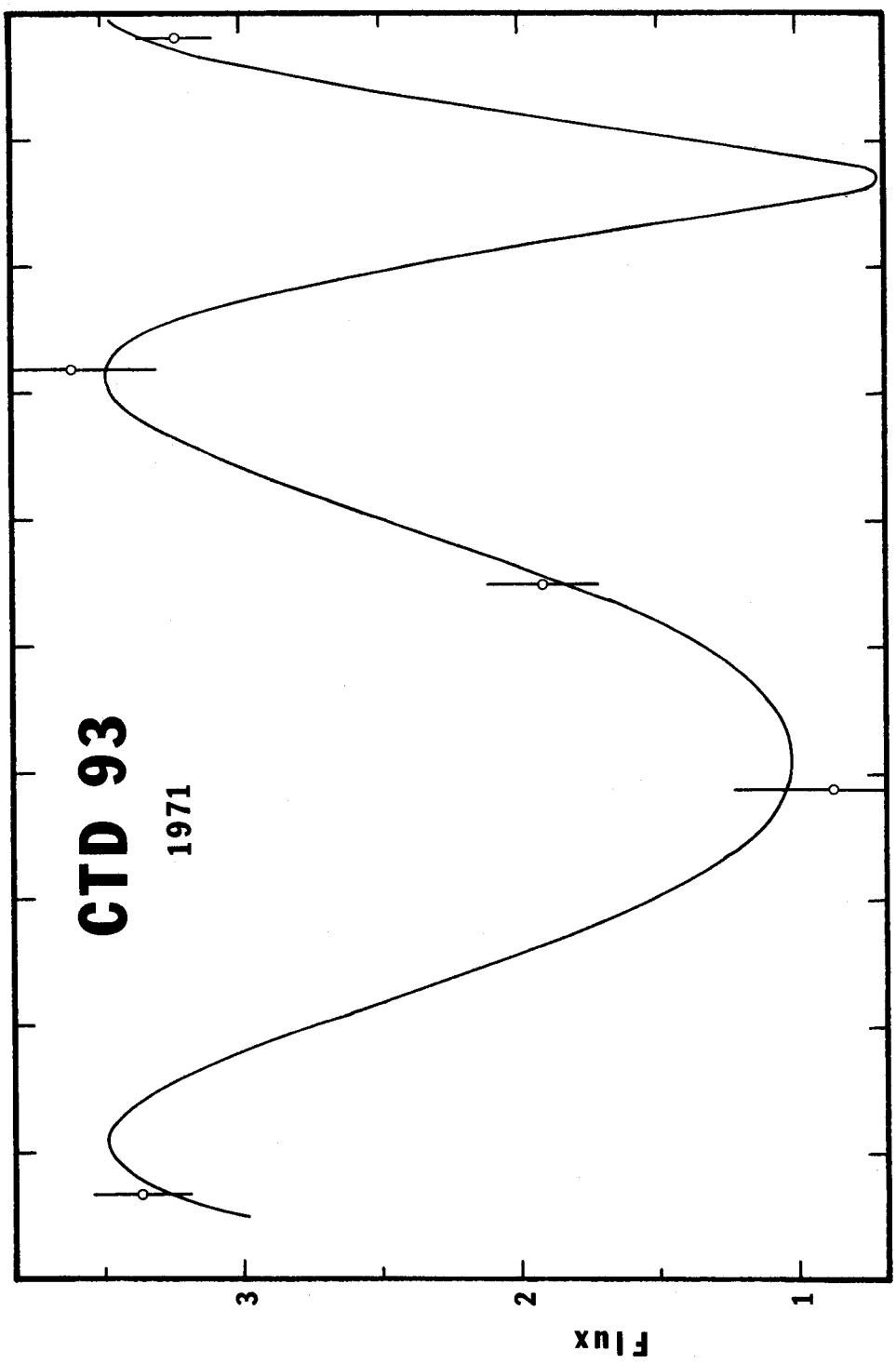

Figure 4-10. Observed correlated fluxes and predictions of model for CTD 93. Epoch 1971. Key on page 49.

3C 345

3C 345 is a quasar strikingly like 3C 273 and 3C 279. Sandage and Wyndham *(88)* made the identification, and Lynds and others *(69)* measured the redshift. The optical flux is strongly polarized, and both the total emission and the polarization vary markedly in intervals as short as a week, as they do in 3C 279 *(63)*. Another intriguing peculiarity is the variability in the flux and frequency of the strong Mg II λ2798 doublet, first noticed by the Burbidges *(15)* and later confirmed by Wampler *(105)*.

At radio frequencies too the emission is polarized, and both the polarization and flux vary in time *(38,3,61)*. Together with the complex form of the spectrum, this variability constituted the first evidence of compact structure. It was soon supplemented by intermediate-baseline interferometry between Malvern and Jodrell Bank, which established that all or nearly all of the flux at 11 and 21 cm is confined to a region smaller than a few tenths of a second of arc *(5,79,40)*. Observations with the Mark I VLBI system at 6, 13, and 18 cm *(24,58,59,60,10)* confirmed the earlier findings and added details. Apparently the source consists of three components. A, the most extended part, seems to be no larger than a few tenths of a second of arc at centimeter wavelengths, but at 158 MHz *(2)* it appears to be much larger, perhaps 10″ in diameter. B, the next smaller

component, is around $0.''01$; and C, the smallest, is in the neighborhood of $0.''0007$. The most recent measurements *(31)* indicate that C may be double. All this evidence is consistent with the shape of the flux spectrum.

At relatively low frequencies the only substantial body of previous VLBI observations is that of the Canadian group, who worked at 408 and 448 MHz *(12,13)*. The model they propound *(28)* merely confirms the one described above, however. They put 48 percent of the flux in component A, $>0.''05$, and the rest in a component $\sim 0.''005$ that corresponds to B.

Surprisingly, the present observations reveal considerable detail not detected in the Canadian work. The data are tabulated in Table 4-18 and plotted, along with the models, in Figure 4-11, while the models themselves are listed in Table 4-19. In the 1971 data I rejected the points at 0.77 and 1.26 hours, which seem too low, as do the points at -5.18, -5.01, -4.85, and -4.68 hours in the 1972 data. The 1972 point at -3.83 hours resulted from an incorrect system temperature measurement. For both series of observations the preferred model, A, consists of three components, only one of which is appreciably resolved. Since the third component is very weak I have also plotted, for comparison, model B, which is simply A without the weak component.

Several features attract immediate attention. The structure is manifestly different in the two sets of observations, but the character of the curves is similar, and they show pronounced resolution over the range of observed baselines. This result was unexpected on the basis of the Canadian model noted above, although it does not contradict the higher-frequency observations by any means. Closer study makes it clear that neither circularly symmetric models nor single gaussian components fit the observations adequately. The elliptical core-halo structure of model B works well, however, even though the distribution of flux between the core and halo is rather poorly determined.

As usual we should try to interpret the present observations in terms of the preexisting model, and in this case the two provide an especially interesting comparison. The 606-MHz model preserves the core-halo structure seen at higher frequencies, although the low-frequency core and halo both seem to correspond to component B alone. C should be almost completely self-absorbed at 606 MHz, and A contributes about 2 flux units, which leaves 6 flux units or so in B -- just about the amount in the model. Furthermore the flux of B appears to decrease below its cutoff frequency (about 800 MHz *(58)*) more slowly than one would expect for a simple component, and it is tempting to associate this flattening of the spectrum with the broadening

of the structure that appears at the same frequency. The broadening also seems to connect well with the more extended low-frequency halo noted above. Overall, a picture emerges of a source possessing a core-halo structure over a wide range of frequencies, with the halo continuously becoming more diffuse as the frequency decreases. It remains to be seen, unfortunately, how the 408- and 448-MHz observations can be made to conform to this representation.

Returning to the data at hand, we see that between the two series of observations there was a definite, if somewhat difficult to characterize, change in the apparent basic structure of the source (model B). The models account for the change adequately, but as mentioned above, the relation between core and halo is rather nebulous.

Then, in addition to the basic core-halo structure there is strong evidence of a third component in both sets of data. This component brings to mind the similar features in the visibility curves of 3C 279 and 3C 84, and points out once more that structure far below the normal detection threshold is easily detectable when it modulates a strong "carrier" component. But here again, the details of the extended structure are open to a wide range of interpretation.

TABLE 4-18

Observations of 3C 345

EPOCH	IHA	u ($\lambda \times 10^6$)	v ($\lambda \times 10^6$)	CORR. FLUX	ERROR
1971	-5.107	1.555	-4.024	3.30	0.12
	-4.678	2.278	-3.886	3.32	0.11
	-4.262	2.952	-3.703	3.23	0.11
	-3.763	3.712	-3.424	3.24	0.11
	-3.231	4.453	-3.059	2.67	0.12
	-2.725	5.078	-2.653	2.53	0.11
	-2.190	5.642	-2.171	2.43	0.16
	-1.478	6.129	-1.461	2.61	0.11
	-0.898	6.531	-0.838	2.46	0.12
	-0.395	6.680	-0.281	2.48	0.12
	+0.444	6.671	+0.663	2.59	0.11
	0.610	6.631	0.849	2.67	0.10
	0.772	6.579	1.028	2.07*	0.14
	0.947	6.511	1.220	2.54	0.11
	1.106	6.437	1.392	2.68	0.11
	1.258	6.355	1.555	2.32*	0.13
	5.144	1.492	4.361	3.85	0.10
	5.729	0.476	4.458	3.63	0.10
1972	-5.345	1.145	-4.078	2.98	0.12
	-5.178	1.434	-4.042	1.97*	0.10
	-5.011	1.719	-3.997	1.99*	0.10
	-4.847	1.997	-3.946	2.02*	0.10
	-4.682	2.271	-3.887	2.17*	0.10
	-4.522	2.535	-3.822	2.84	0.09
	-3.831	3.612	-3.465	3.70*	0.16
	-3.247	4.432	-3.070	2.37	0.10
	-2.746	5.054	-2.671	2.20	0.10
	-2.246	5.588	-2.224	1.91	0.10

TABLE 4-18 -- Continued

EPOCH	IHA	u ($\lambda \times 10^6$)	v ($\lambda \times 10^6$)	CORR. FLUX	ERROR
1972	-1.744	6.028	-1.734	2.09	0.10
	-1.243	6.363	-1.213	2.27	0.10
	-0.184	6.708	-0.044	2.43	0.11
	+0.363	6.686	+0.573	2.86	0.15
	0.613	6.630	0.851	2.63	0.14
	0.867	6.544	1.132	2.94	0.16
	1.441	6.244	1.749	2.96	0.12
	2.200	5.632	2.509	3.28	0.15
	2.871	4.907	3.103	4.16	0.15
	3.507	4.079	3.584	3.98	0.15
	4.040	3.297	3.914	4.30	0.14
	4.620	2.374	4.190	4.21	0.14
	5.128	1.519	4.357	3.89	0.14
	5.620	0.667	4.447	3.88	0.16

TABLE 4-19

Models of 3C 345

	COMP.	FLUX	r	θ	x	α	ζ
1971, Model A Three Components	1	3.53 *L*	0.0	---	0.026 *L*	0.735 *0.26*	142.4 *L*
	2	2.10 *1.49*	0.0	---	0.0	---	---
Error Factor 0.89	3	0.21 *0.07*	0.053 *0.002*	105.3 *5.3*	0.0	---	---
1971, Model B Core and Ell. Halo	1	3.53 *L*	0.0	---	0.026 *L*	0.735 *0.21*	142.4 *L*
Error Factor 1.87	2	2.10 *L*	0.0	---	0.0	---	---
1972, Model A Three Components	1	4.57 *L*	0.0	---	0.026 *0.009*	0.532 *0.25*	139.1 *14.6*
	2	1.34 *0.40*	0.0	---	0.0	---	---
Error Factor 0.96	3	0.19 *0.04*	0.090 *0.001*	94.1 *1.5*	0.0	---	---
1972, Model B Core and Ell. Halo	1	4.57 *L*	0.0	---	0.026 *0.013*	0.532 *0.37*	139.1 *21.9*
Error Factor 1.48	2	1.34 *0.61*	0.0	---	0.0	---	---

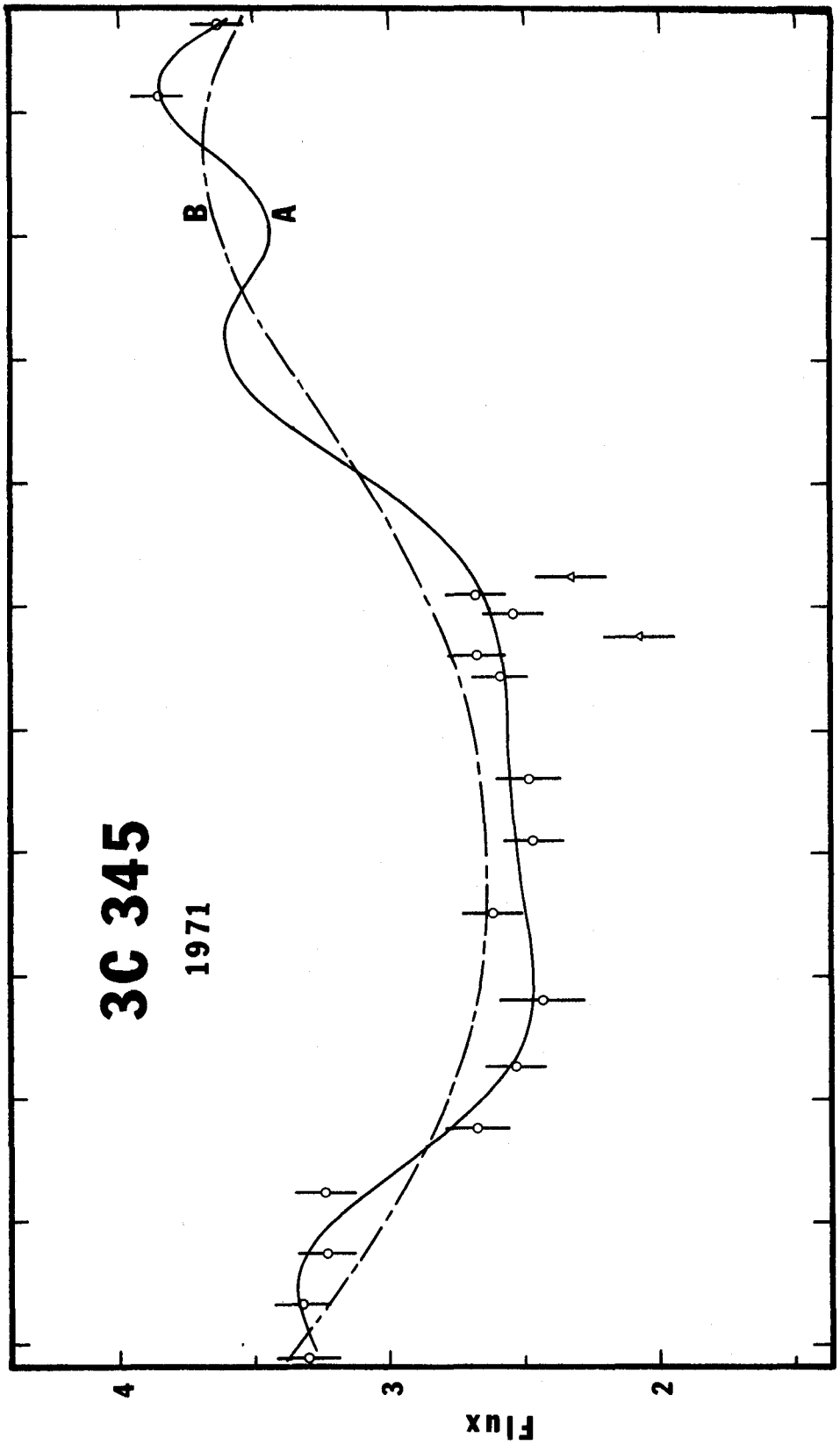

Figure 4-11a. Observed correlated fluxes and predictions of models for 3C 345. Epoch 1971. Key on page 49.

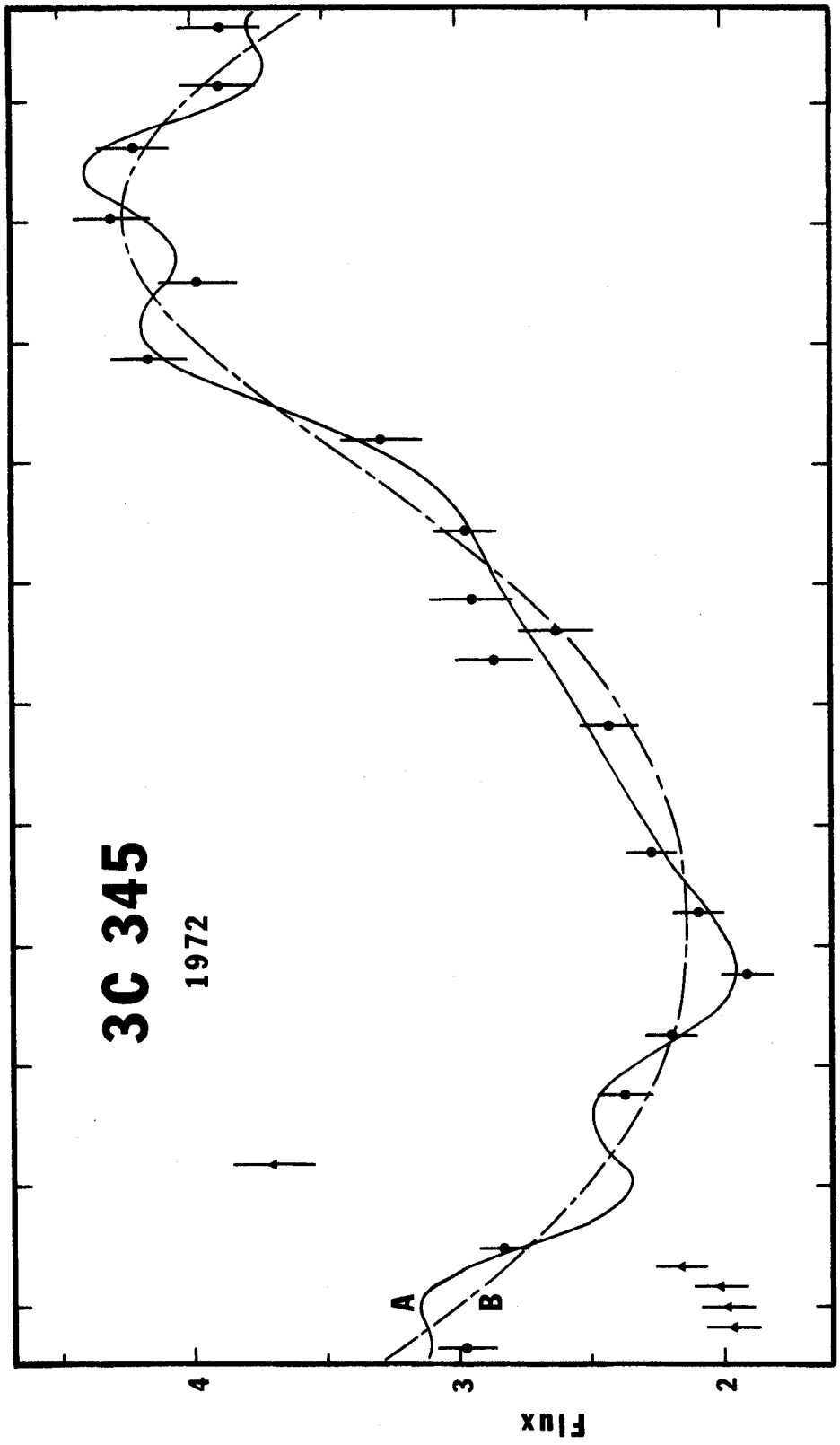

Figure 4-11b. Observed correlated fluxes and predictions of models for 3C 345. Epoch 1972. Key on page 49.

3C 380

Wyndham and Sandage *(88,109)* discovered the quasar associated with 3C 380 in the same search that led to similar identifications for 3C 279, 3C 345, and CTA 102. Lynds, Stockton, and Livingston *(69)*, among others, measured the redshift.

Compared to most of the sources examined in this study 3C 380's history is conspicuously undramatic. At radio frequencies, in particular, its spectrum falls off steadily above 30 MHz; and as noted in Chapter 3 it is only marginally variable even at short centimeter wavelengths *(61)*. As a result VLBI investigators have paid little attention to it. The few observations that have been made *(5,79,40,24,60)* all are compatible with the core-halo model proposed by Kellermann and others *(60)*. In this model the core, $\leq 0''.002$ and optically thick at 6 and 18 cm, provides about 30 percent of the flux at those wavelengths, while a halo, $\sim 0''.03$, supplies the rest. There is also evidence that at 158 MHz the source has an extended envelope several seconds in diameter *(2)*.

The 606-MHz observations shown in Table 4-20 and Figure 4-12 also indicate a core-halo structure, although the core is relatively much weaker than at the higher frequencies cited above. Table 4-21 gives the parameters of the models. Similar models without a core fit the data

nearly as well; but the pronounced flatness of the visibility curve between -3 and -1 hours, where the halo is almost entirely resolved, strongly suggests the presence of an unresolved component. Concerning the halo I made the natural assumption that it provides virtually the total source flux, about 26 flux units. The reader should understand, however, that smaller halos containing much less flux -- as little as 5 flux units -- fit the data just as well. In other words, the data are equally compatible with a model in which most of the 606-MHz emission comes from a much more extended halo like the one seen at 158 MHz.

Notably, 3C 380 is the only source thoroughly observed in both sessions that shows no convincing evidence of structural changes in the interim. The apparent discrepancy between the two curves at large positive hour angles is due almost entirely to the single high point in the 1972 data at 3.60 hours. This point is suspect since the observation to which it refers immediately preceded one that had to be rejected because of a violently discordant system temperature measurement. Otherwise the agreement between the two sessions is good. In fact, as the Table shows, a model fitted to the combined data of both series actually fits slightly better than the model computed on the basis of the second series alone. To facilitate comparison the visibility of this consolidated model (model B) is also plotted in both parts of the Figure.

TABLE 4-20

Observations of 3C 380

EPOCH	IHA	u ($\lambda \times 10^6$)	v ($\lambda \times 10^6$)	CORR. FLUX	ERROR
1971	-5.778	0.391	-4.898	3.39	0.14
	-5.289	1.243	-4.820	3.03	0.12
	-4.758	2.145	-4.643	2.44	0.12
	-4.250	2.971	-4.386	2.56	0.13
	-3.670	3.847	-3.997	1.77	0.16
	-2.998	4.752	-3.426	1.27	0.21
	-2.410	5.423	-2.837	1.42	0.20
	-1.912	5.892	-2.281	1.40	0.19
	-1.621	6.120	-1.937	0.86	0.39
	-1.249	6.360	-1.480	1.22	0.19
	-1.066	6.456	-1.249	1.72	0.16
	-0.905	6.528	-1.044	1.55	0.17
	-0.729	6.594	-0.817	1.24	0.20
	-0.557	6.645	-0.592	1.64	0.17
	+0.266	6.700	+0.492	1.59	0.16
	0.439	6.672	0.720	1.60	0.15
	0.615	6.629	0.950	1.92	0.14
	0.770	6.580	1.152	2.20	0.13
	0.940	6.514	1.370	2.09	0.13
	1.621	6.121	2.219	2.60	0.12
	1.772	6.006	2.400	2.80	0.10
	1.936	5.872	2.590	2.74	0.11
	2.108	5.719	2.787	3.00	0.10
	2.231	5.602	2.924	3.31	0.14
	2.777	5.018	3.495	3.78	0.10
	2.943	4.819	3.656	4.02	0.10
	3.109	4.611	3.810	4.05	0.10
	3.694	3.812	4.296	4.30	0.10

TABLE 4-20 -- Continued

EPOCH	IHA	u ($\lambda \times 10^6$)	v ($\lambda \times 10^6$)	CORR. FLUX	ERROR
1971	+4.199	3.050	4.638	4.48	0.10
	4.987	1.760	5.012	4.17	0.10
	5.590	0.720	5.159	3.27	0.10
1972	-5.848	0.267	-4.903	2.70	0.11
	-5.354	1.131	-4.835	2.58	0.11
	-4.777	2.113	-4.650	2.21	0.10
	-4.274	2.932	-4.401	1.94	0.10
	-3.772	3.698	-4.073	1.65	0.12
	-3.272	4.398	-3.674	1.50	0.10
	-1.669	6.085	-1.996	1.58	0.16
	-1.163	6.407	-1.373	1.66	0.16
	-0.663	6.615	-0.731	1.24	0.19
	+0.030	6.716	+0.180	1.62	0.13
	0.757	6.585	1.135	2.24	0.15
	1.426	6.254	1.981	2.64	0.15
	2.009	5.808	2.675	2.94	0.15
	2.511	5.316	3.225	3.84	0.15
	3.096	4.628	3.799	4.43	0.14
	3.598	3.950	4.223	5.05	0.15
	4.086	3.226	4.568	7.01*	0.21
	4.378	2.766	4.740	6.22*	0.26
	4.598	2.411	4.852	5.82*	0.20
	4.742	2.173	4.917	5.71*	0.20
	5.764	0.414	5.179	3.77	0.16

TABLE 4-21

Models of 3C 380

	COMP.	FLUX	r	θ	x	α	ζ
1971, Model A	1	24.6	0.0	---	0.037 *0.001*	0.717 *0.014*	140.4 *1.6*
Core and Ell. Halo							
Error Factor 1.38	2	1.0 *0.2*	0.0	---	0.0	---	---
1972, Model A	1	24.6	0.0	---	0.042 *0.002*	0.627 *0.026*	137.6 *2.5*
Core and Ell. Halo							
Error Factor 1.86	2	1.4 *0.2*	0.0	---	0.0	---	---
1971 and 1972	1	24.6	0.0	---	0.038 *0.001*	0.690 *0.015*	140.2 *1.6*
Combined Data, Model B							
Core and Ell. Halo	2	1.1 *0.2*	0.0	---	0.0	---	---
Error Factor 1.84							

(For explanation see key on page 48.)

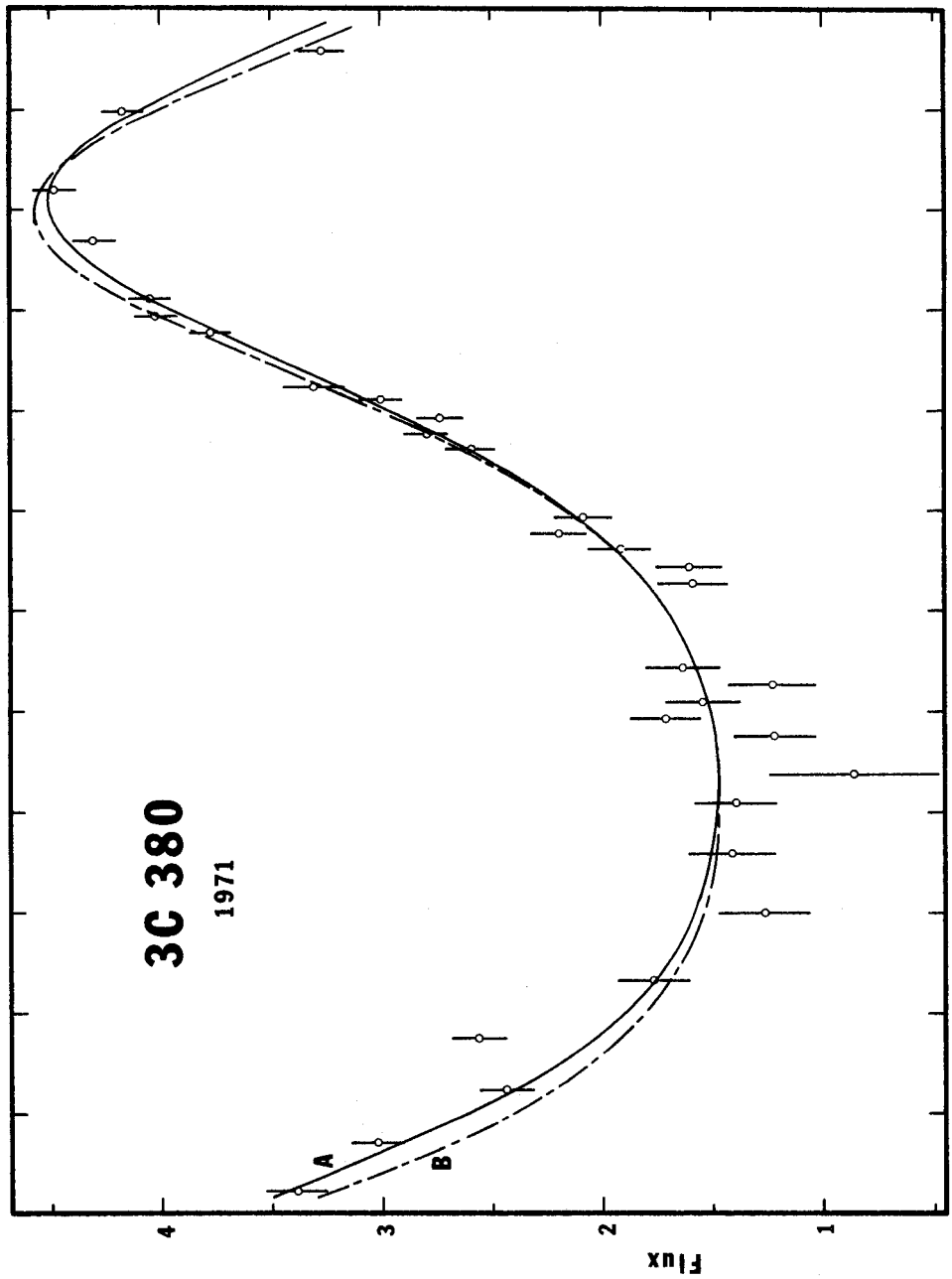

Figure 4-12a. Observed correlated fluxes and predictions of models for 3C 380. Epoch 1971. Key on page 49.

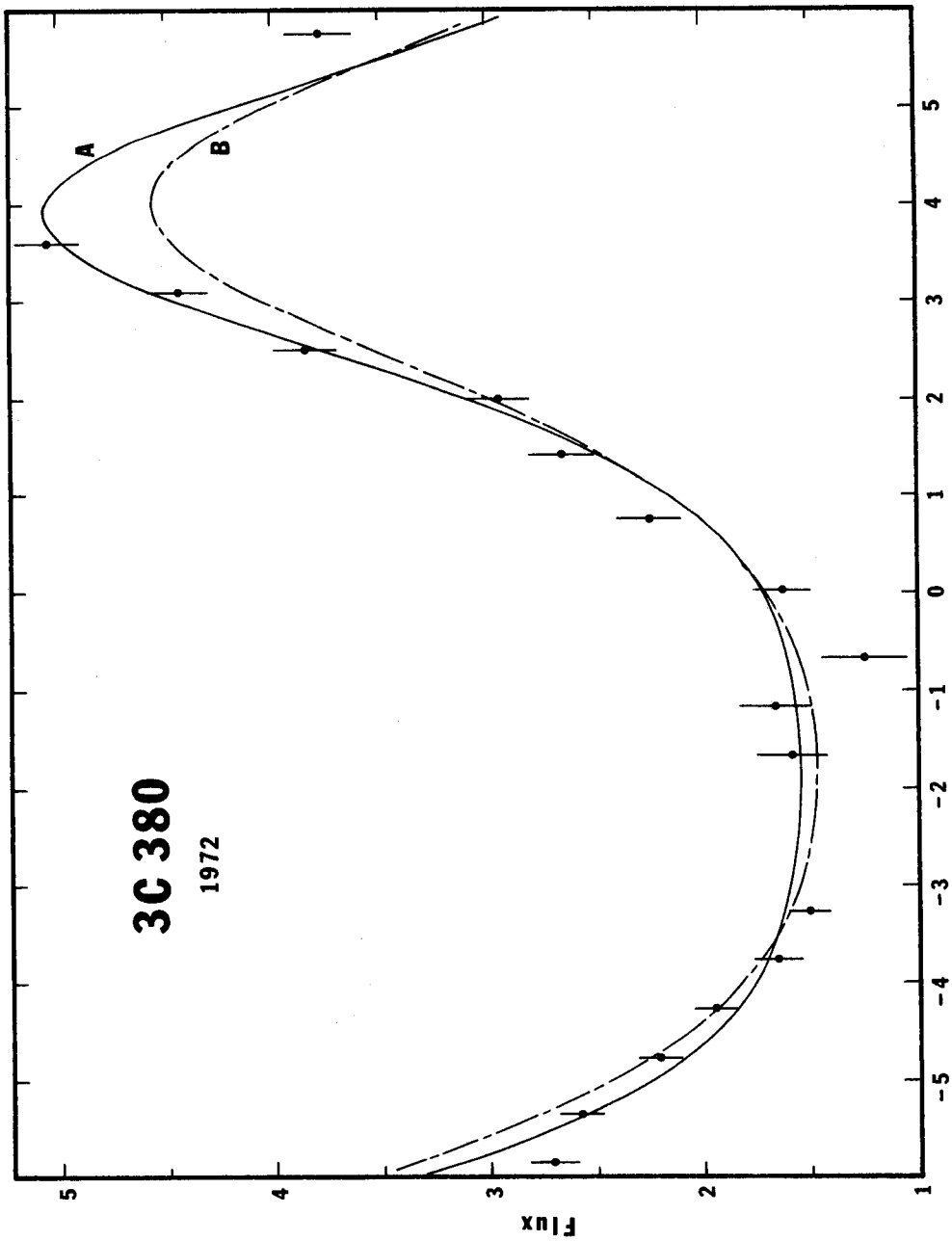

Figure 4-12b. Observed correlated fluxes and predictions of models for 3C 380. Epoch 1972. Key on page 49.

CTA 102

The quasar associated with CTA 102 belongs to the group identified by Wyndham and Sandage *(88,109)*. Schmidt *(93)* measured the redshift.

CTA 102 created a brief sensation in 1965 when Sholomitskii *(99,100)* reported that its 32.5-cm flux was varying quasi-sinusoidally by about 30 percent, with a period of a little more than a hundred days. But after efforts by numerous other observers failed to confirm the report *(7,70,77,104)* it languished in mild disrepute for almost eight years. Recently, however, Hunstead's convincing observations of similar variations in this and other sources, at 408 MHz *(54)*, have thoroughly rehabilitated Sholomitskii's work. In this case at least, it appears that the Soviets really did discover it first.

In view of these intense fluctuations it is not surprising to find that CTA 102 is an exceptionally compact object. The entire source scintillates *(32)*, and intermediate-baseline interferometry at 11 and 21 cm early showed it to be smaller than $0\overset{''}{.}025$ *(1,79,40)*. Mark I VLBI observations at 13 and 18 cm *(23,24,58,59,60)* have resolved part of the source, and they imply a more complicated structure than one would infer from the simple spectrum. There appears to be a core $\leq 0\overset{''}{.}003$ that generates about half the flux at 18 cm, together with a somewhat larger halo,

$\simeq 0''.007$, that supplies most of the rest. There is also some evidence of more extended structure, particularly at the lower frequencies investigated by the Canadian group *(12, 11, 28)*. But since this evidence consists principally in the observers' failure to account for the expected flux -- in a source that has since been discovered to vary in flux by more than the observed discrepancy -- it has to be regarded as precarious.

The present observations (Table 4-22 and Figure 4-13) also admit a core-halo model (Table 4-23), although the halo is definitely larger than at the higher frequencies cited above. Of course the model generated by the three data points of 1971, when the source was supposed to be a calibrator, should not be taken literally; and even the 1972 observations, which had to be terminated prematurely, are open to a considerable range of interpretation. In particular the distribution of flux between the core and halo is so uncertain in both cases that I felt justified in supposing, for modeling purposes, that the flux in the halo was the same at the two epochs. Nevertheless two interesting and unambiguous conclusions do emerge: first, that the source contains appreciable structure larger than $0''.01$; and second, that a substantial change in the apparent structure occurred during the seven months between the two observing sessions.

TABLE 4-22

Observations of CTA 102

EPOCH	IHA	u ($\lambda \times 10^6$)	v ($\lambda \times 10^6$)	CORR. FLUX	ERROR
1971	-2.841	4.942	-0.704	4.83	0.14
	+0.539	6.649	+0.399	4.68	0.15
	4.159	3.113	1.404	5.75	0.14
1972	-3.837	3.604	-0.929	6.18	0.11
	-3.331	4.320	-0.824	6.01	0.12
	-2.822	4.965	-0.699	5.71	0.12
	-2.329	5.506	-0.564	5.78	0.12
	-1.818	5.970	-0.409	5.37	0.13
	-1.326	6.315	-0.250	5.41	0.12
	-0.829	6.559	-0.081	5.48	0.13
	-0.312	6.694	+0.099	5.04	0.13
	+0.847	6.552	0.506	5.22	0.12

TABLE 4-23

Models of CTA 102

	COMP.	FLUX	r	θ	x	α	ζ
1971	1	4.55 L	0.0	---	0.0	---	---
Core and Circ. Halo Error Factor Undefined	2	2.84 L	0.0	---	0.031 L	1.0	---
1972	1	3.99 L	0.0	---	0.0	---	---
Core and Circ. Halo Error Factor 1.19	2	2.84 L	0.0	---	0.015 L	1.0	---

(For explanation see key on page 48.)

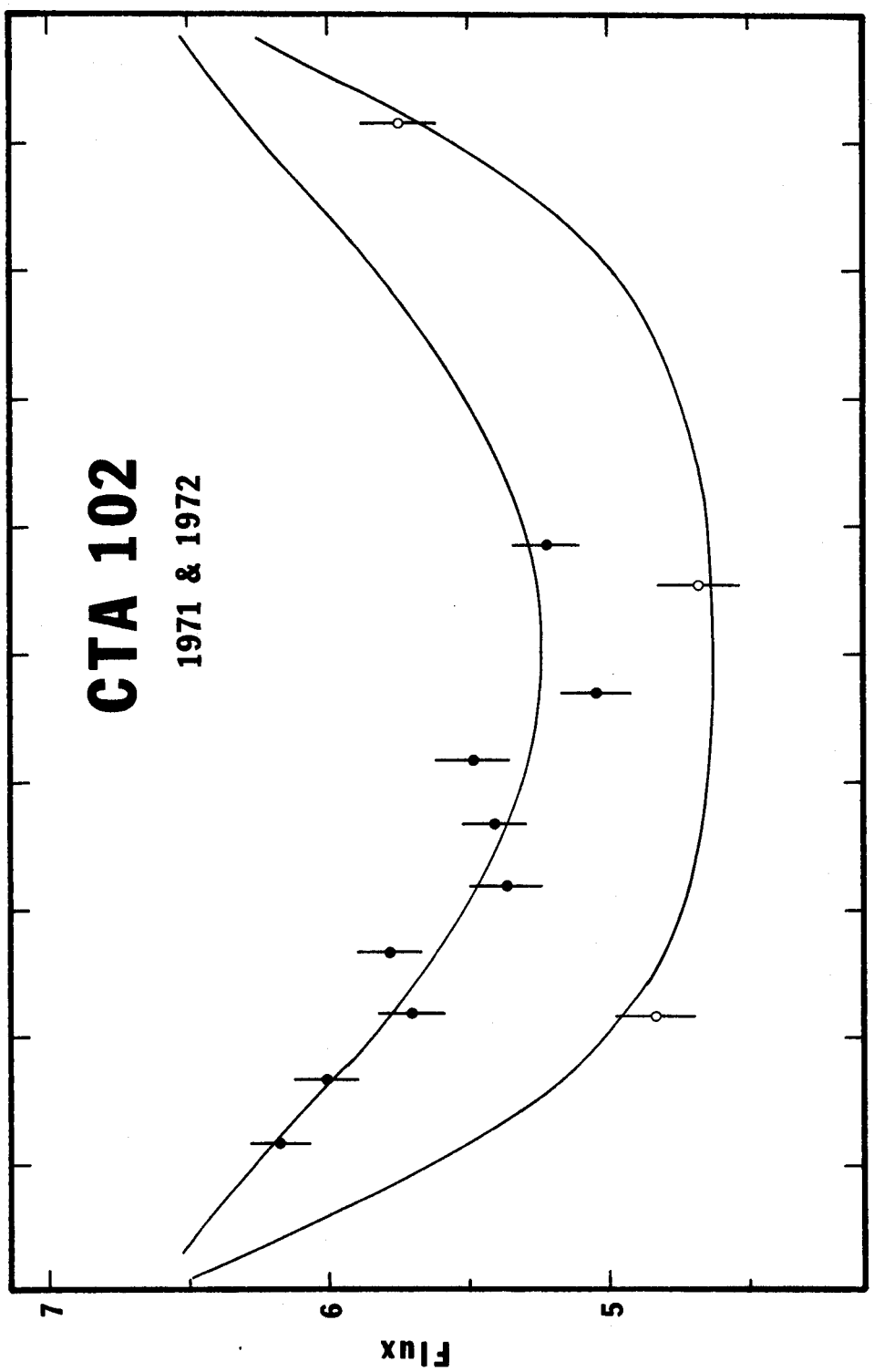

Figure 4-13. Observed correlated fluxes and predictions of models for CTA 102. Open circles are 1971 data. Key on page 49.

3C 454.3

3C 454.3 is a quasar similar in many respects to CTA 102. Wyndham *(110)* corrected the original misidentification and first drew attention to the source's optical variability. Lynds *(67)* measured its redshift.

At radio frequencies the source is known to be exceptionally compact, and like CTA 102 it has a scintillation index of 1.0 at 430 and 611 MHz *(32)*; but unlike CTA 102 it is strongly variable at short centimeter wavelengths and has a peculiar, complicated spectrum that suggests the presence of several components. VLBI measurements made by the NRAO-Cornell-Caltech group *(23,24,58,59,60)* revealed a core-halo structure that accounts for all or nearly all of the flux between 6 and 18 cm. These investigators had difficulty in estimating the size of the halo because of flux variations concurrent with their measurements, but it seems to have been on the order of $0\overset{''}{.}004$. The core, on the other hand, appeared unresolved even at 6 cm and so must have been $\leq 0\overset{''}{.}0004$. Subsequent observations at 3.8 cm by the same group *(31)* indicated an intermediate size of about $0\overset{''}{.}0012$.

Analysis of lower-frequency observations is complicated by the same factor that interferes in the case of CTA 102 -- the large and rapid changes in flux (and by inference structure) first observed by Hunstead *(54)*. In

this connection the Canadian results are especially puzzling. Their early observations at 448 MHz *(13,12)* yielded unexpectedly weak fringes, and they reasonably inferred a source size of about 0".6. Later, in their more extensive investigation *(11,28)*, they again found that the correlated flux accounted for only a fraction of the source. While 62 percent fitted into a compact component of about 0".015 diameter, they had to relegate the remaining 38 percent to an invisible component larger than 1". Extended low-frequency envelopes are not uncommon among quasars, but this particular instance is hard to reconcile with Jauncey and others' *(55)* observation at 610 MHz about a year earlier, in which the source appeared completely unresolved, $\leq$0".015. The scintillation data also bear heavily against it. On the other hand one cannot explain the discrepancy away on the basis that the assumed 448-MHz flux was too high. As a matter of fact comparison with Hunstead's flux curve shows that the Canadians' values were accurate in both 1967 and 1968.

It is hard to say whether the present observations compound the mystery or help to explain it. The data appear in Table 4-24 and the models in Table 4-25; and both are plotted together in Figure 4-14. As in the case of CTA 102 the data are lamentably incomplete, and the models should be considered provisional at best. Since a single circular

component reproduces the data I made no attempt to fit more complicated models, but an elliptical shape is eminently possible, and an unresolved core could easily be substituted for a large fraction of the very compact gaussian brightness distribution.

Notwithstanding the shortcomings of the data, it is clear that quite a profound change has taken place in the apparent structure of the source. Independent of any model the point at 3.79 hours from 1971 represents 79 percent of the assumed source flux, whereas in 1972 the source appears not only weaker, but much less resolved: once again, about 40 percent of the source seems to have vanished. This result provides not only a striking corroboration of Hunstead's findings, but also a basis for reconciling the Canadians' data with the 610-MHz results and the scintillation observations. At the same time the source's behavior makes an interesting contrast to that of the high-frequency variable VRO 42.22.01, which consistently appears *larger* when its flux is relatively low *(25)*.

TABLE 4-24

Observations of 3C 454.3

EPOCH	IHA	u ($\lambda \times 10^6$)	v ($\lambda \times 10^6$)	CORR. FLUX	ERROR
1971	+0.074	6.715	0.241	7.78	0.13
	3.789	3.674	1.754	10.29	0.16
1972	-3.920	3.480	-1.378	7.36	0.13
	-3.436	4.177	-1.244	7.22	0.11
	-2.922	4.845	-1.077	6.94	0.14
	-2.436	5.395	-0.897	7.02	0.12
	-1.933	5.874	-0.692	6.72	0.11
	-1.431	6.250	-0.472	6.85	0.12
	-0.929	6.518	-0.241	6.27	0.12
	-0.387	6.682	+0.018	6.34	0.10
	+0.240	6.703	0.321	6.37	0.12
	0.742	6.590	0.563	6.30	0.12

TABLE 4-25

Models of 3C 454.3

	COMP.	FLUX	r	θ	x	α	ζ
1971 Circular Gaussian Error Factor Undefined	1	12.1 *L*	0.0	---	0.011 *L*	1.0	---
1972 Circular Gaussian Error Factor 1.23	1	7.96 *0.17*	0.0	---	0.0077 *0.0005*	1.0	---

(For explanation see key on page 48.)

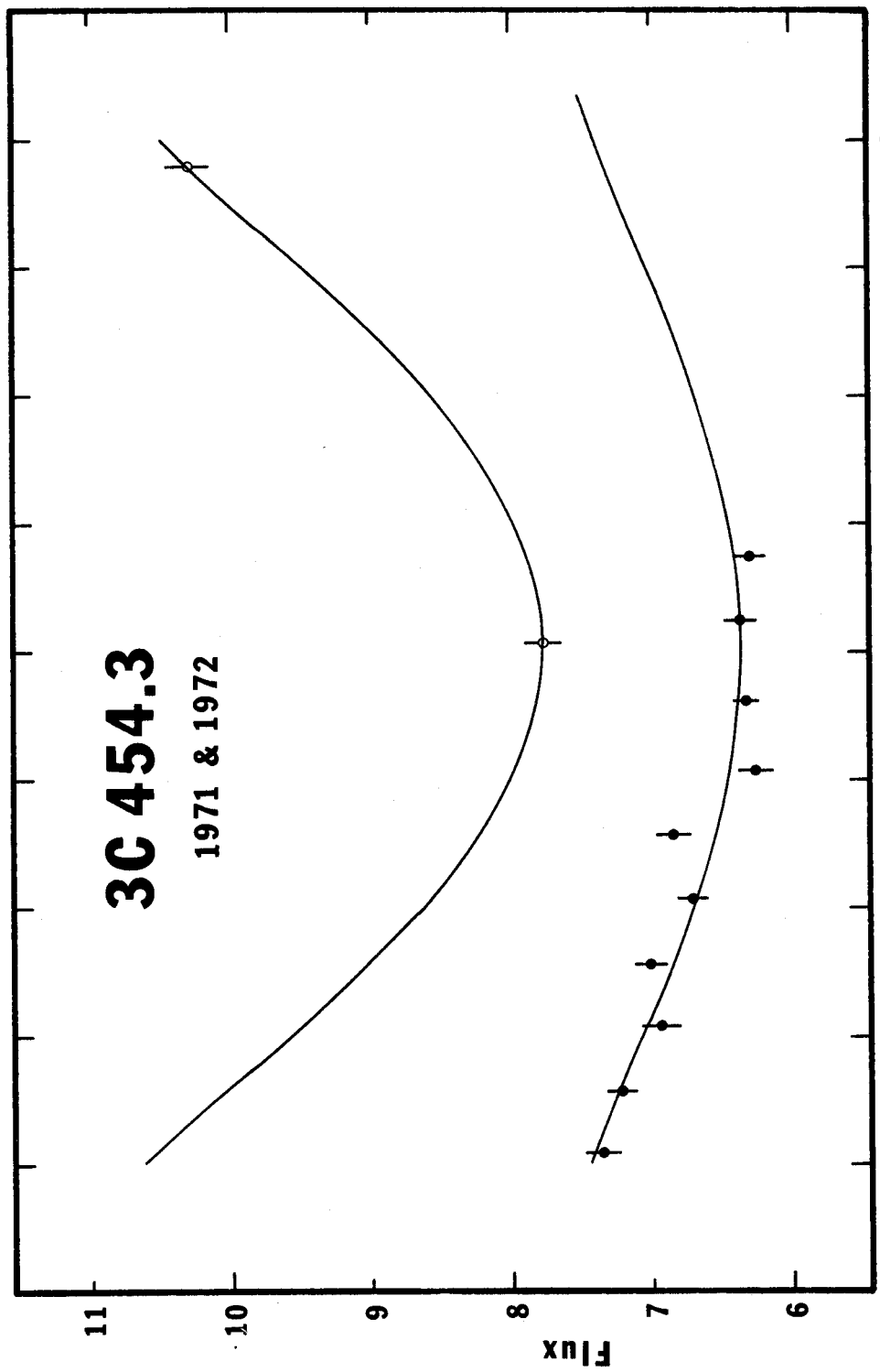

Figure 4-14. Observed correlated fluxes and predictions of models for 3C 454.3. Open circles are 1971 data. Key on page 49.

CHAPTER 5

DISCUSSION

Freely interpreted, the question of what the observations mean would invite a widely ranging discussion of emission mechanisms, source evolution, and cosmology. Within the context of limited information and even more limited understanding, however, it seems preferable to limit consideration to those issues most directly related to the data at hand, with emphasis on what is novel or unexpected. Although the discussion impinges on other areas, it dwells principally on morphology and the problems connected with rapid changes in source structure.

Morphology It is natural to begin by inquiring how well the models derived from the 606-MHz data correspond to those of other observers at neighboring frequencies. Table 5-1 summarizes the individual discussions in Chapter 4 by rating, for each source (column 1), the agreement of the 606-MHz model (column 2) with the model of the NRAO-Cornell-Caltech group (column 3), based mostly on 6- and 18-cm data, and that of the Canadian group (column 4), based on 67- and 73.5-cm observations. For nine of the thirteen sources the three models are basically similar, and in several instances even the details agree well. In

TABLE 5-1

Agreement of Models with Those of Other Observers

SOURCE	606-MHz MODEL	NRAO-CORNELL-CALTECH	CANADIAN
CTA 21	single elliptical component	excellent	poor
3C 84	single elliptical component	excellent	poor
3C 120	point source	excellent	consistent
3C 147	no model (complex)	----	----
3C 273	3 point sources	poor	poor
3C 279	2 strong components	flux excellent configuration poor	insufficient data
3C 286	core-halo	good	excellent
P1345+12	single elliptical component	consistent	consistent
CTD 93	point double?	insufficient data	insufficient data
3C 345	core-halo	excellent	fair
3C 380	core-halo	excellent	insufficient data
CTA 102	core-halo	good	good?
3C 454.3	single small component	good	good?

two other cases, CTA 21 and 3C 84, the discrepancy is due to the Canadians' preference for a double structure rather than a single elongated component. One of the remaining sources, 3C 147, is exceptionally complex and has so far defied all attempts to unify different sets of observations, while the other, 3C 273, is difficult to analyze because of the poor angular discrimination of the data. On the whole, especially in view of the ambiguities inherent in model-fitting, the consistency of the three sets of results is remarkably good. It encourages faith in the individual models and suggests that even in unusually active sources the structure is not likely to depend strongly on the frequency or resolution of the observations.

Table 5-2 examines this dependence in more detail by summarizing the information from Chapter 4 on *all* known structure in the sources studied. Columns 1 and 2 again contain the source name and the basic structure observed in the present study (scale size 0".01 to 0".1), while columns 3 and 4 indicate the structure seen on smaller and larger scales. The most conspicuous feature of the Table is the preponderance of core-halo sources. Though not typical of quasars or radio galaxies in general, this kind of structure is quite characteristic of compact objects with flat spectra. Hogg *(53, notice especially Figure 4)* in particular has pointed out the dichotomy between extended, double

TABLE 5-2

Source Structure Observed at Different Scale Sizes

SOURCE	STRUCTURE 0".01 TO 0".1	SMALLER STRUCTURE	LARGER STRUCTURE
CTA 21	single elliptical comp.	high-frequency core	none known
3C 84	single elliptical comp.	complex and evolving	complex
3C 120	point source	complex and evolving	low-frequency halo ∿10'
3C 147	no model (complex)	none known	complex
3C 273	3 point sources	complex and evolving	second diffuse comp.
3C 279	2 strong components	complex and evolving	low-frequency halo ∿30"
3C 286	core-elliptical halo	none known	low-frequency halo ∿0".2
P1345+12	single elliptical comp.	none known	none known
CTD 93	point double?	none known	none known
3C 345	core-elliptical halo	none known	low-freq. halo ∿ few sec.
3C 380	core-elliptical halo	none known	low-freq. halo ∿ few sec.
CTA 102	core-circular halo	none known	none confirmed
3C 454.3	small circular comp.	high-frequency core	none known

quasi-stellar sources and compact core-halo objects of low spectral index, while Fomalont *(44)* has made the same point with respect to radio galaxies. Thus, eight of the objects listed in the Table are definitely core-halo types, although in two, 3C 84 and 3C 120, the core appears to be compound. In two other cases, P1345+12 and CTD 93, the indications are less clear because the data are so limited, but a core-halo structure is certainly possible. On the other hand 3C 147 and 3C 273 are definitely more complicated, containing several well separated components.

The most troublesome object to classify in this respect is 3C 279. Its structure is certainly core-halo in the sense that it contains components spanning a wide range of scale sizes, with the smallest components ($<0''.001$) dominating the flux at high frequencies and the largest ($\sim 30''$) dominating at low frequencies in the usual way (see Figure 4-6). At the same time it is not at all clear that the various components are even approximately concentric: the present observations, in fact, indicate strongly that they are not. Ignoring for now the fine structure in the visibility function, we still have to explain an asymmetric curve (model B in Figure 4-7) that apparently requires the two strong components -- presumably the ones designated B and C by Kellermann and others *(58)* -- to be about a tenth of a second apart. Yet if this explanation is correct, the separation should surely have been detected in the

numerous 18-cm observations *(23,24,58,60)* as well. This discrepancy is puzzling to say the least.

Aside from 3C 279, however, none of the sources that exhibit core-halo structure in the present study has its halo offset noticeably from the core. This result is of considerable interest theoretically, particularly in its bearing on the various processes that might account for the intermittent explosions which evidently fuel the emission from these objects. As De Young has observed *(39)*, the models proposed to explain these outbursts fall into two general classes: those in which successive outbursts take place in a single relatively small region, and those in which they occur independently at more or less random points in a much larger volume. To the extent that VLBI and other observations show cores and halos to be concentric, they support the first class of models.

At the same time one should keep in mind that the experimental evidence on this point is equivocal in several respects. One difficulty is that although we observe violent activity in the nuclei of a *few* sources, it is far from obvious that the compact and diffuse parts of *most* sources result from distinct events. Fomalont *(44)*, for example, argues from the rarity of simple diffuse source structure that halos and their cores must be coeval. Another problem is that the distinction between core and

halo is often hard to define experimentally. To a certain extent this difficulty arises because some sources, like 3C 286 and 3C 345, exhibit almost a continuum of scale sizes when observed at different frequencies and resolutions. But a more important factor is that in many experiments, including this one, the observations span a relatively narrow range of baselines. In that case, as we have seen in Chapter 4, one may exercise considerable freedom in dividing the source flux between core and halo. A further point, not brought out in Chapter 4, is that the position of the core within the halo is also rather poorly determined -- particularly if one allows the halo to be elliptical. The uncertainty is not unlimited, however; and it is quite clear from the entire body of available data that in general cores and their associated halos are at least approximately concentric.

Another noteworthy feature of the core-halo models, revealed by Table 5-2, is that most of the halos are noticeably elliptical. In fact, only the most compact and poorly observed sources (3C 120, CTA 102, and 3C 454.3) fail to show evidence of elongation. The obvious implication is that either the mechanism producing the source is itself directional (a collision of gas clouds, for example, as in Daltabuit and Cox's model *(36)*); or the source is expanding into a medium that restricts its motion to a

particular axis. It would be interesting to compare these axes of elongation to those observed at higher and lower resolutions, but the information available is not yet complete enough to make such a comparison worthwhile. For core-halo sources at least, previous investigators have usually contented themselves with a single number to represent the scale size of each component.

Information on magnetic field alignment, as derived from polarization measurements, is more plentiful; but the significance of correlations with source structure is open to considerable doubt, as pointed out by Mitton *(75)*. If, as seems likely, the integrated polarization of most sources results from the superposition of several randomly oriented domains, then the absence of a high level of correlation is less than surprising. Table 5-3 compares the polarization and elongation axes of the four sources in the current study for which both angles are reliably known.

Another parameter associated with a source's magnetic field is its maximum possible brightness temperature. In a synchrotron source this temperature is limited by the kinetic temperature of the electron gas (*(91), p. 341*; see also *(62)* and the summary of a more rigorous derivation given by Terrell *(103)*):

$$(T_b)_{max} \sim \gamma m_0 c^2/3k \sim \left(\frac{\nu}{\nu_g}\right)^{1/2} m_0 c^2/3k \qquad (5\text{-}1a)$$

TABLE 5-3

Comparison of Elongation and
Polarization Axes for Four Sources

SOURCE	ELONGATION P.A. (DEGREES)	POLARIZATION P.A. (DEGREES)	DIFFERENCE (DEGREES)
3C 273	∿44	152	108
3C 286	∿46	31	15
3C 345	∿141	46	95
3C 380	∿140	68	72

(The intrinsic polarization angles were kindly provided by Wright *(108)*. Note that for an optically thin synchrotron source the intrinsic polarization angle is perpendicular to the projected magnetic field.)

where $\gamma m_0 c^2$ is the energy of a typical electron,

k is the Boltzmann constant, 1.38×10^{-23} joule/K,

ν is the observed frequency, and

ν_g is the electron gyrofrequency, given (in Gaussian units) by $\nu_g = eB/2\pi m_0 c$.

Substituting their values for the constants, we can rewrite (5-1a) as

$$(T_b)_{max} \sim 1.18 \times 10^9 \left(\frac{\nu}{B}\right)^{1/2} \qquad (5\text{-}1b)$$

where T_b is expressed in kelvins, ν in MHz, and B in gauss. Thus, for $\nu = 606$ and $B = 10^{-4}$, $(T_b)_{max} \sim 2.9 \times 10^{12}$ K. Experimentally the brightness temperature is given by

$$T_b = \frac{Sc^2}{2k\nu^2\Delta\Omega} \qquad (5\text{-}2a)$$

where S is the observed flux and

$\Delta\Omega$ is the solid angle subtended by the source.

For the case of an elliptical Gaussian brightness distribution, with $\nu = 606$ MHz, we can rewrite (5-2a) as

$$T_b = 3.33 \times 10^6 \frac{S}{W_x W_y} \qquad (5\text{-}2b)$$

in which T_b is the brightness temperature at the center of the source,

S is expressed in flux units, and

W_x and W_y are the full widths to half

maximum intensity along the major and minor axes of the source.

Computing T_b for the various models in Chapter 4, we find values typically well below the limit imposed by (5-1). The highest T_b -- for a resolved component, at least -- is 4.2×10^{11} K for 3C 454.3 in 1972. Consequently the models are entirely consistent with magnetic fields in the emitting regions of 10^{-4} gauss or even higher.

Certainly the most remarkable morphological feature of the models is the presence of weak structure far from the strong components in 3C 84, 3C 279, and 3C 345. The evidence for the existence of this structure is strong: it resides in the fact that simple one- and two-component models fail to fit the data adequately and that the deviations of the data from the simple models are systematic. At the same time the evidence is highly ambiguous. From the character of the deviations one can get an idea of the separations involved, but more specific inferences are unreliable. Hence the models proposed in Chapter 4 should be considered as merely *suggestive* of the undetermined structure.

Nonetheless, even the existence of the weak components is a matter of considerable interest. Contrary to the conclusion drawn earlier from the symmetry of core-halo sources, the large distances separating these weak sources

from the strong components suggest that they result from independent events. Much more precise and thorough observations are necessary, however, before we can discuss with confidence the details of this weak, extended structure.

Changes in Source Structure The most dramatic result of the experiment was the discovery of apparent changes in the structure of at least six of the nine sources that were observed in both 1971 and 1972. This finding was unexpected because early searches for low-frequency variability had been uniformly unsuccessful (see *(61, p. 419 ff.)* for a summary), and because it contradicts the canonical model of a variable compact source *(66,61)*. According to this model a variable component originates as an extremely compact, highly energetic outburst of particles in a region containing a magnetic field. Initially the compact source is optically thick at low radio frequencies, so that it appears first at millimeter and short centimeter wavelengths, where a typical outburst can increase the total flux of a source by a factor of two or more. As time goes on and the radiating region expands, it becomes optically thin and radiates at progressively lower frequencies, but with reduced flux. By the time the disturbance becomes visible at long decimeter wavelengths, after two years or so, its amplitude is practically negligible.

Recently, however, Hunstead *(54)* and others have observed rapid changes in the 73.5-cm fluxes of several compact sources, including CTA 102 and 3C 454.3. These findings conflict with the canonical model in that the fluctuations are large and appear to be unrelated to any similar activity at higher frequencies. But at the same time they form a basis for confidence in the current observations of changes in structure -- especially for CTA 102 and 3C 454.3, which exhibited the most dramatic changes.

The interpretation of the variations, both in flux and in structure, is frustrating because every hypothesis encounters serious objections. There are three possibilities: (1) the variations are an artifact of the measuring process; (2) they are imposed on a constant source by the intervening medium; or (3) they are intrinsic to the source. Possibility (1) we can dismiss immediately since the flux changes, at least, have been corroborated by several independent groups using different equipment and procedures.

Possibility (2) requires more detailed consideration, however. Evidently the medium imposing the scintillations, if that is what they are, is neither the ionosphere nor the interstellar plasma, because the time scale of the observed variations (on the order of a year) is far too long. The modulating material has to be intergalactic,

then, and the situation must be more or less as depicted in Figure 5-1.

The behavior of signals passing through such a medium has been considered by numerous writers, including Salpeter *(84)* and Scheuer *(90)*, who summarizes the results in a compact and readable form. Yoshioka *(111)* has applied these results to the intergalactic scintillation of compact sources, but his treatment is rather superficial. For our present purposes we can summarize the relevant relations as follows. (In the numerical relations $\Delta\phi$ is measured in radians, Δn_e in cm^{-3}, a and L in parsecs, and ℓ_0 in Mpc.)

$$\Delta\phi \sim (2\pi)^{1/4} r_e \lambda (aL)^{1/2} \Delta n_e \sim 6.82 \times 10^7 (aL)^{1/2} \Delta n_e > 1 \qquad (5\text{-}3)$$

$$\theta_{sc} \sim (2\pi^3)^{-1/4} (L/a)^{1/2} \Delta n_e r_e \lambda^2 \sim 2.46 \times 10^{-10} (L/a)^{1/2} \Delta n_e \qquad (5\text{-}4)$$

$$\ell_0 \sim 2\pi a^2/\lambda\Delta\phi \sim 5750\, a^{3/2} L^{-1/2} \Delta n_e^{-1} < 3000 \qquad (5\text{-}5)$$

$$\frac{1}{3} \leq \frac{\Delta I}{I} \sim \frac{x}{\ell_0} \quad \text{if } x << \ell_0 \qquad (5\text{-}6)$$

$$z\theta_{sc} > a \qquad (5\text{-}7)$$

$$x\theta_{int} < a \qquad (5\text{-}8)$$

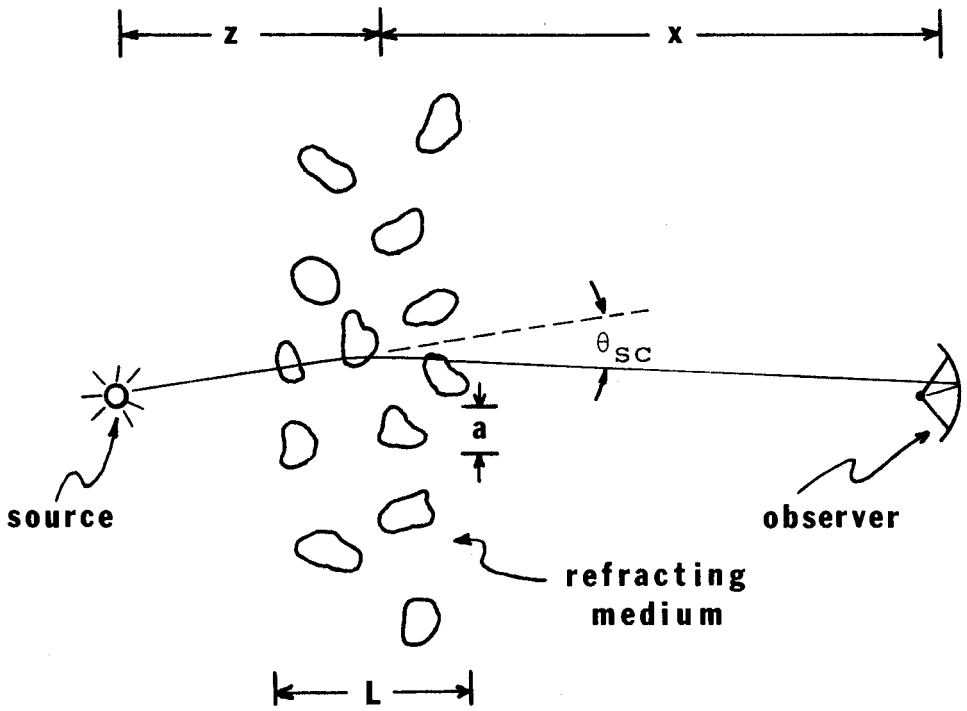

Figure 5-1. Schematic representation of intergalactic scintillation, with the important parameters labeled.

$$0.0033 < \frac{\Delta\lambda}{\lambda} \sim \frac{\lambda}{z\theta_{sc}^2} \lesssim \frac{1}{2} \qquad (5\text{-}9)$$

$$\tau \simeq 3 \times 10^7 \text{ seconds} \lesssim \frac{a}{v} \qquad (5\text{-}10)$$

In these formulas,

r_e is the classical radius of the electron, 2.8×10^{-13} cm,

λ is the observing wavelength,

a is the scale size of the electron density fluctuations, which are supposed to have a Gaussian spectral distribution,

Δn_e is the rms amplitude of the density fluctuations,

z is the distance between the refracting layer and the source,

L is the thickness of the refracting layer,

x is the distance between the refracting layer and the observer,

ℓ_0 is a typical focusing distance for the refracted rays,

$\Delta\phi$ is the rms phase perturbation of a ray traversing the refracting layer,

θ_{int} is the angle subtended by the (unrefracted) source at the location of the observer,

θ_{sc} is the rms scattering angle for a ray traversing the refracting layer,

$\frac{\Delta I}{I}$ is the rms fractional intensity fluctuation of the

observed signal,

$\Delta\lambda$ is the bandwidth over which the observed intensity fluctuations are correlated,

v is the speed of the refracting layer transverse to the line of sight to the source, and

τ is the time scale of the observed intensity fluctuations.

The inequalities in the various formulas are consequences of the observations, under the assumption that a typical source distance is 1000 Mpc. In particular the restriction in (5-5) results from the observation that the intensity fluctuation amplitude in (5-8) exceeds thirty percent in some sources; and the inequalities in (5-9) are due to the fact that the fluctuations are correlated over the bandwidth of the present observations (2 MHz) but show little correlation between 408 and 318 MHz (see Figure 3-1).

These relations can be manipulated in various ways to obtain limits on the parameters of the intergalactic medium. All these results tend to show that intergalactic scintillation is unlikely to be the cause of the observed variations, but the most direct and telling argument follows from solving (5-7) for θ_{sc} and substituting the resulting expression in the left-hand inequality of (5-9). We can then rearrange the resulting formula to show that $a < (300\lambda z)^{1/2}$ or, since $z < 1000$ Mpc, $a < 0.0022$ pc.

However the intrinsic source size must be comparable to a, or smaller (as indicated by (5-8)) in order for the rays passing through different irregularities to interfere coherently. Hence, if scintillation is causing the apparent changes in flux and structure, we are compelled to suppose that the scintillating part of the source is less than 0.0022 pc in diameter. A source of that size, with an apparent flux of one flux unit, would require a brightness temperature in excess of 6×10^{18} K even if it were as close as 3C 273. Consequently we would have to invoke a coherent emission process, and with such a mechanism at our disposal we would no longer need scintillation to produce the observed time variations. The interferometric observations, on the other hand, indicate much larger sizes for at least some of the varying regions, and brightness temperatures well within the limits set by inverse Compton scattering. Another objection to the scintillation mechanism is that the pattern speed of the fluctuations, given by (5-10), is uncomfortably large ($\simeq$2000 km/sec) even for the small scale size derived above. In short, all the evidence we can bring to bear militates strongly against possibility (2).

We are left, then, with the single remaining alternative: that the observed variations in flux and structure are intrinsic to the sources. As a working hypothesis this seems the least objectionable possibility, even though it

creates more problems than it solves.

Foremost among these problems is the apparent irreconcilability of the spatial and temporal scales of variation. The linear size of a source component is related to its apparent angular size by the formula

$$d = \Theta_0 D \qquad (5\text{-}11a)$$

where d is the linear size of the source,

Θ_0 is its apparent angular size, and

D, the metric distance to the source, is given by *(85,86)*

$$D = \frac{c}{H_0 q_0^2 (1+z)^2} \{q_0 z + (q_0 - 1)[(1 + 2q_0 z)^{1/2} - 1]\} \qquad (5\text{-}11b)$$

Here, c is the speed of light,

q_0 is the cosmological deceleration parameter, assumed in the following discussion to be +1,

z is the (cosmological) redshift, and

H_0 is the Hubble constant, taken to be 55 km/sec/Mpc.

Thus, for a typical source in this investigation an angular size of 0".01 corresponds to linear dimensions of about 60 parsecs. If we accept the models of Chapter 4 and the cosmological nature of the redshifts, then we have to conclude that at least some of the observed changes are taking place in sources of about that size. At the same time, the variations occur in intervals of a year or less, and these

intervals are reduced by a factor of (1+z) in a frame moving with the source. The apparent rate of propagation of the disturbances, therefore, is more than 200 times the speed of light.

How are we to avoid these unacceptable speeds? Whitney and others *(106)* have considered the same problem in connection with their own observations of 3C 273 and 3C 279 at 3.8 cm, in which they found apparent expansion rates of a few times the speed of light. They suggested several possible loopholes in the reasoning that deserve reconsideration in the light of the new data:

1) The simple source models are incorrect. This is certainly a plausible supposition, but the basic observational evidence depends very little on the particular models used to represent it. The maximum resolution of the present observations was about $0''.01$, and substantial changes were observed in partially resolved structure during an interval of seven months. Any model similar in character to those suggested in Chapter 4, that accounted for the time variations, would necessarily involve comparable speeds.

2) The emitting regions do not move or change in size; rather, several components simulate motion by blinking on and off independently (the "Christmas tree" model). This model has some attractive features but also raises

additional difficulties. There is no doubt that models of this type can be constructed so as to reproduce the observations made to date. Such models would be very hard pressed, however, to explain any long-term consistency in the evolution of a source.

On the theoretical level, if the individual "blinkers" were made small enough to overcome the propagation-time problem, they would have such high brightness temperatures (greater than 10^{14} K) that a coherent emission mechanism would probably be needed in order to sustain them. Mechanisms of this kind are certainly not implausible; in fact, the lack of correlation between the low-frequency outbursts and those seen at short centimeter wavelengths lends considerable support to the idea that different emission processes are operating. If this supposition is correct, then an important observational consequence is that the high- and low-frequency variations may well be spatially, as well as temporally, independent.

3) The apparent rates are phase, not group speeds. This possibility is credible for apparent rates of a few times c, but not for 100c.

4) The observations result from relativistic motion of source components near the line of sight. This suggestion is open to grave objections even for modest rates and is entirely implausible in the present context.

5) The fluctuations are due to scintillation -- an unlikely possibility because of the arguments advanced earlier.

6) The redshifts are not cosmological. No tenable alternative has been proposed, but the idea is most seductive.

Suggestions for Further Research In the light of our present knowledge it would be presumptuous to suggest a line of inquiry *not* likely to bear fruit. There is a pressing need for more observations of compact sources at all resolutions from a second of arc to a thousandth of a second and beyond, particularly in the frequency ranges that have been neglected. The observations reported here should be repeated at intervals of no more than six months in order to follow the history of the time variations and determine their nature. Concurrent observations at other frequencies are badly needed to establish the spectral dependence of the variable structure and shed light on the underlying mechanism. Additional baselines will also be required in order to determine the structure more reliably, particularly for the sources at low declination. Future observations should emphasize low system temperatures, fastidious calibration, and continous hour-angle coverage so as to extract as much information as possible from each baseline.

APPENDIX A

THE EFFECT OF NOISE ON COMPUTED CORRELATION AMPLITUDES

This appendix deals with the most important statistical considerations involved in the reduction of continuum data on the Mark II VLBI system. Some of the pertinent probability distributions are derived in the first section. Most of these results are germane to a wide class of signal-processing problems, and other writers have evolved them from a more rigorous mathematical foundation. I hope, however, that my heuristic approach will be more suggestive to readers with a particular interest in VLBI. In the second section experimental data are combined with the results of the first section to estimate the bias and error in fringe amplitude measurements.

Probability Distributions Consider the operation of one delay channel in the Mark II reproduce terminal. The inputs to the channel are the bit streams from two record terminals. Each record terminal has limited its incoming i-f signal to a frequency range from near zero to about 2 MHz, sampled the sign of the band-limited i-f at intervals of 0.25 microsecond, and encoded the samples on video tape. In general a portion of the signals on the two tapes, due to a compact source, is correlated and will produce "fringes" -- that is, a correlation coefficient

varying sinusoidally in time. The rest, including the remainder of the signal from the source, is statistically independent at the two stations.

In the correlation process the reproduce terminal first retards one of the two entering bit streams (call them B_1 and B_2) by an integral number of bits to compensate for the difference in propagation time from the source to the two stations. Then it multiplies one of the inputs (B_1, say) by two auxiliary bit streams that approximate sine and cosine waves at the expected fringe rate, producing the outputs B_{1a} and B_{1b}. (The purpose of this multiplication is to shift the fringe rate to near zero. Both components of the auxiliary sinusoid are necessary, because the phase of the fringes is unknown and may, in fact, vary irregularly during an observation.) Finally the terminal correlates B_2 with both B_{1a} and B_{1b} and writes the resulting correlation coefficients on an output tape at intervals of 0.2 second.

In the next step of the reduction procedure a series of correlation coefficients in a particular delay channel of the correlator output tape is Fourier transformed to give the residual rate, the phase, and the amplitude of the fringes in that channel. At this stage the "cosine" and "sine" parts of the correlation coefficient assume the roles of the "real" and "imaginary" parts of the time series.

Given this correlation procedure we can derive the statistical properties of the resulting correlation amplitudes. First consider the simple case of pure noise, in which no part of the two i-f signals is correlated. Suppose also that successive bits on each of the input tapes are uncorrelated. (That this assumption is correct for i-f signals having a square bandpass and sampled at the Nyquist rate, as they are in this case, is evident from a direct application of the Wiener-Khinchine theorem.)

Let N pairs of bits be correlated. The correlation coefficient may be defined as

$$\rho = \frac{\sum_i f_{1,i} f_{2,i}}{\left\{ \sum_i f_{1,i}^2 \sum_i f_{2,i}^2 \right\}^{1/2}} \qquad \text{(A-1a)}$$

where $f_{1,i}$ and $f_{2,i}$ are corresponding members of the two time series. An equivalent formula is

$$\rho = \frac{\langle f_1 f_2 \rangle}{\left\{ \langle f_1^2 \rangle \langle f_2^2 \rangle \right\}^{1/2}} \qquad \text{(A-1b)}$$

in which angle brackets indicate a measured mean value (not a statistical expectation). In this example $f_{1,i}$ and $f_{2,i}$ assume the values +1 and -1 with equal probability, so that the expectation values of both $f_{1,i}$ and $f_{2,i}$ are zero. Furthermore, the correlation of each pair of bits is a Bernoulli trial with a probability of success of 0.5,

when success is defined as $f_{1,i}f_{2,i} = +1$. The probability of n successes in N trials is then the binomial distribution function,

$$b(n;N,0.5) = 2^{-N}\binom{N}{n} \tag{A-2}$$

and using our knowledge of f we can rewrite (A-1a) as

$$\rho = \frac{n - \frac{N}{2}}{\frac{N}{2}} \tag{A-3}$$

Finally, combining (A-2) and (A-3) with the familiar asymptotic relation between the discrete binomial distribution and the continuous normal distribution, namely

$$b(n;N,p) \sim G(n;Np,Np(1-p)) \tag{A-4}$$

where

$$G(x;\mu,\sigma) = (2\pi\sigma^2)^{-1/2} \exp[-(x-\mu)^2/(2\sigma^2)] \tag{A-5}$$

we can easily show that when the correlator operates on pure noise the correlation coefficient has a normal probability density function:

$$P\{\rho\} = G(\rho;0,N^{-1/2}) \tag{A-6}$$

Next consider what happens when the time series of correlation coefficients undergoes a Fourier

transformation. Suppose that a sequence of M correlation coefficients is transformed to yield the spectral coefficients

$$A_t = \frac{1}{M} \sum_{k=0}^{M-1} \rho_k \, e^{-i2\pi tk/M} , \qquad t = 0,1,\ldots,M-1 \qquad \text{(A-7)}$$

Remember that ρ_k has both real and imaginary parts (the cosine and sine correlations), and the A_t are complex as well. Recall also that if ρ_1 and ρ_2 are normally distributed random variables with means $\langle\rho_1\rangle$ and $\langle\rho_2\rangle$, respectively, and standard deviations σ_1 and σ_2, and if $\rho_3 = A\rho_1 + B\rho_2$, then ρ_3 is normally distributed too, with $\langle\rho_3\rangle = A\langle\rho_1\rangle + B\langle\rho_2\rangle$ and $\sigma_3^2 = A^2\sigma_1^2 + B^2\sigma_2^2$. Then by isolating the real and imaginary parts of (A-7) it is again perfectly straightforward to show that the real and imaginary parts of A_t, $\mathrm{Re}[A_t]$ and $\mathrm{Im}[A_t]$, both are normally distributed with means

$$\mu(\mathrm{Re}[A_t]) = \mu(\mathrm{Im}[A_t]) = 0, \quad t = 0,1,\ldots,M-1 \qquad \text{(A-8a)}$$

and standard deviations

$$\sigma(\mathrm{Re}[A_t]) = \sigma(\mathrm{Im}[A_t]) = M^{-1/2}\sigma(\rho) = (MN)^{-1/2} , \qquad t = 0,1,\ldots,M-1 \qquad \text{(A-8b)}$$

in which MN is simply the total number of pairs of bits correlated.

Of course our primary interest is in the fringe visibility, which is proportional to the modulus of A_t:

$$\text{modulus}(A_t) = |A_t| = \{(\text{Re}[A_t])^2 + (\text{Im}[A_t])^2\}^{1/2} \qquad \text{(A-9)}$$

We can derive the probability density function $P\{|A_t|\}$ from (A-8) by using a relation that will be helpful again later on, the convolution formula for probability distributions. Given the probability density functions $P_1\{x_1\}$ and $P_2\{x_2\}$ of the random variables x_1 and x_2, let $y = F(x_1,x_2)$ and $x_1 = f(y,x_2)$. Then the probability density function $P\{y\}$ is given by

$$P\{y(x_1,x_2)\} = \int P_2\{x_2\}P_1\{f\} \left|\frac{\partial f}{\partial y}\right| dx_2 \qquad \text{(A-10)}$$

where the integration is performed over all values of x_2 permitted by a particular value of y. Here, with $x_1 = \text{Re}[A_t]$, $x_2 = \text{Im}[A_t]$, $P\{x_1\}$ and $P\{x_2\}$ as specified in (A-8), and $y = |A_t|$ from (A-9), we find, carrying out the integration (A-10), that

$$P\{|A_t|\} = \frac{|A_t|}{A_0^2} \exp[-|A_t|^2/(2A_0^2)] = R(|A_t|;A_0), \qquad 0 \leq |A_t| < \infty \qquad \text{(A-11a)}$$

where

$$A_0 = (MN)^{-1/2} = \sigma(\rho) \qquad \text{(A-11b)}$$

The function R in (A-11a) is called a Rayleigh distribution.

One can also show by the same method that the phase of A_t is uniformly distributed:

$$P\{\text{phase}(A_t)\} = 1/2\pi, \quad 0 \leq \text{phase} < 2\pi \tag{A-11c}$$

A related function we shall need in the second section is the probability density distribution of the largest value among m independent samples drawn from a Rayleigh-distributed population. In general, for a distribution function $\phi(x)$, associated with a cumulative probability distribution function $\Phi(x) = \int_{-\infty}^{x} \phi(\xi)\, d\xi$, the probability distribution of the largest among m independent samples from ϕ is

$$\phi_m(x) = m\phi(x)[\Phi(x)]^{m-1} \tag{A-12}$$

For the Rayleigh distribution,

$$R_m(x;x_0) = \frac{mx}{x_0^2} e^{-x^2/2x_0^2} \{1 - e^{-x^2/2x_0^2}\}^{m-1}, \quad 0 \leq x < \infty \tag{A-13}$$

So much for the pure noise case. Now suppose that a source signal (the correlated part of the radio source flux) is a component of both of the i-f bit streams. In this case (A-1b) may be written

$$\rho = \frac{<(n_1 + s_1)(n_2 + s_2)>}{[<(n_1 + s_1)^2><(n_2 + s_2)^2>]^{1/2}} \tag{A-14a}$$

where n_1, s_1, n_2, s_2, are the noise and signal parts of the i-f voltages at the two terminals. But since all the cross-correlation terms except $s_1 s_2$ vanish,

$$\rho = \frac{\langle s_1 s_2 \rangle}{[\langle (n_1 + s_1)^2 \rangle \langle (n_2 + s_2)^2 \rangle]^{1/2}} \qquad \text{(A-14b)}$$

where both sides of the formula are now to be interpreted in terms of expectations. The two factors in the denominator of (A-14b) are proportional to the total (signal plus noise) power available at the terminals of the two receivers; that is, to

$$P = kT\Delta\nu \qquad \text{(A-15a)}$$

where P is the available power,

k is Boltzmann's constant, 1.38×10^{-23} joule/kelvin,

T is the total receiver noise temperature, and

$\Delta\nu$ is the receiver i-f bandwidth.

Furthermore the two factors in the numerator of (A-14b) are proportional to the square root of the *signal* power available, which can be written as

$$P_s = kT_s\Delta\nu = S\eta A\Delta\nu/2 \qquad \text{(A-15b)}$$

where P_s and T_s denote the signal (correlated) contributions to P and T,

S is the correlated source flux,

η is the antenna aperture efficiency, and

A is the geometrical antenna aperture.

Therefore we can use the relations (A-15) to rewrite (A-14b). Remembering also to insert the Van Vleck clipping correction,

$$\rho_{clipped} = (2/\pi)\ \sin^{-1}(\rho_{unclipped}) \qquad \text{(A-16)}$$

(for which Clark *(21)* gives a good, simple derivation), to account for the degradation of the correlation caused by clipping, we may rewrite the correlation formula (A-14b), in the low-correlation limit, as

$$\rho = \frac{2}{\pi}\left[\frac{T_{1,s}T_{2,s}}{T_1T_2}\right]^{1/2} = \frac{S(\eta_1A_1\eta_2A_2)^{1/2}}{\pi k(T_1T_2)^{1/2}} \qquad \text{(A-17)}$$

where subscripts 1 and 2 now refer to the two antenna systems, and subscript s again isolates that portion of the system temperature due to the correlated source flux.

Equation (A-17) shows that the first-order effect of uncorrelated system noise, whether due to the receiver, antenna spillover, uncorrelated source flux, or other causes, is to reduce the observed correlation by a factor proportional to the geometric mean of the two system temperatures. There is also a second-order effect, which arises from the uncertainty introduced into the measurement of ρ by the presence of the uncorrelated noise. The

following paragraphs show how this effect introduces bias into the correlation measurements.

Figure A-1 depicts schematically how the Fourier transform operates on a waveform containing both correlated and uncorrelated parts. The amplitude of the correlated part (the signal) is S, and its phase is ϕ. It is composed of the real and imaginary (or if you prefer, sine and cosine) parts S_R and S_I, which are added in quadrature as indicated in the Figure. In addition to the signal contribution to the total amplitude, A, there is also a noise part of amplitude N, whose components N_R and N_I combine with S_R and S_I to give the component amplitudes A_R and A_I, for which probability distribution functions are plotted along the corresponding axes. The variances in the distributions of A_R and A_I are precisely those of (A-8b), but the means are no longer zero because of the presence of the signal.

We can now compute the probability distribution function of A. Consider A as the composition of S, a fixed vector in the plane, and N, whose distribution is given by (A-11). Using (A-10) with $P_1(N) = R(N;N_0)$; $P_2(\theta) = 1/2\pi$, $0 \leq \theta < 2\pi$; $y = A = (S^2 + N^2 - 2SN\cos\theta)^{1/2}$; and performing the integral, we find that

$$P\{A\} = \frac{A}{N_0^2}\exp[-(S^2+A^2)/2N_0^2]\ I_0(AS/N_0^2),\ 0 \leq A < \infty \qquad \text{(A-18a)}$$

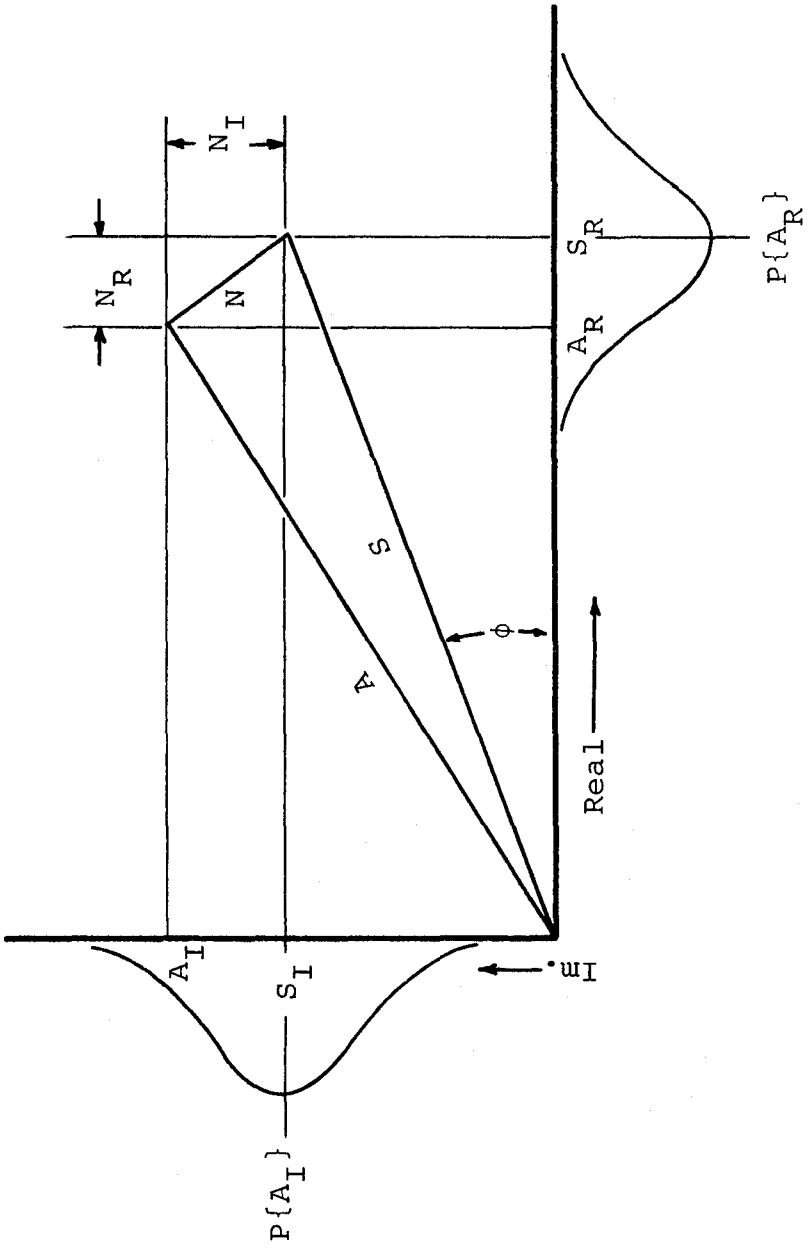

Figure A-1. Analysis of a sinusoidal signal modified by Gaussian noise.

where I_0 is the Bessel function of imaginary argument. A more convenient form results when we scale the distribution in units of N_0: letting $\gamma = A/N_0$, $\delta = S/N_0$,

$$P\{\gamma|\delta\} = \gamma e^{-(\delta^2+\gamma^2)/2} I_0(\delta\gamma), \quad 0 \leq \gamma < \infty \qquad \text{(A-18b)}$$

in which the left member, to be read, "P of γ given δ," emphasizes the fact that the distribution of γ is specified in terms of a *known*, *fixed* value of δ. The distribution (A-18a,b) is named the Rice distribution after the man who first investigated it thoroughly *(81)*. It approaches $R(A;N_0)$ as $\delta \to 0$ and approaches $G(A;S,N_0)$ as $\delta \to \infty$.

By the same method we can also determine the distribution of the phase error of A, $\theta = \arg(A) - \arg(S)$:

$$P\{\theta|\delta\} = (1/2\pi)e^{-\delta^2/2} + \frac{\delta\cos\theta}{\sqrt{8\pi}} e^{-\delta^2\sin^2\theta/2} \times \qquad \text{(A-18c)}$$

$$\times[1 + \operatorname{erf}(\delta\cos\theta/\sqrt{2})], \quad 0 \leq \theta < 2\pi$$

where

$$1 + \operatorname{erf}(\delta\cos\theta/\sqrt{2}) = (2/\pi)^{1/2} \int_{-\infty}^{\delta\cos\theta} e^{-x^2/2}\, dx \qquad \text{(A-18d)}$$

(A-18b,c) are virtually identical to equations (8-115) and (8-118) of Davenport and Root *(37)*, who give a more formal derivation in a less restricted context.

(A-18b) is not yet the form we want, however. It

gives information about γ when δ is known; but in practice we measure A (that is, γ, if we know N_0) and want to draw inferences concerning S (or δ). In order to "invert" (A-18b) we have to interpret the right member as a bivariate distribution, in γ and δ, and make some assumption about the marginal density function for δ. (There are philosophical difficulties at this point which the reader will have to resolve to his own satisfaction.) Proceeding from the weakest possible assumption, that all values of δ are *a priori* equally probable, we obtain the desired relation by simply renormalizing (A-18b):

$$P\{\delta|\gamma\} = P\{\gamma|\delta\}/\int_0^\infty P\{\gamma|\delta\}\, d\delta \qquad (A\text{-}19)$$

$$= (2/\pi)^{1/2} e^{-[(2\delta^2+\gamma^2)/4]} I_0(\delta\gamma)/I_0(\gamma^2/4),\ 0 \leq \delta < \infty$$

(A-11, 13, 17, 18, 19) are the fundamental relations needed to transform uncorrected correlation coefficients to a scale strictly proportional to correlated flux. How they are used in a particular case, however, depends on the details of the reduction procedure. The next section describes how they were applied to the data of this experiment.

Applications First let us understand a little better the relationship between (A-18b) and (A-19). The moments of the two distributions are of interest and can be expressed in terms of familiar functions. In general,

$$E\{\gamma^n|\delta\} = (2)^{n/2}\,\Gamma(\tfrac{n}{2}+1)\,e^{-\delta^2/2}\,{}_1F_1(\tfrac{n}{2}+1;1;\tfrac{\delta^2}{2}) \quad \text{(A-20a)}$$

where $E\{x\}$ denotes the statistical expectation of x,

$\Gamma(x)$ is the ordinary gamma function, and

${}_1F_1(a;b;x)$ is the confluent hypergeometric function.

For the values of the parameters with which we are concerned ${}_1F_1(a;b;x)$ can be expressed in terms of exponentials or Bessel functions. Using these relations we find, for the first two moments,

$$E\{\gamma|\delta\} = \sqrt{\pi/2}\,e^{-\delta^2/4}\,[(1+\tfrac{\delta^2}{2})I_0(\delta^2/4) + \tfrac{\delta^2}{2}I_1(\delta^2/4)] \quad \text{(A-20b)}$$

$$E\{\gamma^2|\delta\} = \delta^2 + 2 \quad \text{(A-20c)}$$

(Observe the implication of (A-20c): the power in the signal-plus-noise is the sum of the signal power and the noise power.)

Similarly,

$$E\{\delta^n|\gamma\} = (2^n/\pi)^{1/2}\,\Gamma(\tfrac{n}{2}+\tfrac{1}{2})\,\frac{e^{-\gamma^2/4}}{I_0(\gamma^2/4)}\,{}_1F_1(\tfrac{n}{2}+\tfrac{1}{2};\,1;\,\tfrac{\gamma^2}{2}) \quad \text{(A-21a)}$$

and in particular,

$$E\{\delta|\gamma\} = \sqrt{2/\pi}\ e^{\gamma^2/4}/I_0(\gamma^2/4) \qquad \text{(A-21b)}$$

$$E\{\delta^2|\gamma\} = 1 + \gamma^2\{[I_0(\gamma^2/4) + I_1(\gamma^2/4)]/2I_0(\gamma^2/4)\} \qquad \text{(A-21c)}$$

Now we can compute corrected correlation amplitudes in a simple case. Suppose that we have a single reliable measurement of a correlation, A_1. First we compute the noise level, A_0, using either (A-11b) or an experimental determination, and find $\gamma = A_1/A_0$. Then we merely multiply A_1 by $E\{\delta|\gamma\}/\gamma$ (using (A-21b)) to remove the bias and multiply the product by $\sqrt{T_1T_2}$ -- or if necessary by $\sqrt{T_1T_2/\eta_1\eta_2}$ -- to give a corrected value that is independent of the variable system parameters. If we like we can even estimate the error in the result with the help of (A-21c).

In practice, however, two important considerations disrupt this simple scheme. First, it is rarely practical to Fourier transform a long observation -- fifteen minutes, say -- *en masse*. When the signal-to-noise ratio is high enough it is usually better to subdivide the observation into shorter segments, each typically a minute long, and take the scalar average of the results. In this case it is *not* correct to apply (A-21b) to the scalar average. In fact the proper correction is a function not only of γ, but also of n (the number of segments being averaged) as well; and as n becomes large without limit, the correction

converges to the function $E\{\gamma|\delta\}$ given by (A-20b).

This paradoxical result is actually easy to understand if we retrace a few steps of the derivation. When γ is the average of n independent measurements, $P\{\gamma|\delta\}$ is no longer the right member of (A-18b), but rather the n-fold self-convolution of that expression. Making the required substitution, and calling the result $P\{\gamma|n,\delta\}$, we can then proceed as before to calculate $P\{\delta|n,\gamma\}$ and its moments. Notice that as $n\to\infty$, $P\{\gamma|n,\delta\}$ approaches a delta function at $\gamma = E\{\gamma|\delta\}$. In that case $P\{\delta|n,\gamma\}$ approaches a delta function also, and $E\{\delta|n\to\infty,\gamma\}$ becomes simply the inverse of $E\{\gamma|\delta\}$, as mentioned above.

The general expression for $P\{\gamma|n,\delta\}$, so far as I know, cannot be expressed compactly in closed form; but in most practical situations n is large enough so that we can make a very good approximation by using the central limit theorem -- namely,

$$P\{\gamma|n\to\infty,\delta\} \sim G(\gamma;\ E\{\gamma|\delta\},\ [\tfrac{1}{n}(E\{\gamma^2|\delta\} - E^2\{\gamma|\delta\})]^{1/2}) \quad \text{(A-22)}$$

in which the variance of the normal distribution is evidently just 1/n times the variance of $P\{\gamma|\delta\}$. This approximation makes the succeeding numerical computations quite tractable, and I used it throughout the reductions.

The second additional consideration is most important when the signal is only marginally detectable above

the noise. It arises because the residual delay and fringe rate are not precisely known *a priori*. Consequently it is necessary to search for the fringes over a substantial range of both delay and rate, with the result that the effective noise level is enhanced, and sometimes an especially intense noise point is mistaken for the signal.

Figure A-2 depicts the procedure schematically. The reduction program computes correlation amplitudes on a rectangular grid of thirty-five points in the delay-rate plane and locates the point of largest amplitude. Then it interpolates in the immediate neighborhood of that point to estimate the true amplitude, rate, and delay of the fringes. We need to know how often this procedure will pick a "wrong" point -- that is, a noise point remote from the signal -- and how these errors will affect the distribution of the measured amplitudes.

Details of the reduction procedure complicate the analysis. To simplify it, suppose at first that the signal falls precisely on a point in the grid (so that no interpolation is necessary) and that the measurements at all thirty-five points are statistically independent. In that case the amplitude distribution at the signal point is $P\{\gamma|\delta\}$ (A-18b), and at the thirty-four noise points it is $R(\gamma N_0; N_0)$ (according to (A-11a)). The probability distribution of the largest among the noise points is

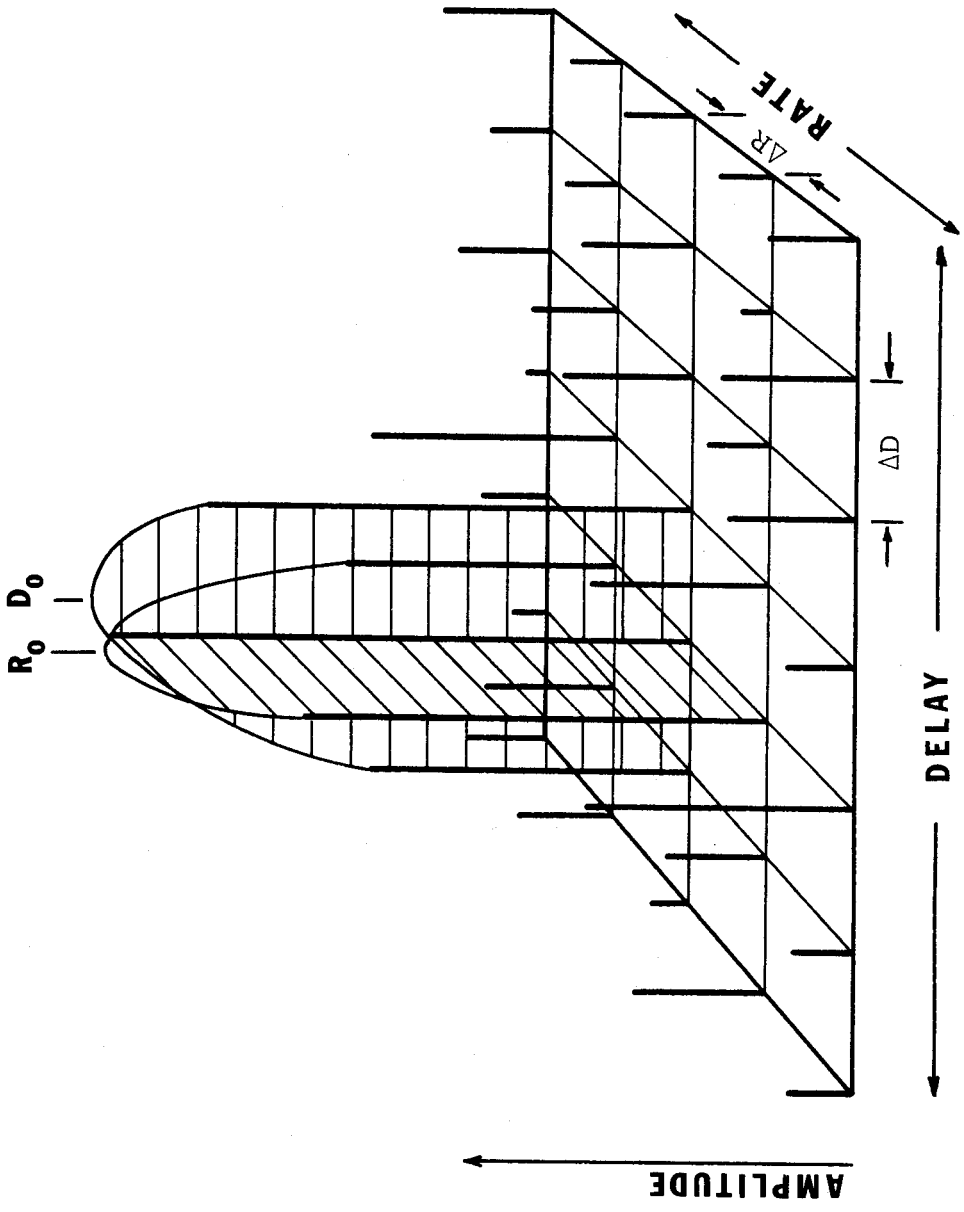

Figure A-2. Determination of fringe amplitude, delay (D_0), and rate (R_0) using amplitudes measured on a lattice of points in the delay-rate plane. ΔD = 0.25 microsecond, and ΔR is variable.

$R_{34}(\gamma N_0;\ N_0)$, *à la* (A-13). If we define the cumulative probability distribution functions associated with $P\{\gamma|\delta\}$ and $R_m(x;x_0)$ as

$$P\{\gamma|\delta\} = \int_0^{\gamma} P\{g|\delta\}\ dg \qquad \text{(A-23)}$$

and

$$R_m(x;x_0) = \int_0^{x} R_m(\xi;x_0)\ d\xi \qquad \text{(A-24)}$$

then the probability that the largest noise amplitude will be larger than the signal-plus-noise amplitude, for a given signal-to-noise ratio, is simply

$$\int_0^{\infty} R_{34}(\gamma N_0;\ N_0)\ P\{\gamma|\delta\}\ d\gamma \qquad \text{(A-25)}$$

Of more immediate concern is the effect of these errors on the distribution of the measured amplitudes -- an effect which obviously depends on how one deals with the errors. There are several plausible ways. Probably the most straightforward is to ignore them -- to allow them to persist through the succeeding stages of data reduction. In that case the distribution $P\{\gamma|\delta\}$ is replaced by

$$P_a^*\{\gamma|\delta\} = P\{\gamma|\delta\}R_{34}(\gamma N_0;N_0) + P\{\gamma|\delta\}R_{34}(\gamma N_0;N_0) \qquad \text{(A-26a)}$$

Another way is to try to identify the errors (by their discrepant fringe rates or delay values, for example)

and excise them from the data. In this scheme, if the detection procedure is perfect, $P\{\gamma|\delta\}$ is replaced by

$$P_b^*\{\gamma|\delta\} = P\{\gamma|\delta\}R_{34}(\gamma N_0;N_0)\Big/\int_0^\infty P\{\gamma|\delta\}R_{34}(\gamma N_0;N_0)\,d\gamma \quad \text{(A-26b)}$$

Now we had better return to our simplifying assumptions and gauge their effect on the results. Neighboring points in the delay-rate grid are, in fact, correlated, so that the number of statistically independent measurements must be rather less than thirty-five. To compensate, at least partially, for this correlation we can allow the parameter m in the analysis (formula (A-13)) to assume a value smaller than thirty-four. The fact that the signal is not concentrated in one point of the grid, but is actually distributed over several points, also has an effect, in that it increases the likelihood that some noise point will be strongest. We can reasonably hope to counteract this effect too by varying m (in this instance by raising it). Other factors are significant only when the signal-to-noise ratio is so low that the measurement is practically worthless.

At this point it finally appears that we have a complete prescription for correcting correlation amplitudes:

1) Determine the noise level, N_0, either by using (A-11b) or, preferably, by observing actual noise.

2) Begin with $P\{\gamma|\delta\}$ (A-18b). If the signal-to-noise ratio is low, replace P by P_a^* (A-26a), P_b^* (A-26b), or another appropriate form, using a suitable value of m in the R_m and $\mathcal{R}_m$ distributions. One way to choose m is to treat it as a variable parameter, reduce some of the correlation tapes twice using two different coherent integration times, and pick the value of m that produces the best agreement between the two sets of corrected results.

3) If the correlations being reduced are averages of a small number of coherent integrations convert $P^*\{\gamma|\delta\}$ to $P^*\{\gamma|n,\delta\}$ and thence to $P^*\{\delta|n,\gamma\}$. The approximation (A-22) may be helpful.

4) Compute $E\{\delta\}$ and $E\{\delta^2\}$. Correct the measured amplitude and estimate the error accordingly.

5) Eliminate the effects of variable system parameters by using (A-17).

Figure A-3 shows the result of applying the foregoing method to the data of this investigation. I reduced the data from the second observing session with coherent integration times of fifteen and seventy-five seconds. For fifteen-second integrations the measured noise level was $\langle\rho\rangle = 0.0002938$, in good agreement with expectation. I used n = 30, a typical value for the fifteen-second reductions, and varied m to fit the data of Figure A-3a, in which the systematic difference between the two sets of

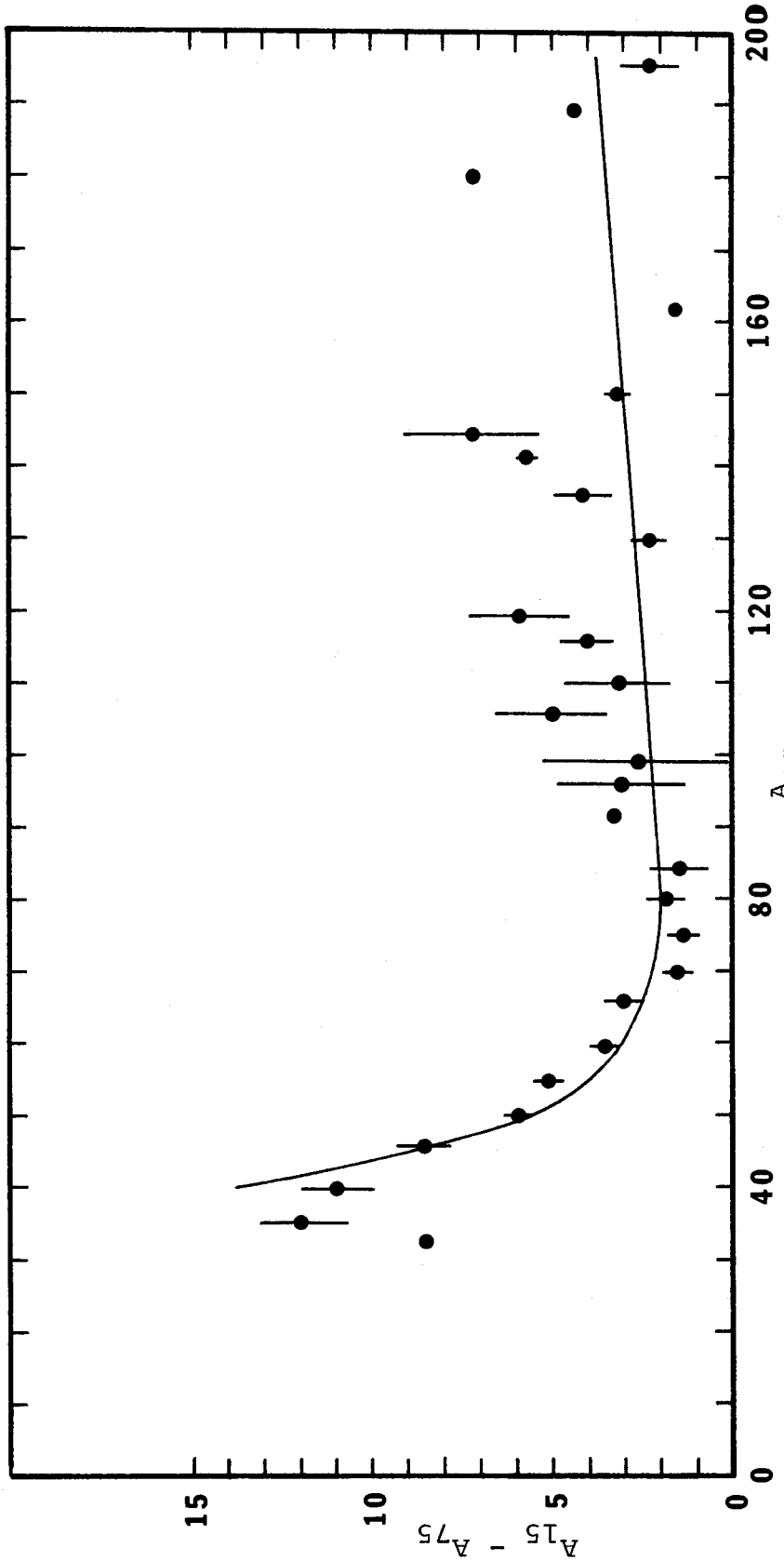

Figure A-3a. Systematic differences between raw correlation amplitudes obtained from 15- and 75-second coherent integrations (A_{15} and A_{75}, respectively). Each point represents a cluster of measurements, and the curve is predicted by the model described in the text. One correlation unit corresponds to $\rho = 10^{-5}$.

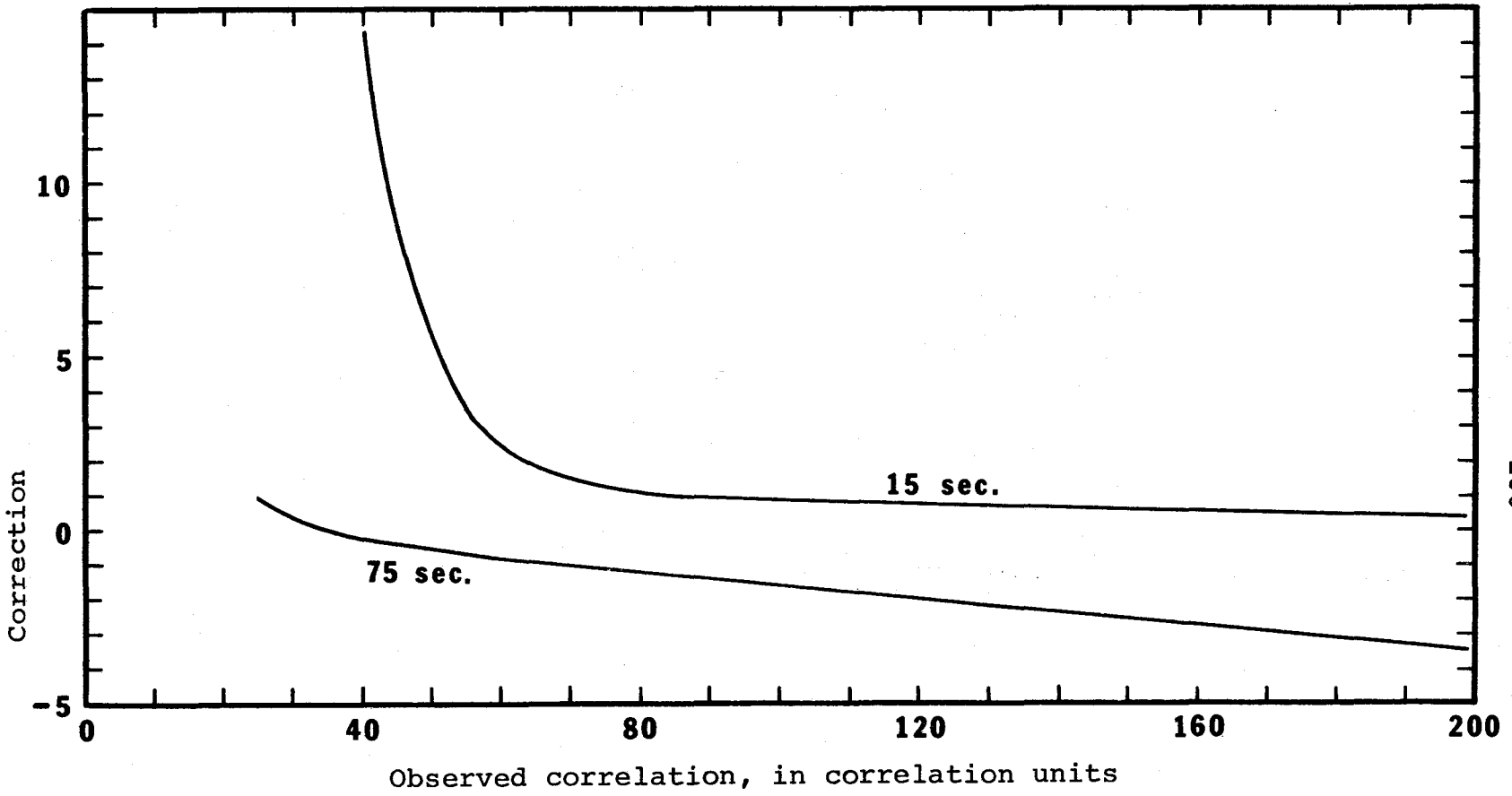

Figure A-3b. Corrections applied to raw correlation amplitudes, for 15- and 75-second coherent integrations. The correction is to be subtracted from the observed value. One correlation unit corresponds to $\rho = 10^{-5}$.

amplitudes (in correlation units) is plotted as a function of the fifteen-second amplitudes. The solid line is the computed curve for m = 17, the optimum value. The computation also includes a 1.8 percent linear correction to the seventy-five-second data. This correction compensates for systematic decorrelation in the longer integrations, due to fluctuations in the apparent fringe rate. In Figure A-3b are plotted the corresponding correction curves for the two sets of reductions.

APPENDIX B

THE MODEL-FITTING ALGORITHM

This appendix discusses briefly the nonlinear least-squares fitting procedure used in this investigation to refine source models. Numerous writers have developed the theory, including Hamilton *(48, Ch. 4)*, whose treatment is straightforward and thorough and whose notation I have adopted; and Chapter 4 deals with some related practical problems. Therefore I restrict myself here to stating the theoretical results and describing the procedure.

If the two-dimensional brightness distribution of a radio source can be partitioned into components in such a way that each component is transformed into itself by a 180-degree rotation about its own center, then the complex visibility of the ensemble can be written as

$$V = \left\{ \sum_i S_i v_i e^{-i2\pi B r_i \cos(\phi - \theta_i)} \right\} \Big/ \sum_i S_i \qquad \text{(B-1)}$$

where V is the complex visibility,

S_i is the flux of the i-th component,

v_i is the modulus of the visibility of the i-th component,

B and ϕ are the length (in wavelengths) and position angle, respectively, of the projection of the

interferometer baseline onto a plane perpendicular to the line of sight to the source, and

r_i and θ_i are the radius (in radians) and position angle of the i-th component with respect to an arbitrary origin in the source.

If the isophotes of the components are concentric, similar ellipses, then each v_i in (B-1) is the (zero order) Hankel transform of the brightness distribution along the semi-major axis of that component. That is,

$$v(Q) = \int_0^\infty f(x)\ J_0(2\pi Q x)\ x\ dx \Big/ \int_0^\infty f(x)\ x\ dx \qquad \text{(B-2a)}$$

where f(x) (with x in radians) is the brightness distribution along the semi-major axis, and

$$Q = B[\cos^2(\phi-\zeta) + \alpha^2\sin^2(\phi-\zeta)]^{1/2} \qquad \text{(B-2b)}$$

in which ζ is the position angle of the semi-major axis, and

α is the axial ratio ($0 \leq \alpha \leq 1$).

The normalization factor in (B-2a) assures that $v(0) = 1$.

The reduction program allows the user to specify four particular types of elliptical components:

1) Gaussian: $f(x) = (1/16)^{+x^2/x_0^2}$ (x_0 being the full width to half-maximum intensity)

$$v = e^{-(\pi^2/4\ \ln\ 2)(Qx_0)^2} \qquad \text{(B-3)}$$

2) Uniformly bright disk: $f(x) = \begin{cases} 1, & 0 \leq x \leq x_0 \\ 0, & x > x_0 \end{cases}$

$$v = J_1(2\pi Q x_0)/(\pi Q x_0) \tag{B-4}$$

3) Tapered disk: $f(x) = \begin{cases} [1 - (x^2/x_0^2)]^{1/2}, & 0 \leq x \leq x_0 \\ 0, & x > x_0 \end{cases}$

$$v = 3(\pi/2)^{1/2} J_{3/2}(2\pi Q x_0)(2\pi Q x_0)^{-3/2} \tag{B-5}$$

$$= \frac{3}{(2\pi Q x_0)^3}[\sin(2\pi Q x_0) - 2\pi Q x_0 \cos(2\pi Q x_0)]$$

4) Ring: $f(x) = \delta(x - x_0)$

$$v = J_0(2\pi Q x_0) \tag{B-6}$$

A component of a given type, then, is completely specified by six numbers: its flux (S), the position of its centroid (r,θ), its semi-major axis (x_0), its axial ratio (α), and the position angle of the major axis (ζ). The aggregate of these numbers, for all the components, is the set of parameters sought by the fitting procedure. They constitute a parameter matrix $[X]_{m,1}$.

(A note on notation: $[Z]_{x,y}$ means the matrix Z, of x rows and y columns, containing the elements $\{z_{i,j}\}$. Its inverse is $[Z]^{-1}$ and its transpose is $[Z]'$.)

The observation matrix, $[F]_{n,1}$, is a set of n

observations of mod(V)(as defined by (B-1)). In the linear case [F] and [X] are related by the formula

$$[F]_{n,1} = [A]_{n,m}[X]_{m,1} + [E]_{n,1} \qquad \text{(B-7)}$$

where [A], called the design matrix, is known (usually from theory), and [E] is the matrix of random errors in observation. The $\{e_i\}$ are supposed to have a joint distribution with zero means and a variance-covariance matrix $[M_f]_{n,n}$ in which

$$(m_f)_{i,j} = E\{e_i e_j\} = \text{cov}(f_i, f_j) \qquad \text{(B-8)}$$

where $E\{x\}$ denotes the statistical expectation of x.

In many experimental situations, including this one, all the errors may be assumed to be statistically independent. In other words, $(m_f)_{i,j} = 0$ when $i \neq j$. It may also be that the scale of the errors is uncertain:

$$[M_f]_{n,n} = \sigma^2[N]_{n,n} \qquad \text{(B-9)}$$

where we know [N] but not σ^2. In this experiment we have excellent estimates of the errors, both from theory (see Appendix A) and from the data themselves (the statistics of the short coherent integrations). Even so it is worthwhile to preserve the factor σ^2 in the calculations and use it, as shown below, to gauge the quality of the models.

Under the foregoing assumptions it can be shown that there exists an estimate $[\hat{X}]$ of $[X]$ that gives an unbiased, minimum-variance estimate of any linear combination of the $\{x_i\}$. Defining $[P]_{n,n} = [N]^{-1}$, we can write that estimate as

$$[\hat{X}]_{m,1} = [[A]'[P][A]]^{-1}[A]'[P][F] \tag{B-10}$$

or alternately, if

$$[B]_{m,m} = [A]'[P][A] \tag{B-11}$$

then

$$[\hat{X}] = [B]^{-1}[A]'[P][F] \tag{B-12}$$

$[B]$, or more commonly $\sigma^2[B]$, is called the matrix of the normal equations. Notice that $[\hat{X}]$ is independent of σ^2.

The method also enables us to compute the covariance matrix for the desired estimates. Specifically, if

$$[M_x]_{m,m} = E\{[[\hat{X}] - [X]][[\hat{X}] - [X]]'\} \tag{B-13}$$

then

$$[M_x] = \sigma^2[B]^{-1} \tag{B-14}$$

If σ^2 is known we can calculate $[M_x]$ directly. Otherwise

we can use an unbiased estimate of σ^2, namely

$$\hat{\sigma}^2 = [V]'[P][V]/(n-m) \qquad \text{(B-15a)}$$

where

$$[V]_{n,1} = [F] - [A][\hat{X}] \qquad \text{(B-15b)}$$

to compute an unbiased *estimate* of $[M_x]$:

$$[\hat{M}_x]_{m,m} = (n-m)^{-1}[V]'[P][V][B]^{-1} \qquad \text{(B-16)}$$

Now let us relate this procedure more directly to the problem of refining source models. The foregoing formulas are not strictly applicable, because the relation between [F] and [X] -- which is to say, the relation between mod(V) and the parameters S_i, r_i, θ_i, x_{0i}, α_i, and ζ_i, as defined by (B-1 to 6) -- is extremely nonlinear. Nevertheless, *if* we are able to make a good initial guess at [X], say, $[X^\circ] = \{x_1^\circ, x_2^\circ, \ldots, x_m^\circ\}$ -- then we can simulate a linear problem by expanding the functional relation between [F] and [X] in a Taylor series around $[X^\circ]$ and truncating the series after the linear terms. That is,

$$f_i - f_i(x_1^\circ, x_2^\circ, \ldots, x_m^\circ) \simeq \sum_{j=1}^{m} \frac{\partial f_i}{\partial x_j}(x_j - x_j^\circ) \qquad \text{(B-17)}$$

In this form the relation can be identified with (B-7)

if we make the replacements

$$[A] = \{a_{i,j}\} = \{ \frac{\partial f_i}{\partial x_j} (x_1^\circ, x_2^\circ, \ldots, x_m^\circ) \} \qquad \text{(B-18a)}$$

$$[F] = \{\Delta f_i\} = \{f_i - f_i(x_1^\circ, x_2^\circ, \ldots, x_m^\circ)\} \qquad \text{(B-18b)}$$

$$[X] = \{\Delta x_j\} = \{x_j - x_j^\circ\} \qquad \text{(B-18c)}$$

With these substitutions and the error estimates [N] we can complete the computations (B-10 to 16) just as though the problem were truly linear.

In its crudest outline, then, the fitting proceeds as follows. The program begins with the observations [F], the diagonal error matrix [N], an initial estimate [X°] of the parameters, and the relations needed to compute analytically the partial derivatives in (B-18). The elements used in the error matrix are not the experimental sample variances but rather theoretical values computed by the methods of Appendix A. In addition to giving a better estimate of the population variance this choice eliminates the undesirable possibility of assigning an artificially high relative weight to a single point. The initial model usually is the mutual product, in varying proportions, of previous experience, crude graphical analysis of the visibility curve, and guesswork.

From the inputs the program first computes [A],

[B], and [F°] = [A][X°]. Then it inverts [B], substitutes [F] - [F°] for [F], and computes $[\hat{X}]$ according to (B-12). Finally it increments the initial parameters to obtain a (presumably!) improved set, $[X^1] = [X^\circ] + [\hat{X}]$. The program continues to iterate on the new parameters, following the same pattern, until no further improvement is possible.

After each iteration the criterion of goodness-of-fit is the parameter $\hat{\sigma}^2$, as given by (B-15), except that the exact nonlinear relation is substituted for the linear approximation [F] = [A][X]. In other words, at the i-th iteration $\hat{\sigma}^2$ is simply the weighted sum of the squares of the residual differences between the observations and the predictions of the model, divided by (n - m):

$$\hat{\sigma}^2 = (n - m)^{-1} \sum_{j=1}^{n} (n_{j,j})^{-1} [f_j^{(obs.)} - f_j(x_1^i, x_2^i, \ldots, x_m^i)]^2 \qquad \text{(B-19)}$$

in which the $n_{j,j}$, diagonal elements of the matrix [N], are not to be confused with unsubscripted n, the total number of observations.

The parameter $\hat{\sigma}^2$ bears one of two interpretations, depending on whether the error analysis or the model is more reliable. If the scale of the errors is uncertain, it is an unbiased estimate of the scale factor in (B-9). But if, as in this case, the errors are known, then $\hat{\sigma}^2$ is a

parameter that characterizes how well the model fits the data. It is, in fact, the statistic known as "chi-square per degree of freedom," commonly used in hypothesis testing. The square root of $\hat{\sigma}^2$ is the number called the "error factor" in Chapter 4. It tells roughly how many times bigger the discrepancies between the model and the observations are, on the average, than one might expect for a correct and complete model.

The simple scheme outlined above does not remove the nonlinearity of the underlying problem, of course -- it merely obscures it; and this essential feature intrudes at numerous points to complicate both the procedure and the interpretation of the results. Interpretation is the subject of Chapters 4 and 5. Here, in closing, two computational stratagems deserve brief attention.

The first arises from the fact that the increments in the parameters recommended by (B-12) frequently are far from the optimum values; occasionally they actually make the fit worse. The program deals with this difficulty by allowing the *actual* increments to take the form $c[\hat{X}]$, where c is a constant to be determined and $[\hat{X}]$ is the recommended set of increments. The program tries several values of c and calculates $\hat{\sigma}^2$ for each one until it detects a minimum in the relation $\hat{\sigma}^2(c)$. Then it locates the minimum -- that is, the best value of c -- by fitting a

parabola to the three nearest points in the relation.

The second stratagem also helps to assure steady convergence. Almost invariably, in the model-fitting, there are parameters whose errors are highly correlated -- for example the flux and the size of a component. The direct effect of this correlation on the fitting procedure is that [B], the matrix of the normal equations, is nearly singular and therefore hard to invert accurately (because of round-off errors). Moreover the matrix $[\hat{X}]$ computed from $[B]^{-1}$ according to (B-12) is likely to demand huge increments, utterly beyond the range of the linear approximation, in the correlated parameters. What we need to do, is somehow to identify what linear combinations of the parameters are poorly determined, isolate them, and hold them fixed. In terms of matrix algebra, we want to diagonalize [B]. The matrix of the eigenvectors specifies the independent linear combinations of the parameters, and the associated eigenvalues show immediately which ones are ill-determined. (Recall from (B-14) that the covariance matrix of the parameter estimates is proportional to $[B]^{-1}$. When the diagonalized [B] is inverted, small eigenvalues become large variances.) We simply complete the calculation of the increments in the rotated parameter space, suppress variation of the poorly determined parameters, and retransform the results to the old coordinate system.

By neutralizing the near-singularity of the normal equations, this trick has been notably successful in promoting smooth convergence.

REFERENCES

1. Adgie, R. L., Gent, H., Slee, O. B., Frost, A. D., Palmer, H. P., and Rowson, B., *Nature*, *208*, 275 (1965).
2. Allen, L. R., Anderson, B., Conway, R. G., Palmer, H. P., Reddish, V. C., and Rowson, B., *Monthly Notices Roy. Astron. Soc.*, *124*, 477 (1962).
3. Aller, H. D., and Haddock, F. T., *Astrophys. Journ.*, *147*, 833 (1967).
4. Anderson, B., and Donaldson, W., *Monthly Notices Roy. Astron. Soc.*, *137*, 81 (1967).
5. Barber, D., Donaldson, W., Miley, G. K., and Smith, H., *Nature*, *209*, 753 (1966).
6. Bare, C., Clark, B. G., Kellermann, K. I., Cohen, M. H., and Jauncey, D. L., *Science*, *157*, 189 (1967).
7. Bologna, J. M., McClain, E. F., and Sloanaker, R. M., *Science*, *153*, 294 (1966).
8. Bracewell, R. N., "Radio Astronomy Techniques," in *Handbuch der Physik, Vol. XIV: Astrophysik V: Verschiedenes*, ed. by S. Flügge (Berlin: Springer-Verlag, 1962), p. 42.
9. Broderick, J. J., Clark, B. G., Cohen, M. H., Ephanov, V. A., Hansson, B., Jauncey, D. L., Kellermann, K. I., Kogan, L. R., Kostenko, V. I., Matveyenko, L. I., Moiseyev, I. G., Payne, J., and Vitkevitch, V. V., *Radio Sci.*, *5*, 1281 (1970).
10. Broderick, J. J., Kellermann, K. I., Shaffer, D. B., and Jauncey, D. L., *Astrophys. Journ.*, *172*, 299 (1972).
11. Broten, N. W., Clarke, R. W., Legg, T. H., Locke, J. L., Galt, J. A., Yen, J. L., and Chisholm, R. M., *Monthly Notices Roy. Astron Soc.*, *146*, 313 (1969).

12. Broten, N. W., Clarke, R. W., Legg, T. H., Locke, J. L., McLeish, C. W., Richards, R. S., Yen, J. L., Chisholm, R. M., and Galt, J. A., *Nature, 216*, 44 (1967).

13. Broten, N. W., Locke, J. L., Legg, T. H., McLeish, C. W., Richards, R. S., Chisholm, R. M., Gush, H. P., Yen, J. L., and Galt, J. A., *Nature, 215*, 38 (1967).

14. Burbidge, E. M., and Burbidge, G. R., *Astrophys. Journ., 142*, 1351 (1965).

15. Burbidge, E. M., and Burbidge, G. R., *Astrophys. Journ., 143*, 271 (1966).

16. Burbidge, E. M., Burbidge, G. R., and Prendergast, K. H., *Astrophys. Journ., 130*, 26 (1959).

17. Burbidge, E. M., and Rosenberg, F. D., *Astrophys. Journ., 142*, 1673 (1965).

18. Burbidge, G. R., *Annual Rev. Astron. Astrophys., 8*, 369 (1970).

19. Burbidge, G. R., Burbidge, E. M., Hoyle, F., and Lynds, C. R., *Nature, 210*, 774 (1966).

20. Burbidge, G. R., Burbidge, E. M., and Sandage, A. R., *Rev. Modern Phys., 35*, 947 (1963).

21. Clark, B. G., *Annual Rev. Astron. Astrophys., 8*, 115 (1970).

22. Clark, B. G., Cohen, M. H., and Jauncey, D. L., *Astrophys. Journ. (Letters), 149*, L151 (1967).

23. Clark, B. G., Kellermann, K. I., Bare, C. C., Cohen, M. H., and Jauncey, D. L., *Astrophys. Journ. (Letters), 153*, L67 (1968).

24. Clark, B. G., Kellermann, K. I., Bare, C. C., Cohen, M. H., and Jauncey, D. L., *Astrophys. Journ., 153*, 705 (1968).

25. Clark, B. G., Kellermann, K. I., Cohen, M. H., Shaffer, D. B., Broderick, J. J., Jauncey, D. L., Matveyenko, L. I., and Moiseyev, I. G., preprint, submitted to *Astrophys. Journ. (Letters)* (1973).

26. Clark, B. G., Weimer, R., and Weinreb, S., *The Mark II VLB System: Principles and Operating Procedures*, Electronics Division Internal Report 118, (Green Bank, West Virginia: National Radio Astronomy Observatory, 1972).

27. Clarke, M. E., Bolton, J. G., and Shimmins, A. J., *Australian Journ. Phys., 19*, 375 (1966).

28. Clarke, R. W., Broten, N. W., Legg, T. H., Locke, J. L., and Yen, J. L., *Monthly Notices Roy. Astron. Soc., 146*, 381 (1969).

29. Cohen, M. H., *Annual Rev. Astron. Astrophys., 7*, 619 (1969).

30. Cohen, M. H., *Astrophys. Letters, 12*, 81 (1972).

31. Cohen, M. H., Cannon, W., Purcell, G. H., Shaffer, D. B., Broderick, J. J., Kellermann, K. I., and Jauncey, D. L., *Astrophys. Journ., 170*, 207 (1971).

32. Cohen, M. H., Gundermann, E. J., and Harris, D. E., *Astrophys. Journ., 150*, 767 (1967).

33. Cohen, M. H., Moffet, A. T., Shaffer, D. B., Clark, B. G., Kellermann, K. I., Jauncey, D. L., and Gulkis, S., *Astrophys. Journ. (Letters), 158*, L83 (1969).

34. Cohen, M. H., and Shaffer, D. B., *Astron. Journ., 76*, 91 (1971).

35. Conway, R. G., Kellermann, K. I., and Long, R. J., *Monthly Notices Roy. Astron. Soc., 125*, 261 (1963).

36. Daltabuit, E., and Cox, D., *Astrophys. Journ. (Letters), 173*, 13 (1972).

37. Davenport, W. B., and Root, W. L., *An Introduction to the Theory of Random Signals and Noise* (New York: McGraw-Hill, 1958).

38. Dent, W. A., *Science*, *148*, 1458 (1965).

39. De Young, D. S., *Astrophys. Letters*, *9*, 43 (1971).

40. Donaldson, W., Miley, G. K., Palmer, H. P., and Smith, H., *Monthly Notices Roy. Astron. Soc.*, *146*, 213 (1969).

41. Donaldson, W., and Smith, H., *Monthly Notices Roy. Astron. Soc.*, *151*, 253 (1971).

42. Erickson, W. C., Kuiper, T. B. H., Clark, T. A., Knowles, S. H., and Broderick, J. J., *Astrophys. Journ.*, *177*, 101 (1972).

43. Fomalont, E. B., *Astrophys. Journ. Suppl. Ser.*, *15*, 203 (1968).

44. Fomalont, E. B., *Astrophys. Journ.*, *157*, 1027 (1969).

45. Galt, J. A., Broten, N. W., Legg, T. H., Locke, J. L., and Yen, J. L., *Nature*, *225*, 530 (1970).

46. Gubbay, J., Legg, A. J., Robertson, D. S., Moffet, A. T., Ekers, R. D., and Seidel, B., *Nature*, *224*, 1094 (1969).

47. Gubbay, J., Legg, A. J., Robertson, D. S., Moffet, A. T., and Seidel, B., *Nature*, *222*, 730 (1969).

48. Hamilton, W. C., *Statistics in Physical Science* (New York: Ronald Press, 1964).

49. Harris, D. E., and Hardebeck, E. G., *Astrophys. Journ. Suppl. Ser.*, *19*, 115 (1969).

50. Hazard, C., Mackey, M. B., and Shimmins, A. J., *Nature*, *197*, 1037 (1963).

51. Hewish, A., Scott, P. F., and Wills, D., *Nature*, *203*, 1214 (1964).

52. Hoerner, S. von, *Astrophys. Journ.*, *144*, 483 (1966).

53. Hogg, D. E., *Astrophys. Journ.*, *155*, 1099 (1969).

54. Hunstead, R. W., *Astrophys. Letters, 12*, 193 (1972).
55. Jauncey, D. L., Bare, C. C., Clark, B. G., Kellermann, K. I., and Cohen, M. H., *Astrophys. Journ., 160*, 337 (1970).
56. Jauncey, D. L., Condon, J. J., and Niell, A. E., private communication (1973).
57. Kellermann, K. I., *Astrophys. Journ., 140*, 969 (1964).
58. Kellermann, K. I., Clark, B. G., Bare, C. C., Rydbeck, O., Ellder, J., Hansson, B., Kollberg, E., Hoglund, B., Cohen, M. H., and Jauncey, D. L., *Astrophys. Journ. (Letters), 153*, L209 (1968).
59. Kellermann, K. I., Clark, B. G., Jauncey, D. L., Cohen, M. H., Shaffer, D. B., Moffet, A. T., and Gulkis, S., *Astrophys. Journ., 161*, 803 (1970).
60. Kellermann, K. I., Jauncey, D. L., Cohen, M. H., Shaffer, D. B., Clark, B. G., Broderick, J. J., Rönnäng, B., Rydbeck, O. E. H., Matveyenko, L., Moiseyev, I., Vitkevitch, V. V., Cooper, B. F. C., and Batchelor, R., *Astrophys. Journ., 169*, 1 (1971).
61. Kellermann, K. I., and Pauliny-Toth, I., *Annual Review Astron. Astrophys., 6*, 417 (1968).
62. Kellermann, K. I., and Pauliny-Toth, I., *Astrophys. Journ. (Letters), 155*, L71 (1969).
63. Kinman, T. D., *Astrophys. Journ. (Letters), 148*, L53 (1967).
64. Knight, C. A., Robertson, D. S., Rogers, A. E. E., Shapiro, I. I., Whitney, A. R., Clark, T. A., Goldstein, R. M., Marandino, G. E., and Vandenberg, N. R., *Science, 172*, 52 (1971).
65. Kristian, J., private communication (1973).
66. Laan, H. van der, *Nature, 211*, 1131 (1966).
67. Lynds, C. R., *Astrophys. Journ., 147*, 837 (1967).

68. Lynds, C. R., *Astrophys. Journ. (Letters), 159,* L151 (1970).

69. Lynds, C. R., Stockton, A. N., and Livingston, W. C., *Astrophys. Journ., 142,* 1667 (1965).

70. Maltby, P., and Moffet, A. T., *Astrophys. Journ., 142,* 409 (1965).

71. Matthews, T. A., and Sandage, A. R., *Astrophys. Journ., 138,* 30 (1963).

72. Merkelijn, J. K., *Australian Journ. Phys., 21,* 903 (1968).

73. Minkowski, R., *I.A.U. Symposium 4: Radio Astronomy,* ed. by H. C. van de Hulst (Cambridge: University of Cambridge Press, 1957), p. 107.

74. Minkowski, R., *Astron. Journ., 73,* 842 (1968).

75. Mitton, S., *Monthly Notices Roy. Astron. Soc., 155,* 373 (1972).

76. Moffet, A. T., Gubbay, J., Robertson, D. S., and Legg, A. J., *I.A.U. Symposium 44: External Galaxies and Quasi-Stellar Objects,* ed. by D. S. Evans (Dordrecht, Holland: D. Reidel, 1972), p. 228.

77. Nicholson, G. D., *Nature, 210,* 611 (1966).

78. Oke, J. B., *Astrophys. Journ., 142,* 810 (1965).

79. Palmer, H. P., Rowson, B., Anderson, B., Donaldson, W., Miley, G. K., Gent, H., Adgie, R. L., Slee, O. B., and Crowther, J. H., *Nature, 213,* 789 (1967).

80. Pauliny-Toth, I. I. K., and Kellermann, K. I., *Astrophys. Journ. (Letters), 152,* L169 (1968).

81. Rice, S. O., *Bell System Tech. Journ., 24,* 46 (1945).

82. Rowson, B., *Monthly Notices Roy. Astron. Soc., 125,* 177 (1963).

83. Ryle, M., and Windram, M. D., *Monthly Notices Roy. Astron. Soc., 138,* 1 (1968).

84. Salpeter, E. E., *Astrophys. Journ., 147*, 433 (1967).
85. Sandage, A. R., *Astrophys. Journ., 141*, 1560 (1965).
86. Sandage, A. R., *Astrophys. Journ. (Letters), 152*, L149 (1968).
87. Sandage, A. R., Véron, P., and Wyndham, J. D., *Astrophys. Journ., 142*, 1307 (1965).
88. Sandage, A. R., and Wyndham, J. D., *Astrophys. Journ., 141*, 328 (1965).
89. Sargent, W. L. W., *Publ. Astron. Soc. Pacific, 79*, 369 (1967).
90. Scheuer, P. A. G., *Nature, 218*, 920 (1968).
91. Scheuer, P. A. G., and Williams, P. J. S., *Annual Rev. Astron. Astrophys., 6*, 321 (1968).
92. Schmidt, M., *Nature, 197*, 1040 (1963).
93. Schmidt, M., *Astrophys. Journ., 141*, 1295 (1965).
94. Schmidt, M., private communication (1973).
95. Schmidt, M., and Matthews, T. A., *Astrophys. Journ., 139*, 781 (1964).
96. Seyfert, C. K., *Astrophys. Journ., 97*, 28 (1943).
97. Shaffer, D. B., Cohen, M. H., Jauncey, D. L., and Kellermann, K. I., *Astrophys. Journ. (Letters), 173*, L147 (1972).
98. Shimmins, A. J., Clarke, M. E., and Ekers, R. D., *Australian Journ. Phys., 19*, 649 (1966).
99. Sholomitskii, G. B., *Information Bull. Var. Stars, Commun. No. 27 of the I.A.U., No. 83* (1965).
100. Sholomitskii, G. B., *Soviet Astron. AJ, 9*, 516 (1965).
101. Smith, H. J., and Hoffleit, D., *Nature, 198*, 650 (1963).
102. Swenson, G. W., *Annual Rev. Astron. Astrophys., 7*, 353 (1969).
103. Terrell, J., *Science, 154*, 1281 (1966).
104. Terzian, Y., *Astron. Journ., 71*, 1030 (1966).
105. Wampler, E. J., *Astrophys. Journ., 147*, 1 (1967).

106. Whitney, A. R., Shapiro, I. I., Rogers, A. E. E., Robertson, D. S., Knight, C. A., Clark, T. A., Goldstein, R. M., Marandino, G. E., and Vandenberg, N. R., *Science*, *173*, 225 (1971).

107. Woltjer, L., *Astrophys. Journ.*, *130*, 38 (1959).

108. Wright, W., unpublished Ph.D. dissertation, California Institute of Technology (1973).

109. Wyndham, J. D., *Astron. Journ.*, *70*, 384 (1965).

110. Wyndham, J. D., *Astrophys. Journ.*, *144*, 459 (1966).

111. Yoshioka, S., *Publ. Astron. Soc. Japan*, *22*, 423 (1970).